2014

RESPONSE OF MARINE COMPOSITES SUBJECTED TO NEAR FIELD BLAST LOADING

Frank LiVolsi
University of Rhode Island, kingporterr@my.uri.edu

RESPONSE OF MARINE COMPOSITES SUBJECTED TO NEAR FIELD BLAST LOADING

BY

FRANK LIVOLSI

A THESIS SUBMITTED IN PARTIAL FULFILLMENT OF THE

REQUIREMENTS FOR THE DEGREE OF

MASTER OF SCIENCE

IN

MECHANICAL ENGINEERING AND APPLIED MECHANICS

UNIVERSITY OF RHODE ISLAND

2014

MASTER OF MECHANICAL ENGINEERING AND APPLIED MECHANICS
THESIS

OF

FRANK LIVOLSI

APPROVED:

Thesis Committee:

Major Professor Arun Shukla

James LeBlanc

K. Wayne Lee

Nasser H. Zawia
DEAN OF THE GRADUATE SCHOOL

UNIVERSITY OF RHODE ISLAND
2014

ABSTRACT

Experimental studies were performed to understand the explosive response of composite panels when exposed to near-field explosive loading in different environments. The panel construction under consideration was an E-glass fiber-reinforced composite laminate infused with vinyl ester resin (Derakane 8084). The panel was layered bi-axially with plain-woven fiber orientations at 0º and 90º. Panel dimensions were approximately 203 mm x 203 mm x 1 mm (8 in x 8 in x 0.04 in). Experiments were carried out with the panel fully clamped in a holding fixture, which was in turn fastened inside a water tank. The fixture was fastened in such a way as to allow for explosive loading experiments in the following environments: water submersion with water backing, water submersion with air backing, and air immersion with air backing. Experiments were performed in room temperature conditions, and additional experiments in the submerged environments were also performed at high and low water temperatures of 40 °C and 0 °C, respectively. A stereo Digital Image Correlation (DIC) system was employed to capture the full-field dynamic behavior of the panel during the explosive event. Results indicated that the immersion environment contributes significantly to the blast response of the material and to the specimens' appreciable damage characteristics. The water submersion with air backing environment was found to encourage the greatest panel center point deflection and the most significant damage mechanisms around the boundary. The air immersion with air backing environment was found to encourage less center point deflection and exhibited significant impact damage from the explosive capsule. The water submersion with water backing environment encouraged the least panel deflection and

minimal interlaminate damage around the panel boundary and center. Water temperature was found to influence the panel center point deflection, but not damage mechanisms. Maximum positive center point deflections associated with the high and room temperature water submersion with air backing environments, while statistically similar to each other, were found to be statistically different from those associated with the low temperature environment.

ACKNOWLEDGMENTS

It is with profound gratitude that I recognize the following individuals and extend my heartfelt thanks to them:

Dr. Arun Shukla, Simon Ostrach Professor and my research advisor, for his invaluable guidance and expertise, his positive and encouraging attitude, and his impeccable work ethic that inspired all of the graduate students in his charge.

Dr. Yapa D. S. Rajapakse, whose Office of Naval Research grant no. N00014-10-1-0662 supplied the principal funding for this study.

Mr. Steve Nolet, of TPI Composites in Warren, R.I., for providing the facility to fabricate the materials used in this study at no cost to the university.

Dr. James LeBlanc, of the Naval Undersea Warfare Center, Division Newport, for his valued input and suggestions, his previous research in related subjects that provided a context for this study, and his concurrent numerical simulations that will, at a later date, compliment these experiments.

Dr. Donna Meyer, for her infectious enthusiasm, her deep devotion to mechanics and mathematics, and the admirable standards that she encouraged in each of her students as a rule.

The Department of Mechanical, Industrial, and Systems Engineering faculty, for the firm engineering foundation and the culture of professionalism that they fostered, reflected in the brilliant assistance that they rendered.

The Department of Mechanical, Industrial, and Systems Engineering office and technical staff, for their crucial help in facilitating both routine and non-routine tasks in the laboratory. These include Joe Gomez and Dave Ferreira, department machinists

who contributed significantly to apparatus fabrication; Rob D'Ámbrosca and Jim Byrnes, department lab technicians who contributed much-needed electrical and plumbing expertise; and Jen Cerullo and A.J. Bothun, department secretaries who aided in procurement of materials and management of fiscal issues.

The students of the Dynamic Photo Mechanics Laboratory (DPML)—by name: Sachin Gupta, Nicholas Heeder, Prathmesh Parrikar, Michael Pinto, Anil Rajesh Kumar, Emad Makki, Nathaniel Gardner, Sandeep Abotula, Payam Fahr, Chris O'Connell, Kim McCarthy, Christopher Shillings, Craig Tilton, and Abayomi Yussuf—for their indispensable support, their optimism and keen interest in their work, and the valuable insight that they provided when challenges looked steep.

Mr. Daniel Gracia, for the basis of research that he laid as a graduate student before I joined the DPML and for his unfailing willingness to answer all of my questions, even to the point of visiting the lab facilities after his regular work day had concluded.

Dr. Shukla's esteemed visiting faculty—by name: Dr. Murat Yazici, Dr. P. Venkitanarayanan, and Dr. Idris Karen—for their assistance in the lab and the theoretical and experimental understanding that they shared with the DPML.

Most especially my parents: my first teachers, who helped me discern my compatibility with mechanical engineering; whose support and encouragement never diminished through the years, even when those years sometimes had as many downs as they had ups; and who gifted me with a firm foundation on which to face the challenges of graduate school.

I also reverently acknowledge the graces and favor of Our Lord, with whose permission and guidance this study bore fruit.

TABLE OF CONTENTS

LIST OF TABLES

TABLE PAGE

LIST OF FIGURES

CHAPTER 1: Introduction

Composites have been employed in a variety of applications for many years in the marine, automotive, and other commercial industries. They are known and valued for qualities such as high strength-to-weight ratios, good corrosion resistance, resistance to water absorption, and reduced maintenance requirements. These characteristics have garnered them recent attention as effective materials in military applications. Military structures are frequently exposed to extreme loads in the field or at sea, and these loads induce high strain rates in the materials that comprise those structures. The response of composite materials at high strain rates, and in unique environments, is not fully known as yet. This lack of understanding often prevents the designing of components that maximize their material advantages. It is thus advisable to conduct experimental research to fully understand how these materials respond to extreme loadings, so as to determine how to best take advantage of their qualities (LeBlanc, Gardner, & Shukla, 2013). The research described herein attempts to accomplish this objective.

It is of additional interest to naval and maritime engineering that the effects of particular extreme loadings be studied with special emphasis. Of singular importance are the consequences of explosive loadings. Among the varieties of explosions classified in the literature, the near-field explosion enjoys a great deal of relevance to naval design, planning, as well as tactics and maneuvers at sea. This is evidenced by the breadth of history concerning the use of torpedoes, undersea mines, and improvised explosive vessels as instruments to damage or sink ships. The near-field

explosion also enjoins uniquely complex interactions on its target, and is thus a worthy candidate for study with a composite specimen.

This study examined the near-field explosive response of an E-glass/Vinyl Ester (EVE) marine composite panel specimen in different immersion environments and at different water temperatures. The panel specimen was a 2-ply plain weave laminate infused with Derekane 8084 vinyl ester resin. In each of the immersion environments, the specimen existed as a fully-clamped panel barrier between two media, either water or air. The face opposite the explosive side was referred to as the "backing" side. Under this arrangement, the immersion environments were assigned as follows: (1) water submersion with air backing (hereafter referred to as "WA"), (2) water submersion with water backing (hereafter referred to as "WW"), and (3) air immersion with air backing (hereafter referred to as "AA"). Each environment was investigated in turn at room temperature. Following the room temperature studies, low temperature experiments were performed in the WA and WW environments for water temperatures of 0 °C, hereafter referred to as "WALT" and "WWLT," respectively. After these, high temperature experiments were performed in the WA and WW environments for water temperatures of 40 °C, hereafter referred to as "WAHT" and "WWHT," respectively. RP-503 detonator caps, with a TNT weight equivalent of 1 g, were the chosen explosives for this study. Free field pressure transducers were employed to record the spherical shockwave pressure histories underwater and in air, and high speed digital photography was employed to capture real-time, full-field deformation histories via the Digital Image Correlation (DIC) method. Panel displacements and damage mechanisms were noted and analyzed to discover the effects of immersion

environment and water temperature on the blast response of the EVE composite specimens.

It is humbly submitted by the author that the results contained herein will contribute to the understanding of the dynamic thermo-mechanical properties of EVE composites, inspire similar research, and exist as a deposit of relevant information for that research. It is hoped that these results will assist the engineering and design communities in developing stronger and more efficient naval structures.

CHAPTER 2: Review of Literature

2.0 Review and General Comments

This study endeavored to examine the near-field blast response of a common marine composite, constructed from materials available on the commercial market, using the principles of Digital Image Correlation (DIC). These principles have been well-established and appear abundantly in the literature (LeBlanc et al., 2013)(Sutton, Orteu, & Schreier, 2009)(Shukla & Dally, 2010)(Haile, Yin, & Ifju, 2009). Explosive theory is also well-established for both underwater and in-air events and has received much attention over the last century (Cole, 1948)(Brinkley & Kirkwood, 1945)(Hartmann & Laboratory, 1976)(Smith & Hetherington, 1994). The uniqueness of the study under consideration is that it incorporated the effects of (1) a near-field explosion, (2) loading environments characterized by water submersion with water backing, water submersion with air backing, and full air exposure, (3) water temperature variation, and (4) a fully-clamped boundary condition around a flat panel.

Available literature does not address this engineering problem exactly. Torabizadeh examined the mechanical behavior of unidirectional glass/epoxy composites, for temperatures ranging from -60 ℃ to 25 ℃, when subjected to static loading (Torabizadeh, 2013). Wang, Zhou, and Mallick demonstrated the temperature and strain rate-dependence of Polyamide-6, an E-glass-reinforced composite, over temperatures ranging from 21 ℃ to 100 ℃ and slow strain rates of 0.05/min, 0.5/min, and 5/min (Wang, Zhou, & Mallick, 2002). Van Lear studied the effects of fluid structure interaction in an underwater explosive (UNDEX) event using numerical

methods (Van Lear, 2008), while Espinosa et al examined UNDEX fluid structure interaction experimentally using a scaled water piston apparatus instead of an explosive charge (Espinosa, Lee, & Moldovan, 2006). Shin simulated the effects of a far-field explosion on the hull of a warship using the LS-DYNA finite element software (Shin, 2004). Leblanc and Shukla examined the effects of far-field blasts on curved composite panels using a conical shock tube apparatus, DIC methods, and computing software (LeBlanc & Shukla, 2011). In a separate study, LeBlanc, Gardner, and Shukla examined the effect of polyurea coatings on curved composite panels, again using a conical shock tube apparatus and DIC methods (LeBlanc et al., 2013). Rajendran and Narasimhan studied the effects of contact UNDEX loading on curved steel plates in an experimental environment characterized by water submersion with air backing (Rajendran & Narasimhan, 2001). Cichocki employed numerical software to model the loading effects of a 40 kg spherical charge on a closely-nearby protective structure around a pipe (Cichocki, 1999). Spranghers et al examined the near-field deformation behavior of aluminum plates when subjected to 40 grams of C4, using DIC methods (Spranghers, Vasilakos, Lecompte, Sol, & Vantomme, 2012). Ngo et al provided an explanation of blast waves and explosion mechanisms in free air, as well as a detailed outline of the effects of explosions in air on structures (Ngo, Mendis, Gupta, & Ramsay, 2007), and Zakrisson et al modeled the response of structures to near-field explosions in air (Zakrisson, Wikman, & Häggblad, 2011). Batra and Hassan, in separate studies, examined the blast resistance of fiber-reinforced composites in air and water environments using specialized numerical software (Batra & Hassan, 2008)(Batra & Hassan, 2007).

Much of the foregoing literature touched on aspects similar to those found in this proposed study, but none addressed each integral part at once, and none examined the effects of temperature variation on the specimen's dynamic response.

2.1 Literature Review of Basic Explosion Theory

An explosion is defined in broad terms as a "large scale, rapid, and sudden release of energy" (Ngo et al., 2007). Ngo et al. list several possible mechanisms for such discharge, namely those associated with chemical, nuclear, or physical events. This present study considered only explosions of chemical origin—that is to say, explosions produced as a result of the chemical combustion of a parent compound into gasses of very high temperature, pressure, and density. In this context, detonation of the explosive material releases energy via the rapid expansion of the combustion gasses. This rapid expansion produces a supersonic wave front, referred to as a shockwave, which is spherical in geometry and is characterized by discontinuities in temperature, pressure, density, and particle velocities through its thickness (Rajendran & Lee, 2009)(Shin, 2004)(Van Lear, 2008)(Spranghers et al., 2012)(Ngo et al., 2007)(Cole, 1948)(Smith & Hetherington, 1994). As a result of the gas expansion, the shockwave propagates radially and increases in size; its intensity also deteriorates radially, influenced by the medium in which is transmitted.

2.1.1 Review of UNDEX Theory

The shockwave produced in an UNDEX event propagates at a velocity much faster than that of the explosive gasses. Upon interfacing with the water medium, the

initial shock front's velocity moves typically on the order of several thousand meters per second—that is, 3 to 5 times the acoustic velocity in water—and its initial pressure is similarly very high (Cole, 1948)(Shin, 2004)(Rajendran & Lee, 2009). In contrast, the spherical gas bubble initially retains a reduced internal pressure after shockwave emission, though this pressure is still of much greater magnitude than the equilibrium ambient plus hydrostatic pressure (hereafter referred to as the "ambient/hydrostatic" pressure). The bubble also expands radially, thus displacing the surrounding water in the process. The bubble expands in radius until a time just after its internal pressure reduces to the ambient/hydrostatic pressure, when, owing to fluid inertial effects, the bubble is caused to "over-expand" to a radius at which the internal pressure falls short of the ambient/hydrostatic pressure (Shin, 2004)(Cole, 1948)(Van Lear, 2008). The resultant pressure differential reverses the motion of the bubble, forcing it from expansion into contraction, during which time the internal pressure begins to increase once more. The effects of the gasses' compressibility, while negligible during expansion, are significant in the final stages of contraction and act to abruptly reverse the bubble's motion at the point of maximum collapse. This abrupt reversal of motion generates a new pressure wave in the water, referred to as the "bubble pulse." Upon collapse and emission of a bubble pulse, the gas bubble will continue in a periodic cycle of expansion and contraction until all of the explosion energy is released into the surrounding water or vented through the surface, if the event depth permits. During these cycles, called "bubble periods," the bubble is known to migrate upwards due to buoyancy effects. For reasons that are less obvious, the bubble is also known to

migrate away from free surfaces and towards rigid boundaries (Shin, 2004)(Cole, 1948).

2.1.2 Review of Air Blast Theory

Differences in physical properties, as well as differences in fluid interactions between explosive gasses and the detonation environment, produce significant contrasts between the physics of air blast events and those of UNDEX events, in spite of superficial, process-related similarities (development of spherical shockwave, discontinuities in fluid properties across the shockwave thickness, supersonic initial shock front propagation, etc.). Some of these notable differences include the following:

1. The shockwave produced in an air blast event is followed closely by the explosive gasses (Ngo et al., 2007)(Rajendran & Narasimhan, 2001).
2. The explosive gasses do not coalesce into an expanding and contracting bubble. Hence, bubble pulses to not occur.
3. After attaining the peak overpressure, the pressure decay behind the shock front ebbs below the ambient conditions, causing a partial vacuum referred to as the “negative” pressure phase, before returning to the ambient pressure.

2.1.3 The Near-Field Problem

This concise review of basic explosion theory allows for a more detailed description of the criteria that this study selected to constitute a near-field explosion, and how these explosions differ from the far-field variety. In this study, a near-field explosion is one for which the standoff distance between the charge and the target are sufficiently short that the following conditions are true:

1. The influence of the shockwave curvature is significant during interaction with the target. In this way, the shockwave's spherical geometry is a prominent characteristic in its contact with the target and prevents planar wave approximations during analysis.
2. The target is either nearby or within a region of the blast zone where fluid structure interactions are made complex by the flow processes encouraged during shockwave generation.

UNDEX events in the near-field may further have special characteristics enjoined by the gas bubble behavior, characterized by either or both of the following:

3. In UNDEX events, the target is either nearby or within a region of the blast zone where bubble expansions and contractions directly and significantly influence the bulk fluid flow around the target.

4. In UNDEX events, the target is either nearby or within a region of the blast zone where bubble expansions and contractions cause direct contact between the bubble and the target, including migratory bubble behavior.

These characteristics may be contrasted with those representative of a far-field explosion, in which the standoff distance between the charge and the target are sufficiently large that the following conditions are true:

1. The influence of the shockwave curvature is reduced or negligible, permitting the approximation of a plane interface between the wave and the target.
2. The target is far enough removed from regions of complex fluid flow, produced from the direct effects of detonation, that fluid structure interactions corresponding to those flows are nonexistent. In UNDEX events this includes bubble contact.
3. Pressure waves induced by bubble pulses may or may not interact with the target.

CHAPTER 3: Methodology

3.0 Material/Specimen

The material considered in this analysis was an E-glass/Vinyl Ester (EVE) laminate, manufactured at TPI Composites in Warren, R.I. The laminate was layered biaxially using two plies of plain weave fiber sheets, and possessed an areal density of 0.61 kg/m^2 (18 oz/yd^2). The mass density of the E-glass fibers was taken to be 2.56 g/cm^3. A vacuum-assisted resin transfer process was employed to saturate the layered sheets with Derakane 8084 vinyl ester resin, the mass density for which was taken to be 1.02 g/cm^3. The resulting laminate possessed a fiber weight content of 70.6%, possessed a fiber volume percentage of 48.2%, and was divided into 203 mm x 203 mm x 1 mm (8 in x 8 in x 0.04 in) panel specimens. These panels were subsequently post cured sequentially at 70º C for 2 hours and 60 ºC for 10 hours. A detailed description on the panel manufacturing process is given in Appendix A. The unsupported panel surface area was 152 mm x 152 mm (6 in x 6 in), allowing for a 25.4 mm (1 in) clamping edge with loose-fit screw holes spaced at intervals around the periphery, as shown in Figure 3.0-1. The experimental area of interest on each specimen was painted white. A black dot matrix was spray painted on the white surface using a perforated metal mesh. A random black speckle pattern was subsequently hand-painted over these coats, for recognition by the Digital Image Correlation (DIC) data acquisition technique, described in section 3.1.5. For select experiments, a high speed side view digital camera was employed to observe the real-

time explosion behavior behind the specimen, particularly the underwater expansion and contraction of the explosive gas bubble.

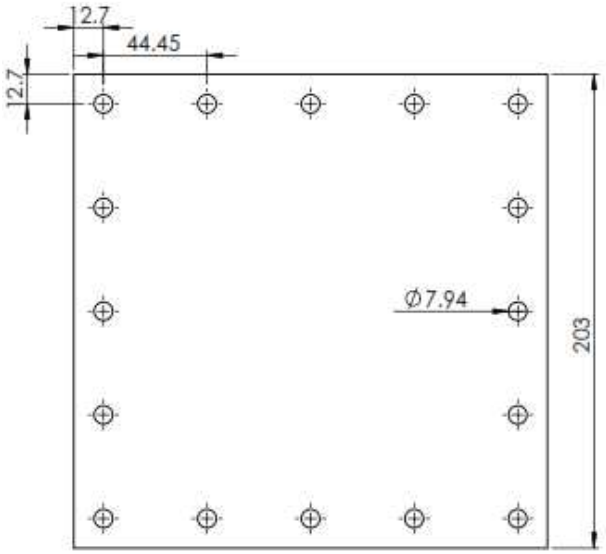

Figure 3.0-1: The composite panel specimen. Units are in millimeters.

3.1 Experimental Apparatus

The apparatus used in this study is illustrated in Figure 3.1-1. The depicted components are discussed in greater detail in sections 3.1.1 through 3.1.6.

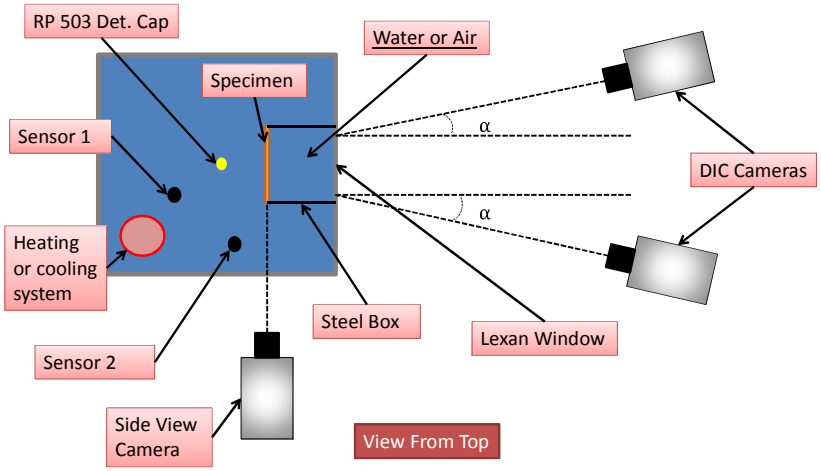

Figure 3.1-1: Experimental apparatus, depicting the specimen, explosive charge, pressure sensors, DIC and side view cameras, specimen fixture, and heating/cooling system. The heating system was composed of 5 heating rods; the cooling system was composed of ice.

3.1.1 Experimental Water Tank

The experimental environment was contained within a special water tank. The tank was constructed of aluminum structural framing, Lexan side panels, and an aluminum floor. The tank stood on legs approximately 58.4 cm (23 in) in length. The tank itself measured approximately 0.914 m x 0.914 m x 0.914 m (36 in. x 36 in. x 36 in.), thus accommodating a maximum fluid volume of approximately 0.75 m^3 (46,656 in^3). Because the operational water depth was only

Figure 3.1.1-1: The experimental water tank

approximately 0.66 m (26 in.), the operational water volume was accordingly 0.551 m^3 (33,696 in^3). The tank may be seen in Figure 3.1.1-1.

3.1.2 Experimental Fixture

Experiments required a unique specimen holding fixture so as to accommodate the panel geometry and provide the appropriate boundary conditions. This fixture consisted of a steel raised platform that was bolted to the floor of the water tank. The edge of the platform stood at a distance of 3.25 mm (0.125 in) from the transparent Lexan observation window. A flanged steel box was in turn bolted to the top of the raised platform. The box accommodated a 203 mm x 203 mm (8 in x 8 in) specimen, the unsupported area of which would become 152 mm x 152 mm (6 in x 6 in) after fully-clamped securement via a mounting bracket. The box, in a similar fashion as the raised platform, was secured at a distance of 3.25 mm (0.125 in) from the transparent Lexan observation window. The 3.25 mm gap between the edge of the box and the viewing window was filled as needed with silicone caulking, to facilitate WA experiments. The holding fixture assembly is shown in Figures 3.1.2-1 and 3.1.2-2.

Figure 3.1.2-1: The experimental holding fixture, absent specimen. <u>Left</u>: view from explosive side, showing the mounting screws for the fully-clamped boundary. The white band around the screws is silicone caulking residue, used as a watertight seal between the specimen and the box. <u>Right</u>: view from the DIC side. Notice the thick white bead of silicone between the box and the window, sealing the edges.

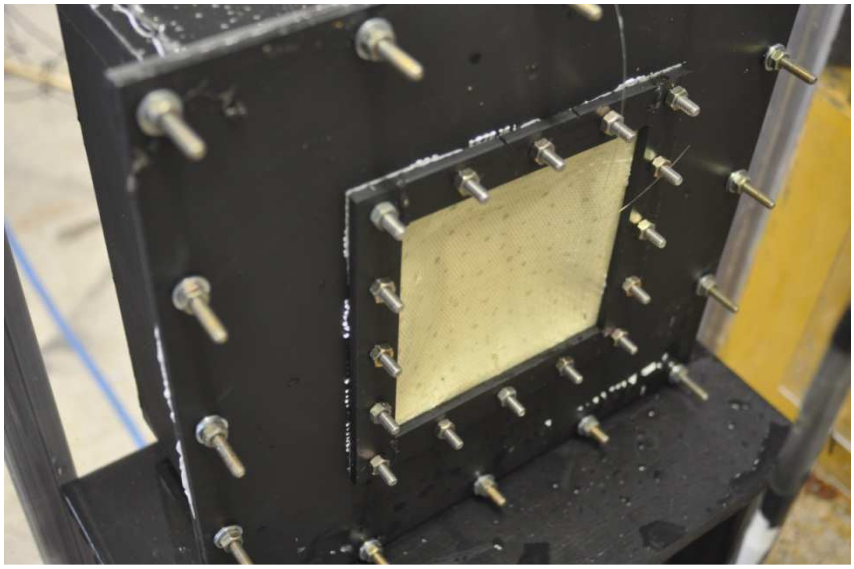

Figure 3.1.2-2: The experimental holding fixture with a specimen clamped beneath the mounting bracket. This photo was taken just after an experiment and the specimen's concavity can be readily seen.

3.1.3 Pressure Sensors

3.1.3.1 Underwater Blast Sensors

The pressure sensors employed in the WA and WW experiments were two series W138A05 integrated circuit piezoelectric (ICP[1]) tourmaline underwater blast probes, serial numbers 9338 and 9656, produced by PCB Piezotronics, Inc. The tourmaline sensing element was suspended in a silicone oil-filled flexible transparent tube of diameter 9.4 mm (0.37 in.). The distance from the conical tip to the sensing element varied between the probes; these distances are noted with further details in section 3.2.1. The overall probe length was 193 mm (7.6 in.). The probes were mounted vertically. Figures 3.1.3.1-1 and 3.1.3.1-2 show the instrument and its technical specifics.

Figure 3.1.3.1-1: Series W138A05 underwater blast probe. The tourmaline sensing element is the spherical shape at the center of the unit. The distance from this element to the end of the conical tip, at right, varied between the sensors.

[1] ICP is a registered trademark of PCB Piezotronics, Inc.

Performance	ENGLISH	SI
Measurement Range (for ±5V output)	5 kpsi	34475 kPa
Useful Overrange (for ± 10V output)	10 kpsi	68950 kPa
Sensitivity (±15 %)	1.0 mV/psi	0.15 mV/kPa
Maximum Pressure	50 kpsi	344750 kPa
Resolution	100 mpsi	0.07 kPa
Resonant Frequency	≥1000 kHz	≥1000 kHz
Rise Time (Reflected)	≤1.5 µ sec	≤1.5 µ sec
Low Frequency Response (-5 %)	2.5 Hz	2.5 Hz
Non-Linearity	≤2.0 % FS	≤2.0 % FS
Environmental		
Temperature Range (Operating)	0 to +100 °F	-17.8 to +37.8 °C
Maximum Shock	20000 g pk	196140 m/s² pk
Electrical		
Output Polarity (Positive Pressure)	Positive	Positive
Discharge Time Constant (at room temp)	≥0.2 sec	≥0.2 sec
Excitation Voltage	20 to 30 VDC	20 to 30 VDC
Constant Current Excitation	2 to 20 mA	2 to 20 mA
Output Impedance	≤100 Ohm	≤100 Ohm
Output Bias Voltage	8 to 14 VDC	8 to 14 VDC
Physical		
Sensing Element	Tourmaline	Tourmaline
Housing Material	Stainless Steel	Stainless Steel
Electrical Connector	10-32 Coaxial Jack	10-32 Coaxial Jack
Weight	0.75 oz	21.0 gm

Figure 3.1.3.1-2: W138A05 blast probe technical information.
Image courtesy of PCB Piezotronics, Inc.

3.1.3.2 Air Blast Sensors

The pressure sensors employed in the AA experiments were two series 137A21 integrated circuit piezoelectric (ICP[2]) free field blast probes, serial numbers 10044 and 10045, produced by PCB Piezotronics, Inc. The distance from the conical probe tip to the quartz sensing element was 157 mm (6.2 in), and the overall probe length was 406 mm (16 in). The sensors were mounted horizontally with the sensing diaphragm oriented sideways. Figures 3.1.3.2-1 and 3.1.3.2-2 show the instrument and its technical specifics.

[2] ICP is a registered trademark of PCB Piezotronics, Inc.

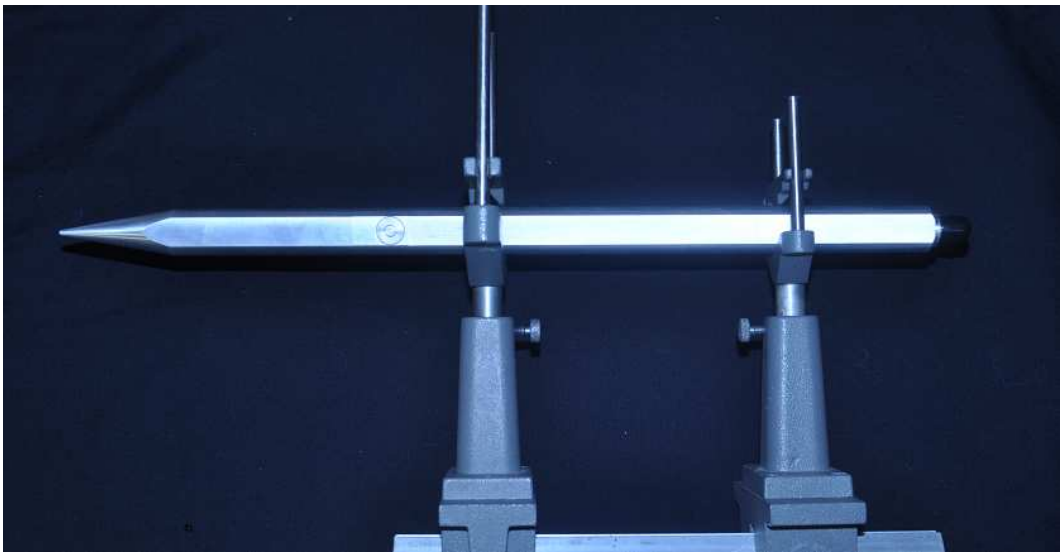

Figure 3.1.3.2-1: Series 137A21 blast probe, mounted in an instrument holding clamp. Notice the circular sensing diaphragm just beside the left holding mount.

Performance	ENGLISH	SI
Measurement Range (for ±1V output)	1 kpsi	6895 kPa
Sensitivity (±15 %)	1.0 mV/psi	0.145 mV/kPa
Maximum Pressure	5 kpsi	34475 kPa
Resolution	100 mpsi	0.69 kPa
Resonant Frequency	≥500 kHz	≥500 kHz
Rise Time (Incident)	≤6.5 µ sec	≤6.5 µ sec
Non-Linearity	≤1.0 % FS	≤1.0 % FS
Environmental		
Temperature Range (Operating)	-100 to +275 °F	-73 to +135 °C
Temperature Coefficient of Sensitivity	≤0.03 %/°F	≤0.054 %/°C
Electrical		
Output Polarity (Positive Pressure)	Positive	Positive
Discharge Time Constant (at room temp)	≥0.2 sec	≥0.2 sec
Excitation Voltage	20 to 30 VDC	20 to 30 VDC
Constant Current Excitation	2 to 20 mA	2 to 20 mA
Output Impedance	≤100 Ohm	≤100 Ohm
Output Bias Voltage	8 to 14 VDC	8 to 14 VDC
Physical		
Sensing Geometry	Compression	Compression
Sensing Element	Quartz	Quartz
Housing Material	Aluminum	Aluminum
Diaphragm	Invar	Invar
Sealing	Epoxy	Epoxy
Electrical Connector	BNC Jack	BNC Jack
Weight	12.7 oz	360 gm

Figure 3.1.3.2-2: 137A21 blast probe technical information. Image courtesy of PCB Piezotronics, Inc.

3.1.4 Explosive Charge

The detonator used was an RP-503 secondary explosive. RP-503 is a plastic-encapsulated, sealed Exploding Bridge Wire (EBW) charge designed for underwater operations of up to 3 m (10 ft) in depth. The chemical content is 454 mg (0.016 oz) RDX and 167 mg (0.006 oz) PETN, combining to produce a TNT weight equivalent of 1 g (0.04 oz). The bridge wire is gold and possesses a threshold voltage of 500 V. A schematic of an RP-503 charge may be seen in Figure 3.1.4-1.

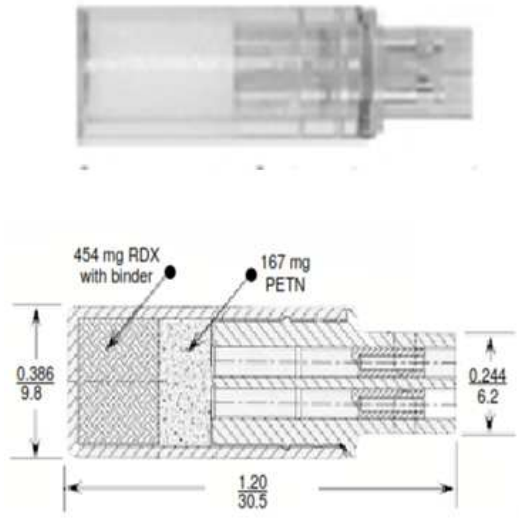

Figure 3.1.4: Illustration of an RP-503 explosive charge. In the figure, numerator values are expressed in inches, denominator values are expressed in millimeters.

3.1.4.1 RP-503 Pressure Decay Test

Placement of the aforementioned blast probes enabled the registering of pressure data at fixed standoff distances from the explosive; but, due to concerns of damaging the sensors, these instruments could not capture pressure information at distances close to the specimen. Available UNDEX literature was consulted to find closed-form

expressions for pressure wave decay under water, but the parameters associated with these solutions did not yield theoretical results that matched the experimental results after detonation (Cole, 1948)(Shin, 2004)(Batra & Hassan, 2007). It was supposed that these discrepancies could be attributed to the small dimensions of RP-503—the size of the bridge wire or detonator cap, for example, relative to the size of the explosive proper, could perhaps influence the detonation behavior in more drastic ways than those components would for heavier explosives. It was decided that the RP-503 pressure decay rate should be experimentally ascertained to produce an expression unique to the conditions used in this study, so as to accurately predict shockwave overpressures at the instant that they interface with the specimen.

Pursuant to this, a line of six tourmaline blast probes were arranged underwater on laboratory stands in the experimental water tank, and were placed at varying distances from an RP-503 explosive, as depicted in Figure 3.1.4.1-1.

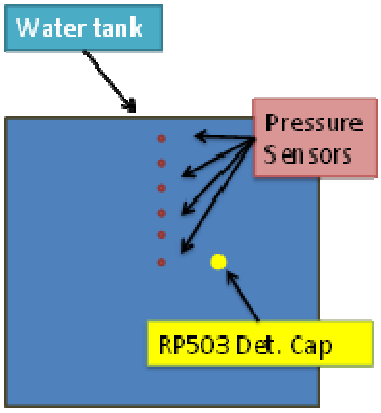

Figure 3.1.4.1-1: Overhead schematic of the RP-503 pressure decay verification setup.

The explosive was detonated and the pressure histories were recorded for each of the six standoff distances, the plots for which are overlaid on each other in Figure 3.1.4.1-2. The resulting peak pressures were plotted together in MATLAB as a function of standoff distance, and a least-squares curve fitting method was employed to establish a trend line function to extrapolate the data across a wider range of standoff distances at 95% confidence, as seen in Figure 3.1.4.1-3.

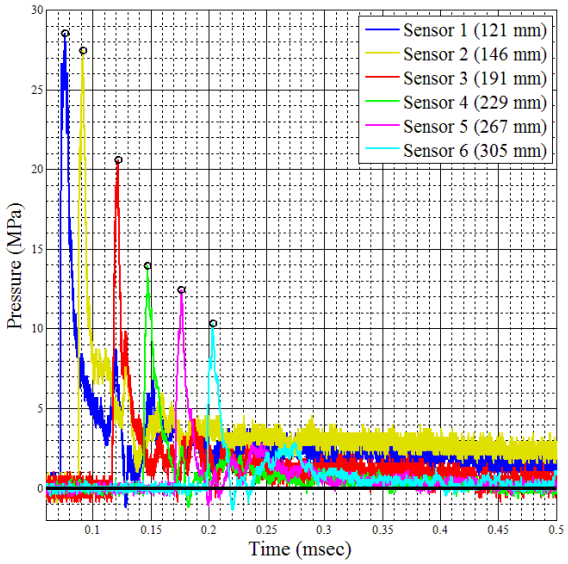

Figure 3.1.4.1-2: Overlaid overpressure histories recorded during the RP-503 pressure decay verification test.

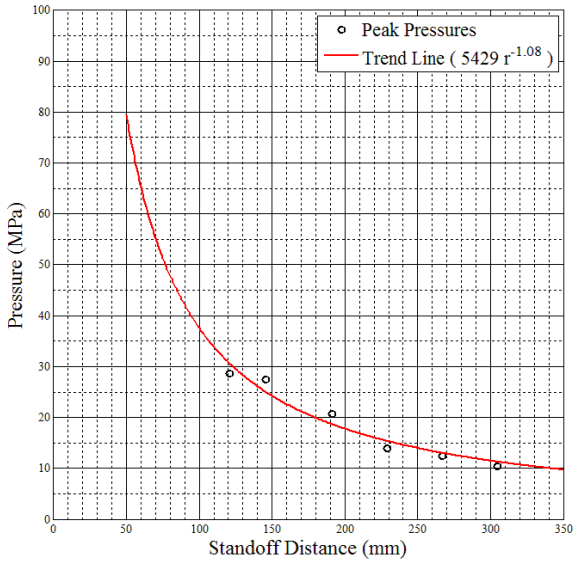

Figure 3.1.4.1-3: Peak pressures as a function of standoff distance, with the accompanying trend line, from the RP-503 pressure decay verification test.

As can be seen in Figure 3.1.4.1-3, the pressure was seen to decay as a function of approximately $1/r$. Key results from the pressure decay test are included in Table 3.1.4.1-1.

Table 3.1.4.1-1: Key values from the RP-503 pressure decay verification test

Sensor #	Peak Pressure (MPa)	Standoff Distance (mm)
1	28.6	121
2	27.5	146
3	20.6	191
4	14.0	229
5	12.5	267
6	10.4	305

The trend line function expressed in Figure 3.1.4.1-3 was used to predict an overpressure of approximately 50.4 MPa experienced at the target at 76 mm. It must be noted however that extrapolating the data so far from the measured range between 120 and 305 mm introduced heightened uncertainty. This is indicated by the MATLAB curve fitting readouts in Figure 3.1.4.1-4, which indicate that the prediction bounds at 95% confidence, when evaluated at approximately 76 mm, are ± 17 MPa.

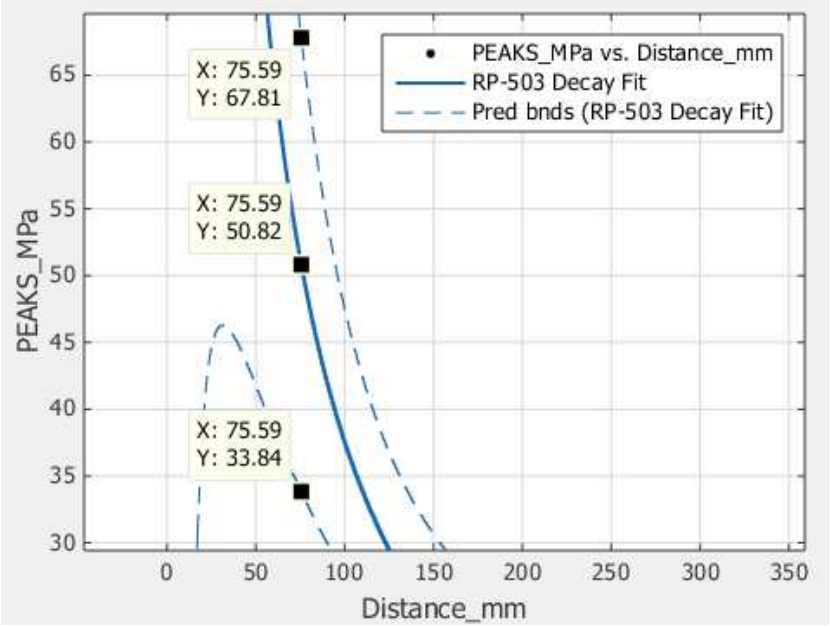

Figure 3.1.4.1-4: MATLAB-generated curve fit based on RP-503 pressure decay test information, indicating the prediction bounds at ~76 mm standoff distance. Pressure in MPa is plotted on the Y axis, and standoff distance in mm is plotted on the X axis.

3.1.5 Digital Image Correlation

Digital Image Correlation (DIC) is a powerful optical tool in experimental mechanics that seeks to non-intrusively ascertain full-field displacement, strain, and velocity fields associated with a deforming body. The method is accomplished via use

of high speed digital cameras and specialized analytical software (Sutton et al., 2009). To record the deformation in real time, two high speed digital cameras are employed in a synchronized stereo arrangement. Calibration of the cameras is achieved via use of an image calibration grid, consisting of a white field and a distinct pattern of evenly-spaced points. The grid is rotated and translated in- and out-of-plane, as a series of individual photographs are taken by the stereo camera system. Since the spacing of the calibration points on the grid is predetermined, the analytical software is allowed to track the points' displacement. These displacements are tracked in a coordinate plane unique to both cameras. The software then correlates the images in these planes to establish a real-world, global coordinate system from which full-field, three-dimensional deformation measurements are made (LeBlanc et al., 2013). A calibration error of 10% or less is generally considered acceptable. As Haile notes, "A [DIC] camera is considered calibrated if the principal distance, principal point offset and lens distortion parameters are known"(Haile et al., 2009). This global three-dimensional coordinate system is unique to the stereo camera layout, and any subsequent alteration of the camera layout necessarily invalidates the calibration (such alterations might include shifting of one or both cameras, replacement of one or both camera lenses, or placement/removal of additional transparent media in front of the cameras). Before experiments, the observation side of the deforming body is painted with a random black-and-white speckle pattern. This random pattern creates a diverse field of unique pixel intensity subsets whose displacements, during specimen deformation, are photographically captured by the high speed cameras. The analytical software tracks and interprets these displacements, which allows consequently for the

three-dimensional assessment of strain, velocity, and other applicable parameters (Shukla & Dally, 2010).

3.1.5.1 DIC Cameras

The high speed cameras employed for the DIC technique were two Photron Fastcam SA1.1 units, of model number 675K-M1, with 8GB internal memory. These cameras can achieve frame rates between 1,000 and 675,000 frames per second with corresponding image resolutions between 1,024 x 1,024 and 64 x 16, respectively.

3.1.5.2 DIC Software

The analytical post-processing software employed for the DIC technique was "Vic-3D," produced by Correlated Solutions, Inc. Vic-3D uses the DIC method to employ various strain tensors in providing full-field, three-dimensional deformation, strain, and shape measurements across the surface of the deforming body.

3.1.6 Heating and Cooling Devices

Experiments investigating the influences of high and low water temperatures—namely WAHT, WALT, WWHT, and WWLT—required unique heating and cooling techniques to achieve the desired environments. These are discussed in sections 3.1.6.1 and 3.1.6.2.

3.1.6.1 Heating Elements

The heating elements used in the WAHT and WWHT experiments were Allied Precision Industries 742G bucket heaters, delivering 1 kW of power each, as seen in Figure 3.1.6.1-1.

Figure 3.1.6.1-1: Allied Precision Industries 1 kW bucket heater. Image courtesy of Allied Precision Industries, Inc.

The nominal water temperature as it entered the experimental water tank was approximately 23 °C. Noting the operational water volume in the tank, the desired water temperature of 40 °C, and a desired heating time of approximately 2 hours, Equation 3.1.6.1-1 was used to determine the required power input.

$$\dot{q} = mc\frac{\Delta T}{\Delta t} \qquad (3.1.6.1\text{-}1)$$

Application of Equation 3.1.6.1-1 yielded a required power input of approximately 5.44 kW. Due to electrical constraints in the experimental facility, the

employed power input was rounded down to 5 kW, and five 1 kW bucket heaters were procured for the study.

The heaters were suspended from rods above the surface of the water, with the heating elements completely submerged. This arrangement can be seen in figure 3.1.6.1-2.

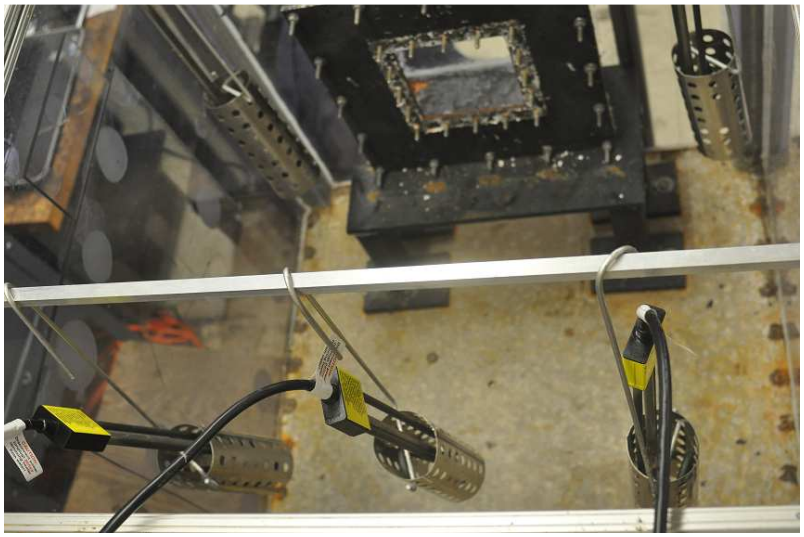

Figure 3.1.6.1-2: Arrangement of the five water heaters

3.1.6.2 Cooling Elements

The cooling element used in the WALT and WWLT experiments was cubed ice. Again, noting the nominal water entrance temperature as approximately 23 °C, the operational water volume in the tank, and the desired water temperature of 0 °C, and assuming ice cubes of -10 °C, equation 3.1.6.2-1 was used to calculate the required mass of ice to sufficiently lower the water temperature, as follows:

$$m_{ice} = \frac{m_{water} c_{water} \Delta T_{water}}{c_{ice} \Delta T_{ice} + h_{ice}} \qquad (3.1.6.2\text{-}1)$$

in which *h* is the latent heat of ice. Appropriate application of equation 3.1.6.2-1 yielded a required mass of 150 kg (330 lb.) of ice per experiment to adequately cool the water.

3.2 Experimental Procedure

3.2.1 Water Submersion, Air Backing (WA)

Experiments were performed to investigate the response of the EVE composite specimen to an UNDEX event in an experimental environment characterized by water submersion and air backing—an environment referred to hereafter as "WA." For each experiment conducted thus, silicone caulk was used to fill the 3.18 mm (0.125 in) clearance between the experimental holding box and the transparent Lexan viewing window, thereby sealing the edges. A thin bead of silicone caulk was likewise applied around the edges of the EVE composite specimen, in an appropriate area as to seal the holding box's interior air environment from the exterior water environment (Figures 3.1.2-1 and 3.1.2-2). A specimen mounting bracket was bolted over the EVE panel to establish a fully-clamped boundary condition. The RP-503 detonator was suspended on the water side of the composite panel by fishing line at a distance of 76.2 mm (3 in.) from the center of the specimen. Two tourmaline underwater blast probes were positioned vertically with their conical tips at radial distances of 127 mm (5 in.) and 203 mm (8 in.) from the detonator, respectively. The minimum probe standoff distance of 127 mm was chosen so as not to damage the instrument. The blast probe that was

positioned closer to the detonator, hereafter referred to as "sensor 1," possessed a tourmaline sensing element located at a distance of 97 mm (3.8 in.)[3] directly above the conical tip. The tourmaline element for sensor 1 therefore stood at a radial distance of 160 mm (6.3 in.) from the detonator. In a similar way, the blast probe that was positioned farther from the detonator, hereafter referred to as "sensor 2," possessed a tourmaline sensing element located at a distance of 99 mm (3.9 in.)[4] directly above the conical tip. The tourmaline element for sensor 2 therefore stood at a radial distance of 226 mm (8.9 in.) from the detonator. 100 mm DIC camera lenses were employed and the camera frame rate was set to 20,000 frames per second (FPS), rendering a DIC image resolution of 512 x 512 with an inter-frame time of 50 μsec. The RP-503 charge was detonated by an independent firing box, which was wired to an isolated electrical circuit to minimize the risk of power surges influencing the recording oscilloscope. The deflections of the speckle patterns on each specimen were observed by the DIC cameras and processed by the DIC software. Out-of-plane deflections were measured from the plane of the un-deformed specimen. The pressure waves induced by the RP-503 explosion were detected by the tourmaline blast probes, whose millivolt signals were amplified to ± 10 VDC signals by an in-line conditioner and relayed to a recording oscilloscope. The oscilloscope was commanded to trigger upon a rising voltage of 400 mV from sensor 1. Key experimental apparatus values are presented for convenience in Table 3.2.1-1.

[3] The sensing element in sensor 1 was measured to exist $3\ {}^{13}/_{16} \pm {}^{1}/_{16}$ in. above the conical tip.
[4] The sensing element in sensor 2 was measured to exist $3\ {}^{15}/_{16} \pm {}^{1}/_{16}$ in. above the conical tip.

Table 3.2.1-1: Key experimental apparatus values invariable throughout the WA experiment set

Parameter	Value
RP-503 Standoff Distance	76.2 mm (3 in.)
Sensor 1 Tip Standoff Distance	127 mm (5 in.)
Sensor 1 Sensing Element Elevation Above Tip	97 mm (3.8 in.)
Sensor 1 Sensing Element Standoff Distance	160 mm (6.3 in.)
Sensor 2 Tip Standoff Distance	203 mm (8 in.)
Sensor 2 Sensing Element Elevation	99 mm (3.9 in.)
Sensor 2 Sensing Element Standoff Distance	226 mm (8.9 in.)
DIC Camera Lens	100 mm
DIC Camera Frame Rate	20,000 FPS
DIC Camera Interframe Time	50 μsec
DIC Image Resolution	512 x 512

3.2.1.1 WA Experiment 1

The first WA experiment was performed with the recording oscilloscope set to a sampling frequency of 10 MHz. The DIC camera angles of incidence with the transparent Lexan viewing window were not recorded during this experiment. The DIC calibration error was found to be 9.8%. The composite specimen's center point deflected sharply outward to a maximum positive deflection of 27.5 mm (1.08 in.) after a total elapsed time of 1.3 msec, before beginning to rebound inward. An X-shaped plateau that occurred across the panel's center during the rebound forced the center point outward briefly, observable at approximately 3 msec (Figure 3.2.1.1-1). This brief response was followed by a rapid center point collapse to an intermediate negative deflection of approximately -14 mm (-0.55 in.) at approximately 7 msec elapsed time. Following a dwell of approximately 2.2 msec at -14 mm, the panel center point collapsed further to a maximum negative deflection of -24 mm (-0.94 in.) at 15.3 msec total elapsed time. The center point deflection tended modestly and

nominally outward for an additional 6 msec, before expanding rapidly outward to a local positive maximum of 17.43 mm (0.69 in.) at 27.15 msec total elapsed time. In later experiments, use of side view imaging would attribute this final outward surge to the effects of the first bubble pulse. *Post mortem* damage was observed to include panel delamination and fiber breakage around the boundary. Such tearing was not observed to have propagated through the specimen. There also appeared to be instances of matrix cracking across the specimen face. A *post mortem* image of the specimen may be observed in Figure 3.2.1.1-2. The panel center point behavior can be observed in Figure 3.2.1.1-3.

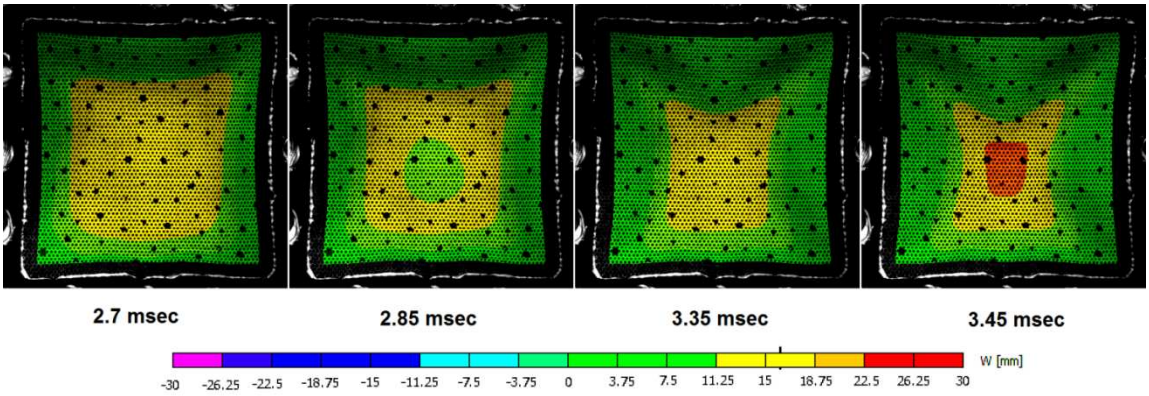

Figure 3.2.1.1-1: 2D DIC contour plot of panel deflection, illustrating the typical development of the X-shaped plateau during the panel's inward rebound. The inward motion (2.7 msec) was realized most about the center, which continued to collapse in spite of the arrested movement towards the boundaries (2.85 msec). This motion was reversed by about 3 msec as the center expanded outward once more (3.35, 3.45 msec).

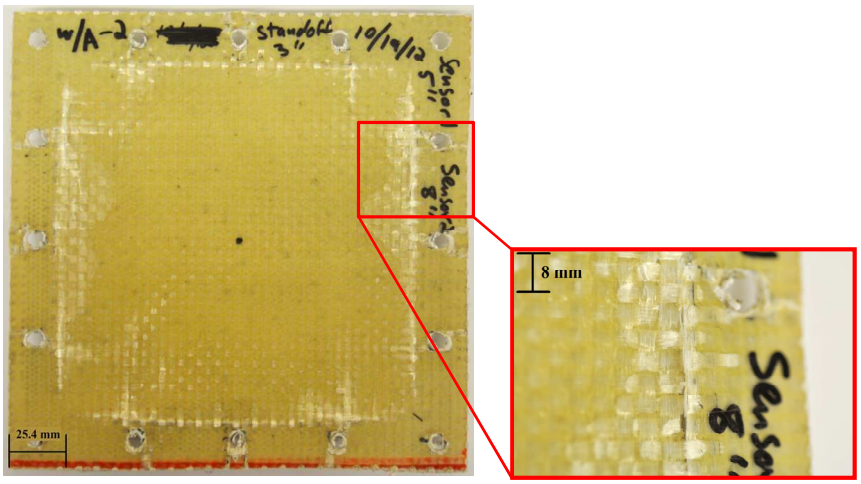

Figure 3.2.1.1-2: *Post mortem* damage typical of the WA experiment set.

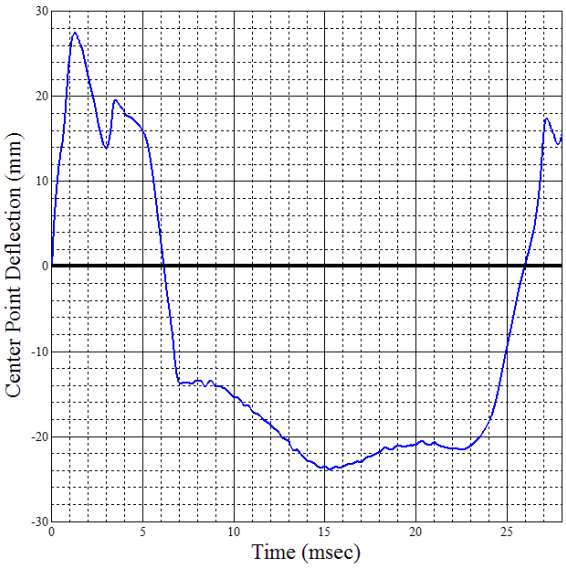

Figure 3.2.1.1-3: Outward center point deflection, WA experiment 1.

Pressure wave data, measured on a time scale from the shockwave's contact with sensor 1, indicated peak overpressures of 22.5 MPa (3260 PSI) at 2.1 µsec elapsed time and 16.7 MPa (2420 PSI) at 55.1 µsec elapsed time, as detected by sensors 1 and 2, respectively. Pressure decay profiles typical of the WA experiment set are overlaid

in Figure 3.2.1.1-4. Key experimental results are presented for convenience in Table 3.2.1.1-1.

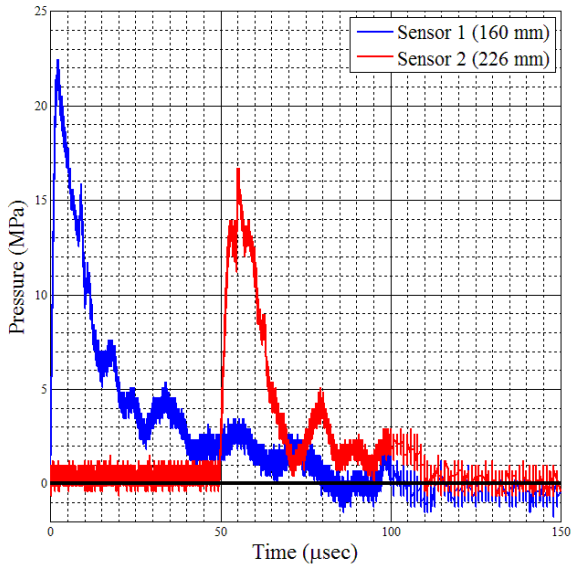

Figure 3.2.1.1-4: Overpressure histories, WA experiment 1

Table 3.2.1.1-1: Key parameters yielded from WA experiment 1

Parameter	Value	Elapsed Time
DIC Calibration Error	9.8%	-
Peak Overpresure, Sensor 1	22.5 MPa (3260 PSI)	2.1 µsec
Peak Overpresure, Sensor 2	16.7 MPa (2420 PSI)	55.1 µsec
Max. Positive Panel Deflection	27.5 mm (1.08 in.)	1.3 msec
Max. Negative Panel Deflection	-24 mm (-0.94 in.)	15.3 msec

3.2.1.2 WA Experiment 2

The second WA experiment, due to an instrument malfunction, was performed without the use of an oscilloscope to record pressure data. The DIC camera angles of

incidence with the transparent Lexan viewing window were also not recorded during this experiment, but the DIC calibration error was found to be 10.0%. Experiment 2 produced DIC results that were repeatable from experiment 1; the center point deflection profile bore remarkable similarity to that of experiment 1, and the X-shaped plateau was again plainly observable and responsible for a brief outward rebound of the center point (see Figure 3.2.1.1-1). Due to an imperfect seal around the holding box's edges at the interface with the transparent Lexan viewing window, a leak occurred that had partially filled the box by the time of detonation. As the panel flexed away from the explosion, the rapid increase in pressure within the box caused the accumulated water to splash. By an elapsed time of 18.45 msec, the splash had so obscured the specimen that all successive DIC data had to be discarded as unreliable. Key results included a maximum positive center point deflection of 29.6 mm (1.17 in.) at 1.15 msec elapsed time and a maximum negative center point deflection of -27.3 mm (-1.07 in.) at 16.45 msec elapsed time. As in experiment 1, *post mortem* damage was observed to include panel delamination and fiber breakage around the boundary. Unlike the damage observed in experiment 1, tearing was observed to have propagated through the specimen. Images of this damage may be observed in Figure 3.2.1.2-1. A deflection plot for this experiment is included in Figure 3.2.1.2-2. Table 3.2.1.2-1 presents relevant data obtained during WA experiment 2.

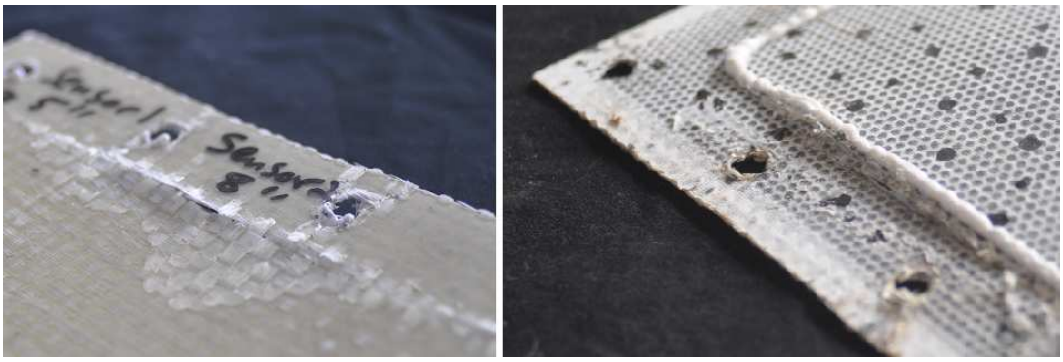

Figure 3.2.1.2-1: *Post mortem* tearing seen through-and-through the specimen, around the boundary. The beaded white line around the periphery (at right) is the remnant of the specimen's caulking seal.

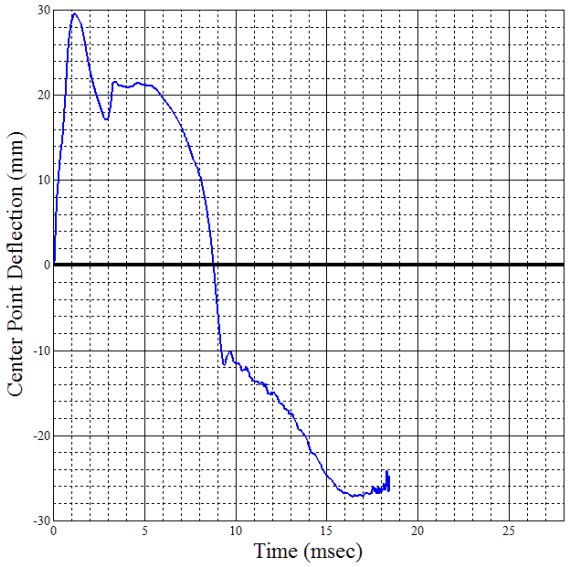

Figure 3.2.1.2-2: Outward center point deflection, WA experiment 2

Table 3.2.1.2-1: Key parameters yielded from WA experiment 2

Parameter	Value	Elapsed Time
DIC Calibration Error	10.0%	-
Max. Positive Panel Deflection	29.6 mm (1.17 in.)	1.15 msec
Max. Negative Panel Deflection	-27.3 mm (-1.07 in.)	16.45 msec

3.2.1.3 WA Experiment 3

The third WA experiment was performed with the recording oscilloscope set to a sampling frequency of 10 MHz. The DIC camera angles of incidence with the transparent Lexan viewing window were 7º for both the Master and Slave 1 cameras, and the corresponding DIC calibration error was found to be 9.0%. A side view camera with a 28 mm lens was employed to observe the expansion and collapse of the gas bubble produced as a result of the explosion. Experiment 3 produced results that were repeatable from experiments 1 and 2. Key results included a maximum positive center point deflection of 26. mm (1.02 in.) at 1.3 msec elapsed time and a maximum negative center point deflection of -25.5 mm (-1.00 in.) at 18.5 msec elapsed time, as seen in Figure 3.2.1.3-1. Sensor 1 detected a peak overpressure of 22 MPa (3200 PSI) at 3.5 μsec after initial shockwave contact, while sensor 2 detected a peak overpressure of 16 MPa (2340 PSI) at 60 μsec, detailed in Figure 3.2.1.3-2.

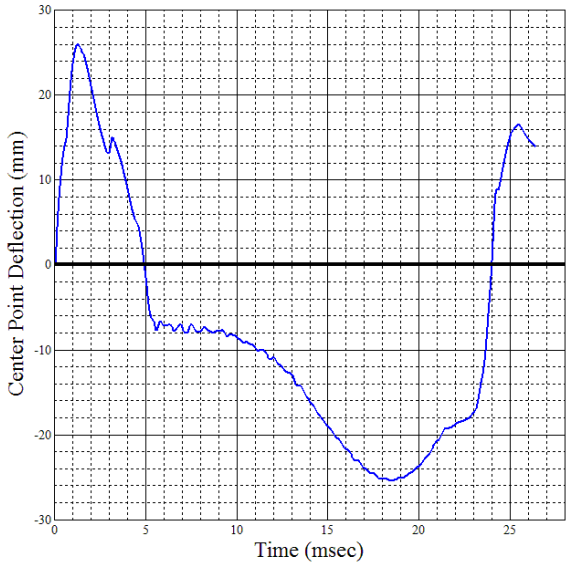

Figure 3.2.1.3-1: Outward center point deflection, WA experiment 3

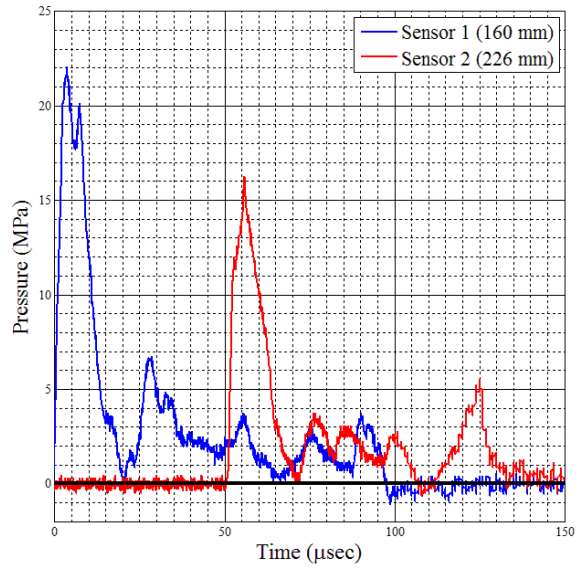

Figure 3.2.1.3-2: Overpressure histories, WA experiment 3

The gas bubble was observed to expand in radius until an elapsed time between 11 and 14 msec, after which it began its collapse. The collapse was accomplished fully

by approximately 22.15 msec, at which time point the first bubble pulse was initiated. Figure 3.2.1.3-3 depicts the typical progress of bubble expansion and contraction. *Post mortem* damage was observed to include delamination and fiber breakage around the specimen boundary, as in experiments 1 and 2, and some matrix cracking across the panel face. Fiber tearing did not extend through the panel. Table 3.2.1.3-1 presents relevant data obtained during WA experiment 3.

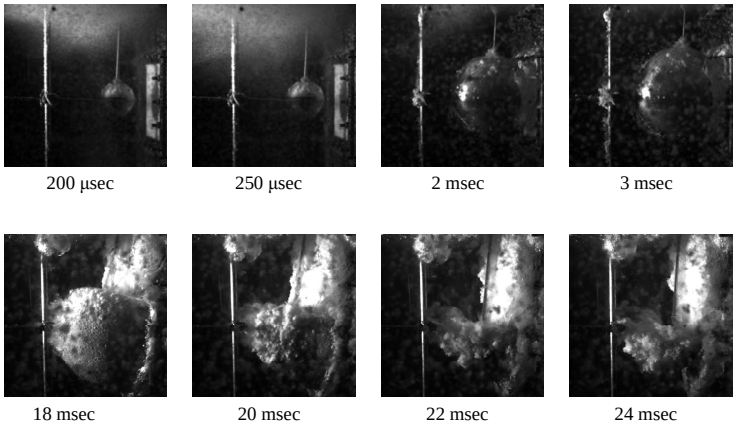

Figure 3.2.1.3-3: Typical progress of a bubble's expansion (upper) and contraction (lower)

Table 3.2.1.3-1: Key parameters yielded from WA experiment 3

Parameter	Value	Elapsed Time
DIC Calibration Error	9.0%	-
Peak Overpresure, Sensor 1	22 MPa (3200 PSI)	3.5 μsec
Peak Overpresure, Sensor 2	16 MPa (2340 PSI)	55.9 μsec
Max. Postive Panel Deflection	26 mm (1.02 in.)	1.3 msec
Max. Negative Panel Deflection	-25.5 mm (-1.00 in.)	18.5 msec
Full Bubble Expansion	-	11 – 14 msec
Full Bubble Collapse	-	~22.15 msec

3.2.1.4 WA Experiment 4

The fourth WA experiment was performed with the recording oscilloscope set to a sampling frequency of 10 MHz. The DIC camera angles of incidence with the transparent Lexan viewing window were 7º for both the Master and Slave 1 cameras, and the corresponding DIC calibration error was found to be 9.5%. A side view camera with a 28 mm lens was employed to observe the expansion and collapse of the gas bubble produced as a result of the detonation. Due to a faulty instrument cable connection, sensor 2 was not able to register any meaningful signal. In spite of this, experiment 4 produced results that were repeatable from experiments 1, 2, and 3. Key results included a maximum positive center point deflection of 28 mm (1.1 in.) at 1.2 msec elapsed time, maximum negative center point deflection of -29 mm (-1.14 in.) at 17.7 msec elapsed time, and sensor 1 peak overpressure of 23 MPa (3340 PSI) at 6.1 μsec after shockwave contact. These results are depicted in Figures 3.2.1.4-1 and -2.

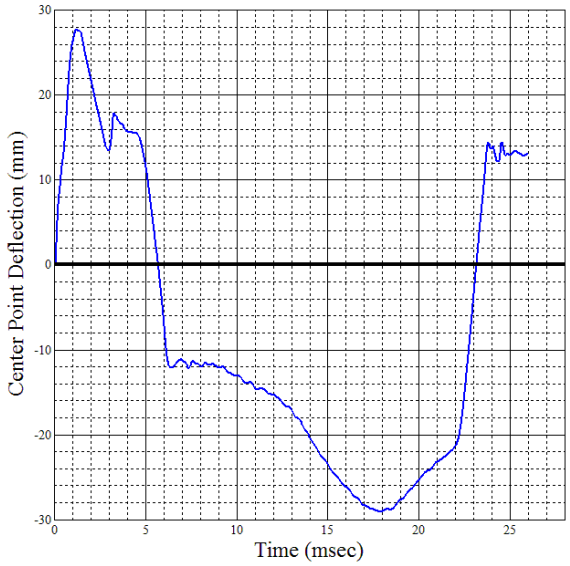

Figure 3.2.1.4-1: Outward center point deflection, WA experiment 4

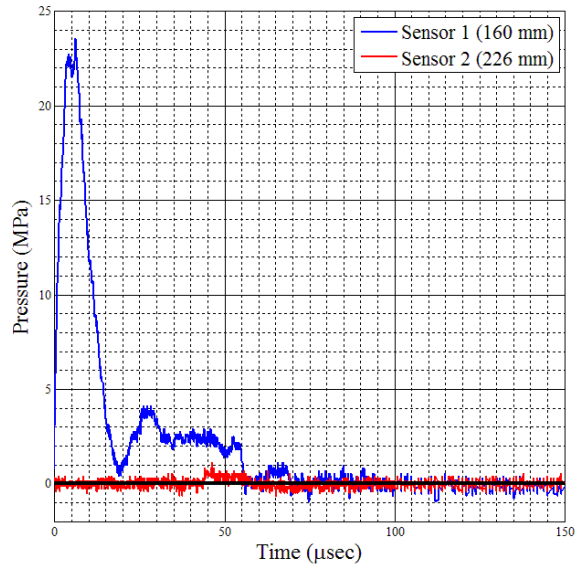

Figure 3.2.1.4-2: Overpressure histories, WA experiment 4

The gas bubble was observed to expand in radius until an elapsed time between 10.25 and 13.30 msec, after which it began its collapse. The collapse was

accomplished fully by approximately 22 msec, at which time the first bubble pulse was generated. *Post mortem* damage was seen to include delamination and fiber breakage around the panel boundary, with through-panel tearing occurring in an isolated area. Table 3.2.1.4-1 presents relevant data obtained during WA experiment 4.

Table 3.2.1.4-1: Key parameters yielded from WA experiment 4

Parameter	Value	Elapsed Time
DIC Calibration Error	9.5%	-
Peak Overpresure, Sensor 1	23 MPa (3340 PSI)	6.1 μsec
Peak Overpresure, Sensor 2	N/A	N/A
Max. Positive Panel Deflection	28 mm (1.1 in.)	1.2 msec
Max. Negative Panel Deflection	-29 mm (-1.14 in.)	17.7 msec
Full Bubble Expansion	-	10.25 - 13.30 msec
Full Bubble Collapse	-	~22

3.2.2 Water Submersion, Water Backing

Experiments were performed to investigate the response of the EVE composite specimen to an UNDEX event in an experimental environment characterized by water submersion and water backing—an environment referred to hereafter as “WW”. The holding box was moved backwards on the mounting stand and re-bolted, so as to provide sufficient clearance to allow proper water circulation while the panel flexed. The mounting/boundary conditions, the detonator/blast probes and their positioning, the camera lenses, settings, and software, and the supporting data acquisition devices employed in the WW experiment set remained identical to those employed in the WA set. These invariable parameters are reflected in Table 3.2.1-1.

3.2.2.1 WW Experiment 1

The first WW experiment was performed with the recording oscilloscope set to a sampling frequency of 10 MHz. The DIC camera angles of incidence with the transparent Lexan viewing window were 6º for the Master camera and 7º for the Slave 1 camera, and the corresponding DIC calibration error was found to be 8.5%. A side view camera with a 28 mm lens was employed to observe the expansion and collapse of the gas bubble produced as a result of the detonation. After the initiation of the explosion, the rapid flexing of the panel caused dense cavitation to develop in front of the specimen's speckle pattern (Figure 3.2.2.1-1). The impenetrability of the cavitation field varied in intensity as the UNDEX event progressed, but the panel center point remained at all times beneath considerable shielding. Because of this, DIC information could only be confidently analyzed up to 200 μsec after the onset of panel deflection, a maximum value of which was recorded as 2.25 mm (0.09 in.). The center point deflection plot from WW experiment 1, typical of the WW experiment set, is given in Figure 3.2.2.1-2.

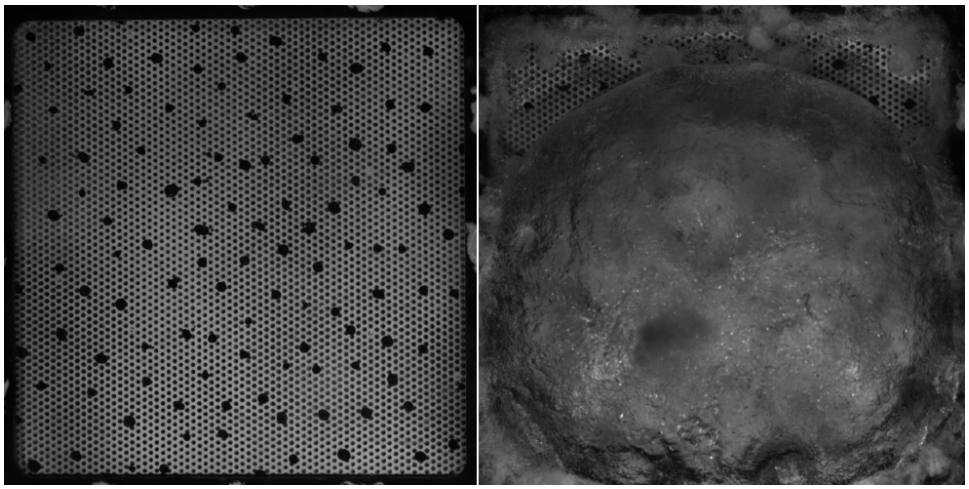

Figure 3.2.2.1-1: A depiction of the cavitation witnessed in the WW experiment set. Left: the undeformed panel. Right: the deforming panel at 6.3 msec.

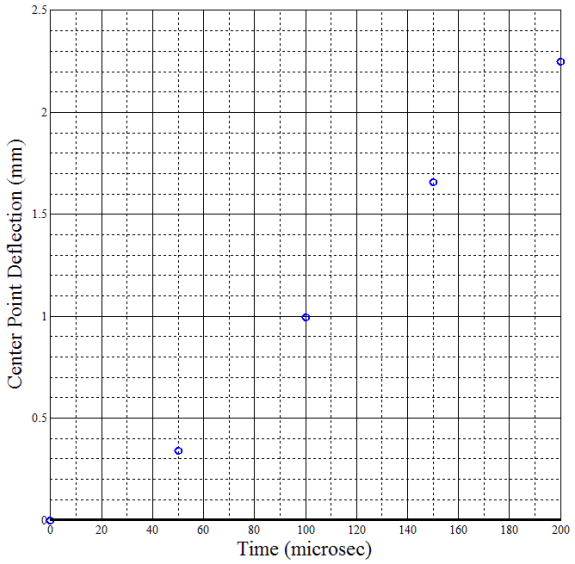

Figure 3.2.2.1-2: Outward center point deflection, WW experiment 1

The WW experiment set exhibited curious pressure histories. These shall be discussed in further detail in section 4.1.2, but for convenience relevant information is also presented here. The closer of the tourmaline blast probes (sensor 1) recorded a peak overpressure of 24.8 MPa (3600 PSI) at an elapsed time of approximately 3 μsec after initial contact with the shockwave. The farther probe (sensor 2) recorded an

initial peak pressure of 12 MPa (1740.5 PSI) at 43 μsec, followed by an intermediate ebb of 9.25 MPa (1341.6 PSI) at 47 μsec, and again followed by a final, more intense overpressure of 12.8 MPa (1862.3 PSI) at 50 μsec. This behavior was typical of the WW experiment set. Pressure profiles for WW experiment 1 are depicted in Figure 3.2.2.1-3. *Post mortem* damage was observed to include matrix cracking and mild delamination around the boundaries, as well as cracking at the panel center. This damage is depicted in Figure 3.2.2.1-4. The gas bubble was observed to expand in radius until an elapsed time of about 11 msec, and the collapse was accomplished fully by approximately 23 msec, initiating the first bubble pulse. Key parameters from WW experiment 1 are listed for convenience in Table 3.2.2.1-1.

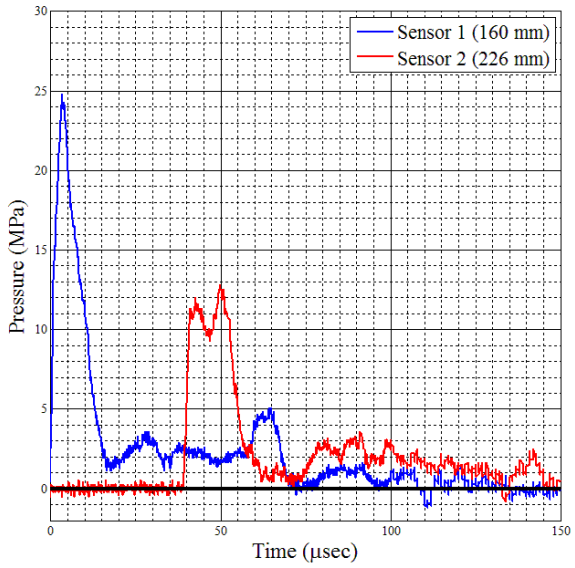

Figure 3.2.2.1-3: Overpressure histories, WW experiment 1

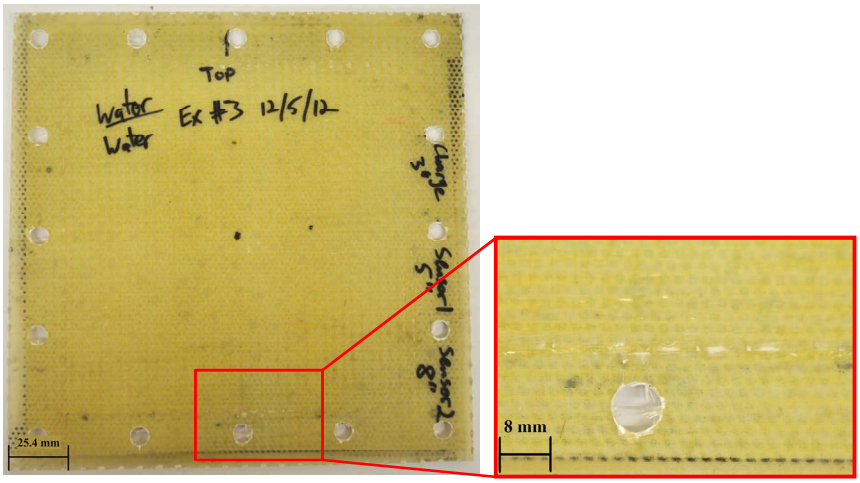

Figure 3.2.2.1-4: *Post mortem* damage typical of the WW experiment set

Table 3.2.2.1-1: Key parameters yielded from WW experiment 1

Parameter	Value	Elapsed Time
DIC Calibration Error	8.5%	-
Peak Overpresure, Sensor 1	24.8 MPa (3600 PSI)	3 µsec
Overpresure, Sensor 2 (I)	12 MPa (1740.5 PSI)	43 µsec
Overpresure, Sensor 2 (II)	12.8 MPa (1862.3 PSI)	50 µsec
200 µsec Panel Deflection	2.25 mm (0.09 in.)	-
Full Bubble Expansion	-	~10.95 msec
Full Bubble Collapse	-	~23 msec

3.2.2.2 WW Experiment 2

The second WW experiment was performed in quick succession after the first, and all of the experimental parameters remained unchanged (see section 3.2.2.1). Similar event behavior was observed in WW experiment 2 as was observed in experiment 1—the onset of cavitation occurred at approximately 200 µsec, by which time the panel had deflected outward 1.5 mm; sensor 1 detected a peak overpressure of 28.3 MPa (4100 PSI) at an elapsed time of 3.4 µsec after contact with the shockwave,

while sensor 2 detected an initial peak overpressure of 12.8 MPa (1860 PSI) at an elapsed time of 51 µsec, followed by an ebb to 9.5 MPa (1378 PSI) at 55.3 µsec and a surge to 13.3 MPa (1929 PSI) at 58 µsec. *Post mortem* damage was similar to that of WW experiment 1. The gas bubble expanded in radius until an elapsed time of about 12.65 msec, after which it achieved its full collapse and generated the first bubble pulse around 25.3 msec. These key parameters are listed for convenience in Table 3.2.2.2-1. Figures 3.2.2.2-1 and -2 illustrate the deflection and pressure histories.

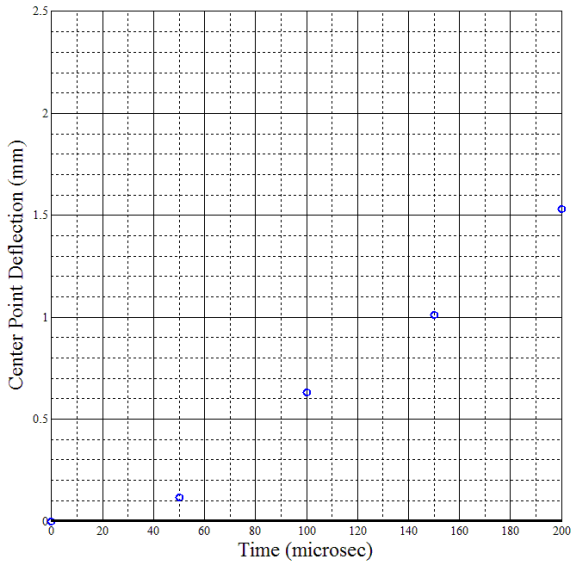

Figure 3.2.2.2-1: Outward center point deflection, WW experiment 2

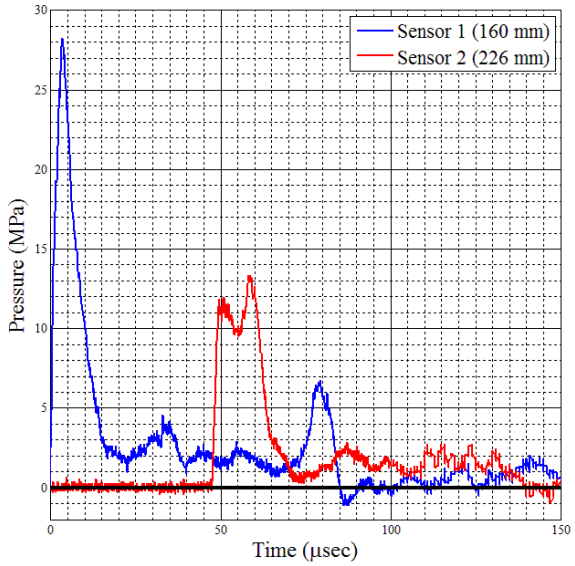

Figure 3.2.2.2-2: Overpressure histories, WW experiment 2

Table 3.2.2.2-1: Key parameters yielded from WW experiment 2

Parameter	Value	Elapsed Time
DIC Calibration Error	8.5%	-
Peak Overpresure, Sensor 1	28.3 MPa (4100 PSI)	3.4 µsec
Overpresure, Sensor 2 (I)	12.8 MPa (1860 PSI)	51 µsec
Overpresure, Sensor 2 (II)	13.3 MPa (1929 PSI)	58 µsec
200 µsec Panel Deflection	1.5 mm (0.06 in.)	-
Full Bubble Expansion	-	~12.65 msec
Full Bubble Collapse	-	~25.3 msec

3.2.2.3 WW Experiment 3

The third WW experiment was performed in quick succession after the second, and all of the experimental parameters remained unchanged (see section 3.2.2.1, 3.2.2.2). Similar event behavior was observed in WW experiment 3 as was observed in experiments 1 and 2—the onset of cavitation occurred at approximately 200 µsec, by

which time the panel had deflected outward 1.73 mm. Sensor 1 detected at peak overpressure of 28.7 MPa (4162.6 PSI) at an elapsed time of 3.2 µsec after initial contact with the shockwave, while sensor 2 detected an initial overpressure of 12.2 MPa (1769.5 PSI) at an elapsed time of 50 µsec, an ebb to 9 MPa (1305.3 PSI) at 54.3 µsec, and a final surge to 13.4 MPa (1943.5 PSI) at 56.3 µsec. *Post mortem* damage was that of experiments 1 and 2. The gas bubble expanded in radius until an elapsed time of about 11 msec after detonation, after which time it achieved its full collapse and generated the first bubble pulse around 22.6 msec. These key parameters are listed for convenience in Table 3.2.2.2-1. Panel center point deflection behavior and the peak overpressure history may be seen in Figures 3.2.2.3-1 and -2.

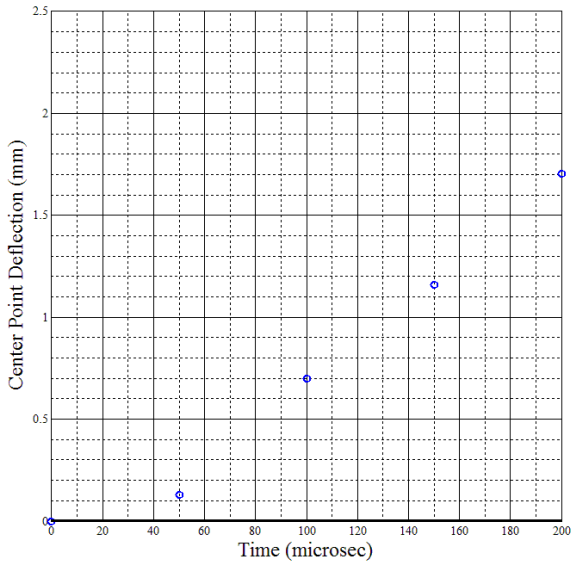

Figure 3.2.2.3-1: Outward center point deflection, WW experiment 3

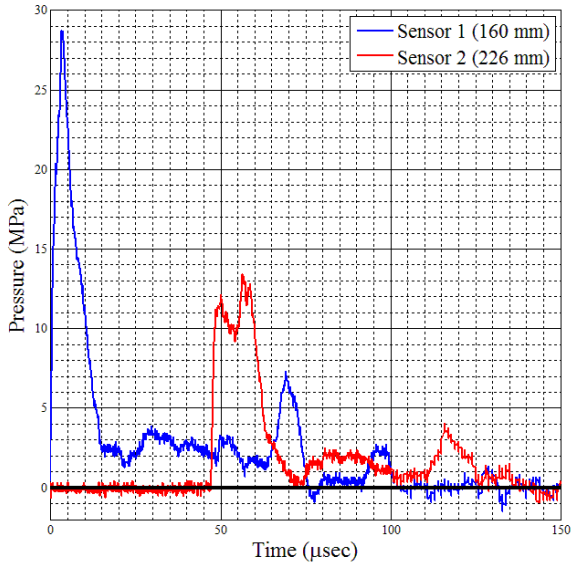

Figure 3.2.2.3-2: Overpressure histories, WW experiment 3

Table 3.2.2.3-1: Key parameters yielded from WW experiment 3

Parameter	Value	Elapsed Time
DIC Calibration Error	8.5%	-
Peak Overpresure, Sensor 1	28.7 MPa (4162.6 PSI)	3.2 µsec
Overpresure, Sensor 2 (I)	12.82 MPa (1860 PSI)	50 µsec
Overpresure, Sensor 2 (II)	13.4 MPa (1943.5 PSI)	56.3 µsec
200 µsec Panel Deflection	1.73 mm (0.07 in.)	-
Full Bubble Expansion	-	~11.00 msec
Full Bubble Collapse	-	~22.55 msec

3.2.3 Air Immersion, Air Backing

Experiments were performed to investigate the response of the EVE composite specimen to an UNDEX event in an experimental environment characterized by air immersion and air backing—an environment referred to hereafter as “AA”. The tourmaline blast sensors were retired during the AA experiments and replaced by air

blast pencil probes. These sensors were mounted horizontally with the sensing element oriented sideways. The size of these instruments imposed different standoff distance requirements than those in the WA and WW experiment sets. The sensor tips were positioned at a minimum of 76 mm (3 in.) from the explosive, to avoid the creation of moments of force against the sensor bodies. With the tips of sensors 1 and 2 standing off at 76 and 152 mm (3 and 6 in.) respectively from the explosive, the 157.5 mm (6.2 in.) distance from the probe diaphragms to the tips imposed actual sensing element standoff distances of 234 mm (9.2 in.) and 310 mm (12.2 in.), respectively. In addition, due to incidental damage to the transparent Lexan viewing window, the window had to be removed from the tank. To protect the DIC lenses after this adjustment, special filter mounts were obtained for affixing to the lenses. Thin plates of Lexan were inserted into the filter mounts, which, owing to compatibility restrictions, could only be attached to 60 mm lenses. All other experimental parameters enumerated in Table 3.2.1-1 remained invariable. For convenience and clarity, the amended parameters are listed in Table 3.2.3-1. These parameters remained invariant for all AA experiments except when explicitly noted.

Table 3.2.3-1: Key experimental apparatus values invariable throughout the AA experiment set.

Parameter	Value
RP-503 Standoff Distance	76.2 mm (3 in.)
Sensor 1 Tip Standoff Distance	76.2 mm (3 in.)
Sensor 1 Sensing Element Standoff Distance	234 mm (9.2 in.)
Sensor 2 Tip Standoff Distance	152.4 mm (6 in.)
Sensor 2 Sensing Element Standoff Distance	310 mm (12.2 in.)
DIC Camera Lens	60 mm
DIC Camera Frame Rate	20,000 FPS
DIC Camera Inter frame Time	50 μsec
DIC Image Resolution	512 x 512

3.2.3.1 AA Experiment 1

It was recognized from theory (Cole, 1948)(Smith & Hetherington, 1994)(Shin, 2004)(Ngo et al., 2007) that the pressure wave decay rate in air would be greater than in water. Without full knowledge of the energy release during an RP-503 detonation in air, the appropriate pressure ranges to be expected at certain radii from the explosive were not clearly known. Because of this uncertainty, it was recognized that the oscilloscope trigger, still initiated by the amplified signal from sensor 1, needed to be lowered as far as possible while at the same time remaining above the instrument noise level. This was achieved by lowering the trigger to 100 mV. However, during detonation the electromagnetic interference induced by the firing box's 2000 V pulse prematurely triggered the oscilloscope and caused high frequency noise that consumed the blast probe signal. For this reason, the first AA experiment yielded no useful pressure data. The tips of sensors 1 and 2 nevertheless stood off at respective distances of 76.2 mm (3 in.) and 136.53 mm (5.375 in.) from the explosive. The DIC camera angles of incidence with the specimen plane were 7º for the Master camera and 6º for

the Slave 1 camera, and the corresponding DIC calibration error was found to be 10%. After detonation, the panel center point deflected to a positive maximum of 7 mm (0.27 in.) after an elapsed time of 0.4 msec. The ensuing center point deflection followed a pattern of successive outward and inward oscillations, first reaching its negative maximum of -9.5 mm (-0.37 in.) at an elapsed time of 1.05 msec. This behavior is illustrated in Figure 3.2.3.1-1.

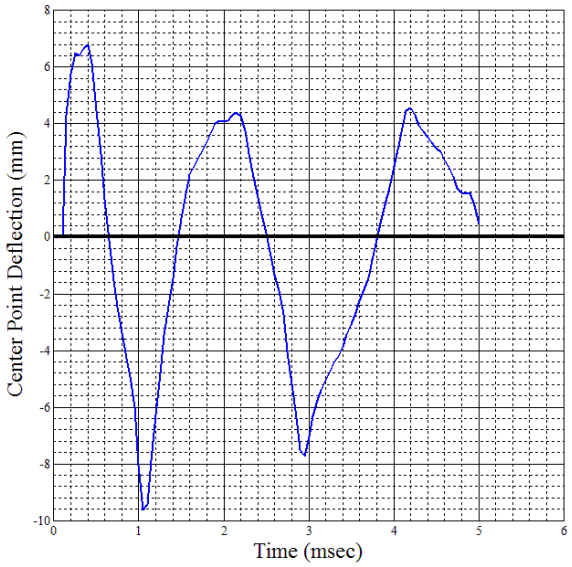

Figure 3.2.3.1-1: Outward center point deflection, AA experiment 1

Post mortem damage included light resin singing around the boundary, and a prominent lacerated cleft that passed horizontally through the panel center. This cleft propagated through the panel's thickness, severing fibers on both sides. On the explosive side of the panel, the cleft appeared as a demarcation line between a dense lower field of impact damage pockmarks and isolated resin singing, and a sparse upper field of impact damage pockmarks. This damage is depicted in Figure 3.2.3.1-2.

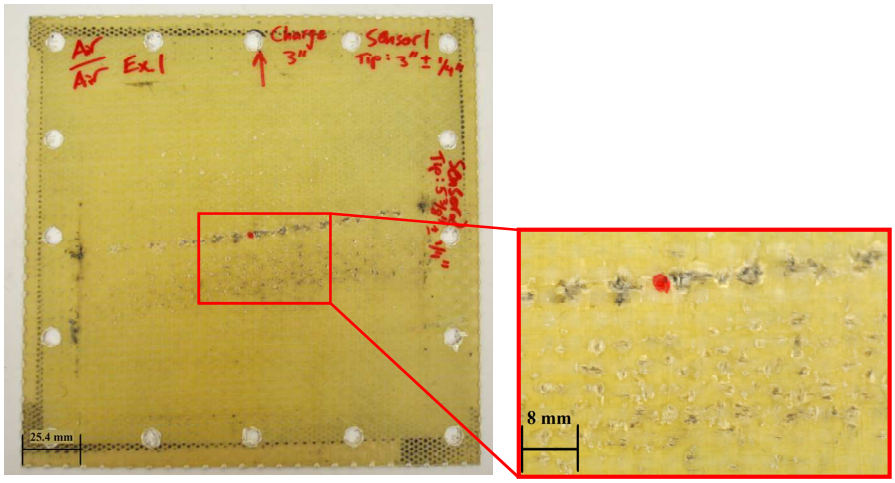

Figure 3.2.3.1-2: *Post mortem* damage typical of the AA experiment set

Key values from AA experiment 1 are listed for convenience in Table 3.2.3.1-1.

Table 3.2.3.1-1: Key parameters yielded from AA experiment 1

Parameter	Value	Elapsed Time
DIC Calibration Error	10%	-
Max. Positive Panel Deflection	7 mm (0.27 in.)	0.4 msec
Max. Negative Panel Deflection	-9.5 mm (-0.37 in.)	1.05 msec

3.2.3.2 AA Experiment 2

The second AA experiment, due again to premature oscilloscope triggering, high-frequency noise, and additional error, yielded neither useful pressure data nor any DIC data. However, *post mortem* damage was consistent with that experienced in AA experiment 1.

3.2.3.3 AA Experiment 3

The third AA experiment was accomplished with two oscilloscopes, both with separate triggering mechanisms. The first oscilloscope (hereafter “oscilloscope 1”) was triggered directly by a new firing box, with the capability of sending an independent 9 V triggering signal to oscilloscope 1 in concert with a 3000 V explosive detonation pulse. The second oscilloscope (hereafter “oscilloscope 2”) was triggered by an external circuit beak. The circuit break supplied a 5 V triggering signal to oscilloscope 2 after a graphite rod, positioned 1 in. from the explosive, fractured during detonation (Figure 3.2.3.3-1). Oscilloscopes 1 and 2 employed sampling frequencies of 50 MHz and 1 MHz, respectively. The DIC camera angles of incidence with the specimen plane were 10º for the Master camera and 11º for the Slave 1 camera, and the corresponding DIC calibration error was found to be 3.8%. After detonation, the panel center point deflected in a similar oscillatory manner as it had in AA experiment 1, reaching its maximum positive deflection of 6.44 mm (0.25 in.) after an elapsed time of 0.25 msec and its maximum negative deflection of -9.74 mm (-0.38 in.) after an elapsed time of 1.05 msec. High frequency/amplitude noise induced by electromagnetic interference, though unexpected, again contaminated the pressure data. In spite of this, pulses were clearly observed—however, because of the intense noise it was still necessary to process the signal with a MATLAB-based interval-dependent denoising filter, using a 4-level wavelet decomposition with a “db1” wavelet family. Based on this filtering scheme, sensor 1 on oscilloscope 1 detected a pulse of 0.11 MPa (16 PSI) at an elapsed time of 9 μsec, and sensor 2 detected a pulse

of 0.06 MPa (8.7 PSI) at an elapsed time of 187 μsec. The positive and negative pressure phases are clearly visible in the sensor 1 signal. The sensor 2 signal tends towards its negative phase, but apparent wave reflections prevent it from experiencing that phase as quickly as the signal from sensor 1. Since oscilloscope 2 operated with inferior resolution than did oscilloscope 1, its detected pulses were lesser in magnitude than oscilloscope 1's. Because of this, only the data from oscilloscope 1 is presented here. A filtered plot of sensor 1 data from oscilloscope 2 is provided in Figure 3.2.3.3-2, and center point displacement behavior is illustrated in Figure 3.2.3.3-3. *Post mortem* damage was consistent with that observed in experiments 1 and 2. Key results are listed in Table 3.2.3.3-1.

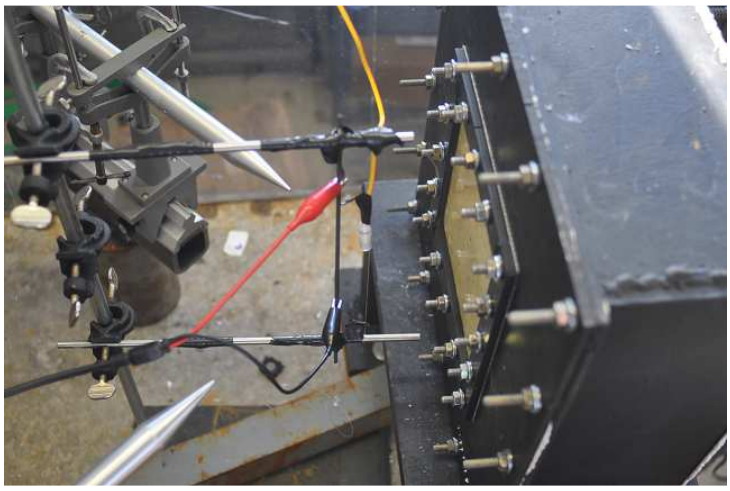

Figure 3.2.3.3-1: Graphite rod circuit break, illustrating the rod (connected to alligator clips) and its orientation to the blast probes and the explosive.

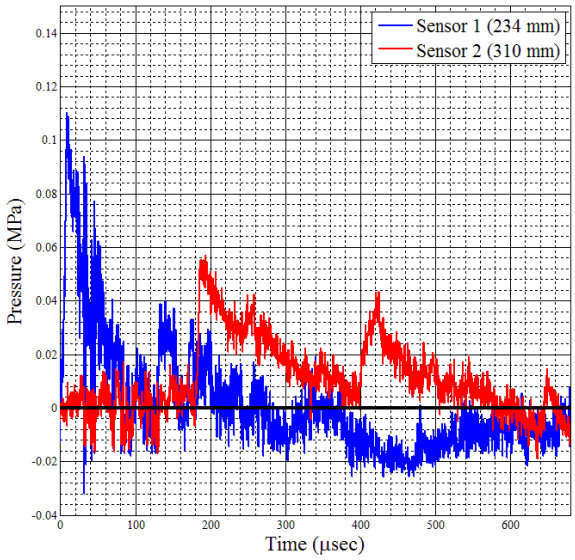

Figure 3.2.3.3-1: Filtered plot of pressure data collected during AA experiment 3

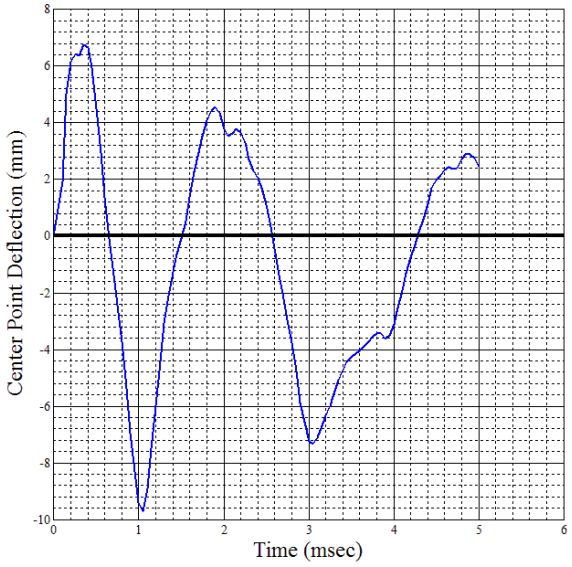

Figure 3.2.3.3-2: Outward center point deflection, AA experiment 3

Table 3.2.3.3-1: Key parameters yielded from AA experiment 3

Parameter	Value	Elapsed Time
DIC Calibration Error	3.8%	-
Peak Overpresure, Sensor 1 (Oscilloscope 1)	0.11 MPa (16 PSI)	9 μsec
Peak Overpresure, Sensor 2 (Oscilloscope 1)	0.06 MPa (8.7 PSI)	187 μsec
Max. Positive Panel Deflection	6.4 mm (0.25 in.)	0.25 msec
Max. Negative Panel Deflection	-9.74 mm (-0.38 in.)	1.05 msec

3.2.3.4 AA Experiment 4

The fourth AA experiment was accomplished with one oscilloscope with a graphite circuit break trigger. The oscilloscope was arranged with a sampling frequency of 10 MHz. This lower sampling frequency was used in AA experiment 4 due to the cumbersome size of the data sets from AA experiment 3, which slowed down processing to such an extent that the data had to be broken into 4 individual files. The DIC camera angles of incidence with the specimen plane were 7º for the Master camera and 12º for the Slave 1 camera, and the corresponding DIC calibration error was found to be 3.0%. The center point deflection behavior was consistent with the behavior observed in the previous experiments of the AA series. The panel reached its maximum positive deflection of 6.5 mm (0.26 in.) at an elapsed time of 0.35 msec and reached its maximum negative deflection of -10.3 mm (-0.41 in.) at an elapsed time of 1.00 msec. Following these were the center point's characteristic oscillations. Sensor 1 registered a pulse of 0.14 MPa (20.3 PSI) at an elapsed time of 13 μsec from contact with the shock wave, and sensor 2 similarly registered a pulse of 0.04 MPa

(5.8 PSI) at an elapsed time of 196 μsec. The displacement plot is given in Figure 3.2.3.4-1, and pressure histories are depicted in Figure 3.2.3.4-2.

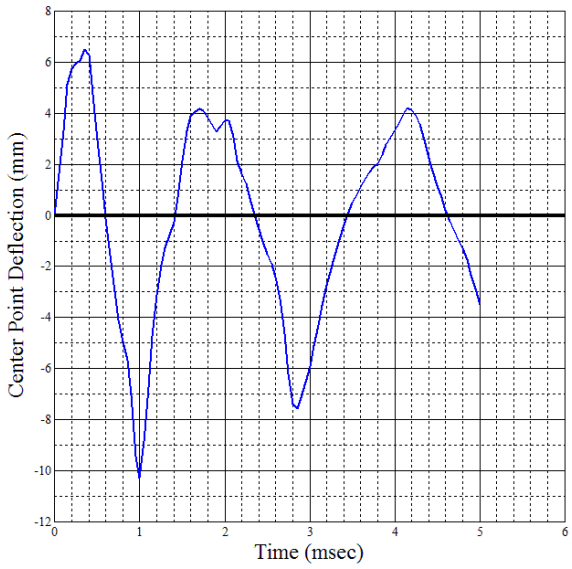

Figure 3.2.3.4-1: Outward center point deflection, AA experiment 4

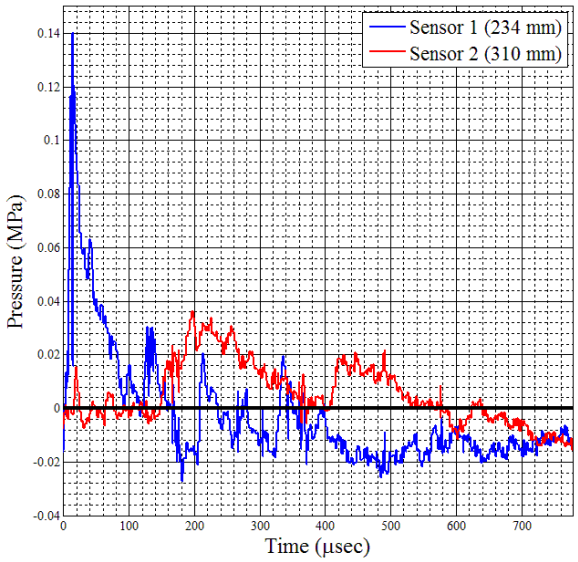

Figure 3.2.3.4-1: Filtered plot of pressure data collected during AA experiment 4.

Post mortem damage was consistent with that seen in the previous experiments. Key results are listed in Table 3.2.3.4-1.

Table 3.2.3.4-1: Key parameters yielded from AA experiment 4.

Parameter	Value	Elapsed Time
DIC Calibration Error	3.0%	-
Peak Overpresure, Sensor 1	0.14 MPa (20.3 PSI)	13 µsec
Peak Overpresure, Sensor 2	0.04 MPa (5.8 PSI)	196 µsec
Max. Postive Panel Deflection	6.5 mm (0.26 in.)	0.35 msec
Max. Negative Panel Deflection	-10.3 mm (-0.41 in.)	1.00 msec

3.2.3.5 AA Experiment 5

The fifth AA experiment was accomplished without pressure sensors, and DIC data was recorded only. A side view camera with a 28 mm lens was employed in an

attempt to observe the phenomena responsible for the unique *post mortem* damage characteristic of the AA experiment set. Of particular interest was the cause of the through-thickness cleft. The DIC camera angles of incidence with the specimen plane were 7º for the Master camera and 12º for the Slave 1 camera, and the corresponding DIC calibration error was found to be 2.8%. The event was sufficiently bright and quick that the side view camera was unable to observe the cause of any damage. In spite of this, the DIC cameras captured panel deformation data consistent with that seen in the previous experiments. The panel flexed outward to its maximum positive deflection of 6.3 mm (0.25 in.) after an elapsed time of 0.35 msec, and rebounded to its maximum negative deflection of -10.2 mm (-0.40 in.) at a total elapsed time of 1.00 msec. This plot can be seen in Figure 3.2.3.5-1. Key results are listed in Table 3.2.3.5-1.

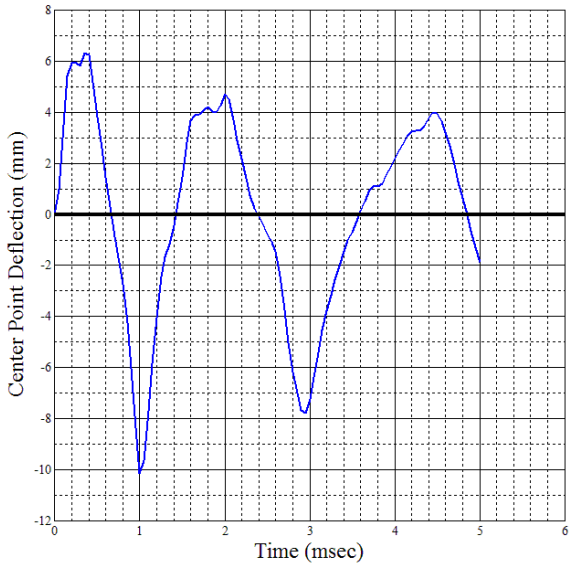

Figure 3.2.3.5-1: Outward center point deflection, AA experiment 4

Table 3.2.3.5-1: Key parameters yielded from AA experiment 5.

Parameter	Value	Elapsed Time
DIC Calibration Error	2.8%	-
Max. Positive Panel Deflection	6.3 mm (0.25 in.)	0.35 msec
Max. Negative Panel Deflection	-10.2 mm (-0.40 in.)	1.00 msec

3.2.4 Low Temperature Water Immersion, Air Backing

Experiments were performed to investigate the response of the EVE composite specimen to an UNDEX event in an experimental environment characterized by water submersion and air backing at water temperatures of approximately 0 °C—an environment referred to hereafter as "WALT." Apart from the water temperature, the WALT experiment series was conducted under largely identical conditions as the WA series: DIC resolution and frame rate, pressure sensor type and standoff distances, RP-503 standoff distance, and waterproofing techniques remained the same between sets. A notable difference in these parameters was the use of 60 mm DIC lens in the WALT series. Side view illumination was also provided this time by an SSG-400 filament-less 400 watt HMI spotlight, manufactured by Frezzi Energy Systems, through the rear observation panel of the water tank. Besides this, the pre-experiment specimen and instrument preparation methods were identical. Key invariable parameters for the WALT experiment set are included in Table 3.2.4-1.

Table 3.2.4-1: Key invariable parameters for the WALT experiment set

Parameter	Value
RP-503 Standoff Distance	76.2 mm (3 in.)
Sensor 1 Tip Standoff Distance	127 mm (5 in.)
Sensor 1 Sensing Element Elevation Above Tip	97 mm (3.8 in.)
Sensor 1 Sensing Element Standoff Distance	160 mm (6.3 in.)
Sensor 2 Tip Standoff Distance	203 mm (8 in.)
Sensor 2 Sensing Element Elevation	99 mm (3.9 in.)
Sensor 2 Sensing Element Standoff Distance	226 mm (8.9 in.)
DIC Camera Lens	60 mm
DIC Camera Frame Rate	20,000 FPS
DIC Camera Interframe Time	50 μsec
DIC Image Resolution	512 x 512

To achieve the required 0 °C water conditions, equation 3.1.6.2-1 was employed to determine the necessary mass of ice to be mixed in the tank, assuming a -10 °C ice temperature. These calculations, accounting for the mass and nominal temperature of the water, indicated that 150 kg (330 lb.) of ice were required per experiment to chill the water sufficiently. Cubed ice was purchased in 9 kg (20 lb.) bags, which were emptied directly into water tank, either before, during, or after filling. The water temperature was monitored with a network of 5 thermometers that were embedded in a small Styrofoam flotation raft. Cooling durations took between two and four hours to accomplish, and water was circulated via manual mixing with a wooden plank.

3.2.4.1 WALT Experiment 1

In the first WALT experiment, the recording oscilloscope was arranged with a sampling frequency of 10 MHz. The DIC camera angles were not recorded for this experiment. The calibration error was found to be 5.1%. A side view camera with a 28

mm lens was employed, and appropriate illumination was supplied through the rear observation window, as stated before. The cooling process was halted when the average registered temperature reached 1.4 °C. Individual qualifying temperatures for each thermometer are given in Table 3.2.4.1-1.

Table 3.2.4.1-1: Qualifying temperatures for WALT experiment 1

Thermometer	Temperature
1	-2 °C
2	2 °C
3	3 °C
4	2 °C
5	1.9 °C

Results for WALT experiment 1 are shown in Figures 3.2.4.1-1 through -3. As seen in the figures, the panel center point achieved its maximum positive deflection of 24.4 mm (0.96 in.) at 1.25 msec before rebounding. A maximum negative displacement of -23.3 mm (-0.92 in.) was achieved by approximately 23 msec, before the effects of the first bubble pulse forced the panel center to a local positive maximum of approximately 11.7 mm (0.46 in.) at 25 msec. This behavior is displayed in Figure 3.2.4.1-1.

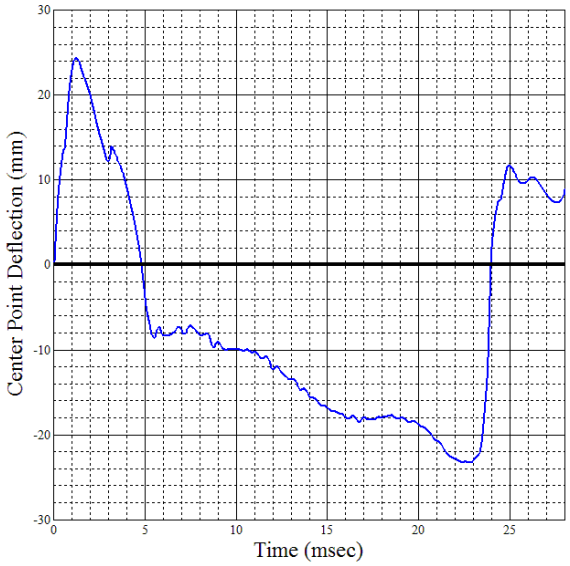

Figure 3.2.4.1-1: Outward center point deflection, WALT experiment 1

Maximum overpressures for the event registered at approximately 25 MPa (3626 PSI) in sensor 1 at 6 μsec after initial contact with the shockwave, and at approximately 14 MPa (2031 PSI) in sensor 2 at 71 μsec after shockwave contact. These are depicted in Figure 3.2.4.1-2.

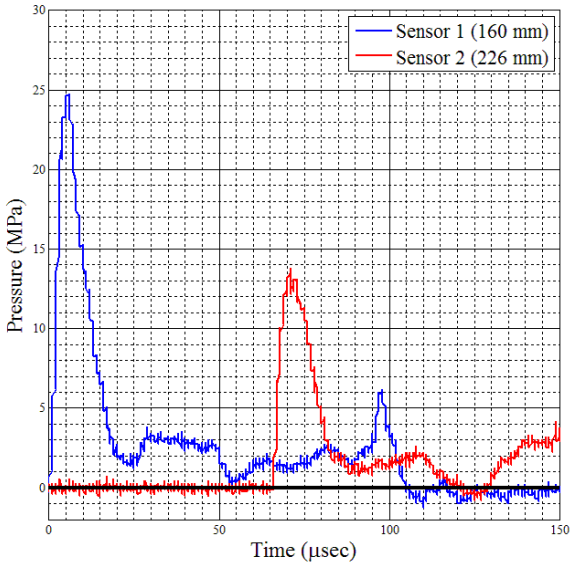

Figure 3.2.4.1-2: Overpressure histories, WALT experiment 1

Post mortem damage included some delamination and minor fiber breakage around the boundaries, similar to that observed in the WA experiment set, but less severe. This is illustrated in Figure 3.2.4.1-3.

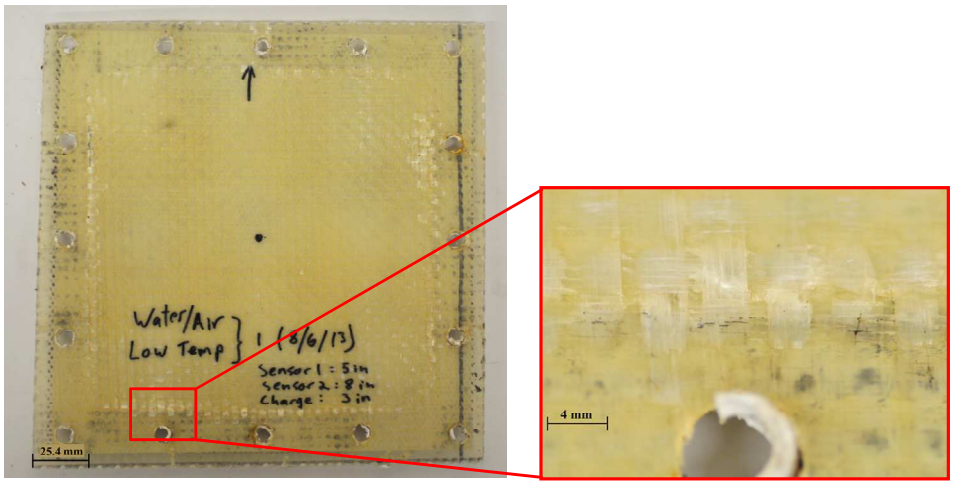

Figure 3.2.4.1-3: *Post mortem* damage typical of the WALT series.

Side view imaging revealed that the bubble reached its maximum expansion by approximately 11 msec after detonation, before achieving full collapse and generating the first bubble pulse by approximately 22.6 msec. Key results of WALT experiment 1 are listed in Table 3.2.4.1-2.

Table 3.2.4.1-2: Key results from WALT experiment 1

Parameter	Value	Elapsed Time
DIC Calibration Error	5.1%	-
Peak Overpresure, Sensor 1	25 MPa (3626 PSI)	6 μsec
Peak Overpresure, Sensor 2	14 MPa (2031 PSI)	71 μsec
Max. Positive Panel Deflection	24.4 mm (0.96 in.)	1.25 msec
Max. Negative Panel Deflection	-23.3 mm (-0.92 in.)	23 msec
Full Bubble Expansion	-	11 msec
Full Bubble Collapse	-	22.6 msec

3.2.4.2 WALT Experiment 2

The second WALT experiment was conducted without having moved the DIC camera system after WALT experiment 1. Because of this, WALT experiment 2 was analyzed using the same calibration images and thus had the same calibration error. In the second WALT experiment the recording oscilloscope was arranged with a sampling frequency of 10 MHz. The DIC camera angles were, again, not recorded for the experiment. A side view camera with a 28 mm lens was again employed, and appropriate illumination was accordingly supplied through the rear observation window. The cooling process was halted when the average registered temperature reached 2.7 °C. Individual qualifying temperatures for each thermometer are given in Table 3.2.4.2-1.

Table 3.2.4.2-1: Qualifying temperatures for WALT experiment 2

Thermometer	Temperature
1	3 °C
2	3 °C
3	3 °C
4	2 °C
5	2.4 °C

In WALT experiment 2, the panel center point achieved its maximum positive deflection of 25.6 mm (1.01 in.) at 1.25 msec before rebounding. A maximum negative displacement of -26.7 mm (-1.05 in.) was achieved by approximately 23 msec, before the effects of the first bubble pulse forced the panel center to a local positive maximum of approximately 13.6 mm (0.53 in.) at 25 msec. *Post mortem* damage was more drastic in WALT specimen 2. Perhaps caused by random variability in the manufacturing process, the first bubble pulse caused the bottom edge of the panel to tear through and through along a long seam. The displacement behavior is displayed in Figure 3.2.4.2-1.

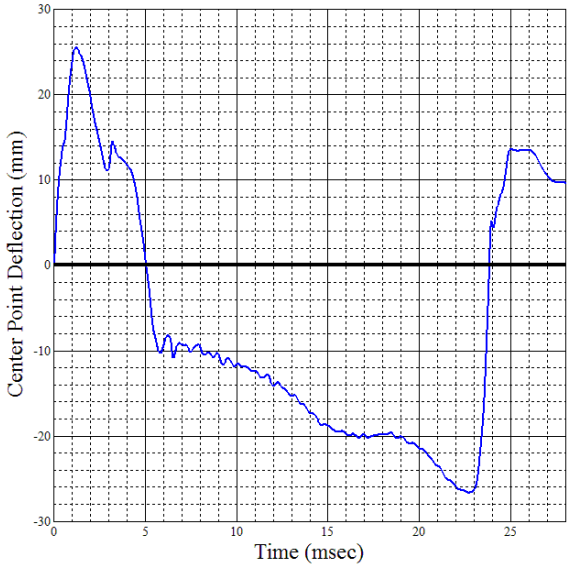

Figure 3.2.4.2-1: Outward center point deflection, WALT experiment 2

Maximum overpressures for the event registered at approximately 23 MPa (3336 PSI) in sensor 1 at 7 μsec after initial contact with the shockwave, and at approximately 18 MPa (2610.6 PSI) in sensor 2 at 40 μsec after shockwave contact, as seen in Figure 3.2.4.2-2.

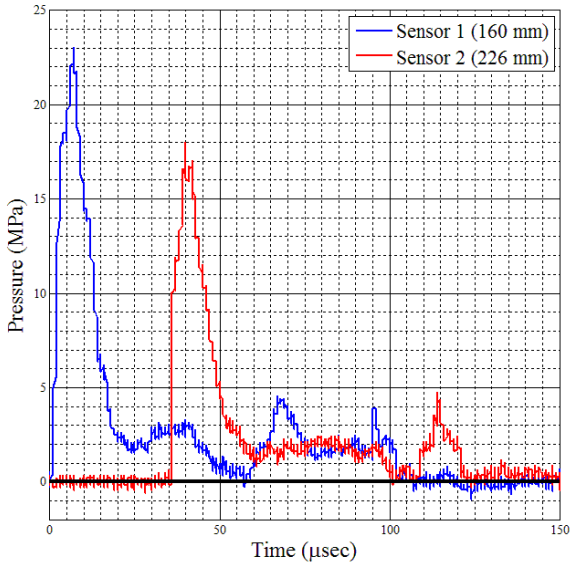

Figure 3.2.4.2-2: Overpressure histories, WALT experiment 2

Side view imaging revealed that the bubble reached its maximum expansion by approximately 10.5 msec after detonation, before achieving full collapse and generating the first bubble pulse by approximately 22.4 msec. Key results of WALT experiment 2 are listed in Table 3.2.4.2-2.

Table 3.2.4.2-2: Key results from WALT experiment 2

Parameter	Value	Elapsed Time
DIC Calibration Error	5.1%	-
Peak Overpresure, Sensor 1	23 MPa (3336 PSI)	7 μsec
Peak Overpresure, Sensor 2	18 MPa (2610.6 PSI)	40 μsec
Max. Positive Panel Deflection	25.6 mm (1.01 in.)	1.25 msec
Max. Negative Panel Deflection	-26.7 mm (-1.05 in.)	23 msec
Full Bubble Expansion	-	10.5 msec
Full Bubble Collapse	-	22.4 msec

3.2.5 Low Temperature Water Immersion, Water Backing

Experiments were performed to investigate the response of the EVE composite specimen to an UNDEX event in an experimental environment characterized by water submersion and water backing at water temperatures of approximately 0 °C—an environment referred to hereafter as "WWLT." The set up and preparation for these experiments was almost completely identical to those of the WALT series, the only prescribed difference being that no sealing was undertaken between the fixture and the Lexan front observation window or between the specimen and the fixture. As with the room temperature WW experiments, the fixture was retracted slightly from the observation window so as to allow for adequate water circulation during the UNDEX event and, as with the WW experiments, only 200 μsec of DIC data could be obtained due to thick cavitation in front of the specimen. Key invariable parameters for the WWLT experiment set, since they were identical to those in the WALT series, are included in Table 3.2.4-1. The cooling method and process remained the same for the WWLT series as it had been in the WALT series, as did the required mass of ice and general cooling duration.

3.2.5.1 WWLT Experiment 1

In the first WWLT experiment, the recording oscilloscope was arranged with a sampling frequency of 100 MHz. The DIC camera stereo angle was 15°, and the calibration error was found to be 6.3%. A side view camera with a 28 mm lens was employed, and appropriate illumination was supplied through the rear observation window. The cooling process was halted when the average registered temperature

reached 3.5 °C. Individual qualifying temperatures for each thermometer are given in Table 3.2.5.1-1.

Table 3.2.5.1-1: Qualifying temperatures for WWLT experiment 1

Thermometer	Temperature
1	4.5 °C
2	3 °C
3	4 °C
4	3 °C
5	3 °C

Results for WWLT experiment 1 are shown in Figures 3.2.5.1-1 through -3. As seen in the figures, by 200 μsec the panel center point achieved a positive deflection of 1.7 mm (0.07 in.). This behavior is displayed in Figure 3.2.5.1-1.

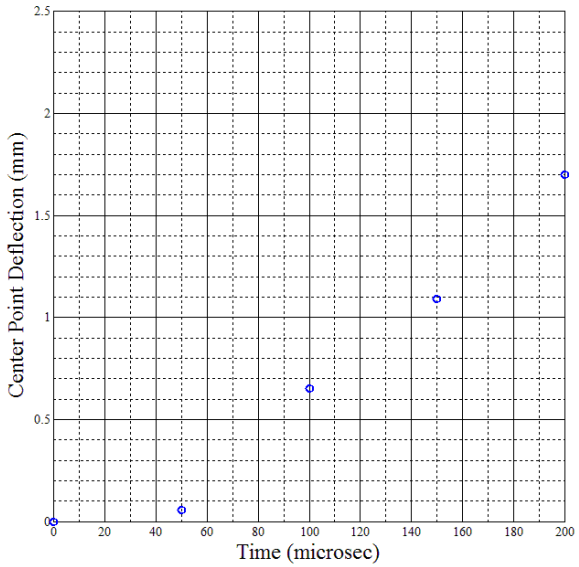

Figure 3.2.5.1-1: Outward center point deflection, WWLT experiment 1.

Maximum overpressures for the event registered at approximately 21.7 MPa (3147 PSI) in sensor 1 at 6 μsec after initial contact with the shockwave, and at approximately 16 MPa (2335 PSI) in sensor 2 at 39 μsec after shockwave contact. These are depicted in Figure 3.2.5.1-2.

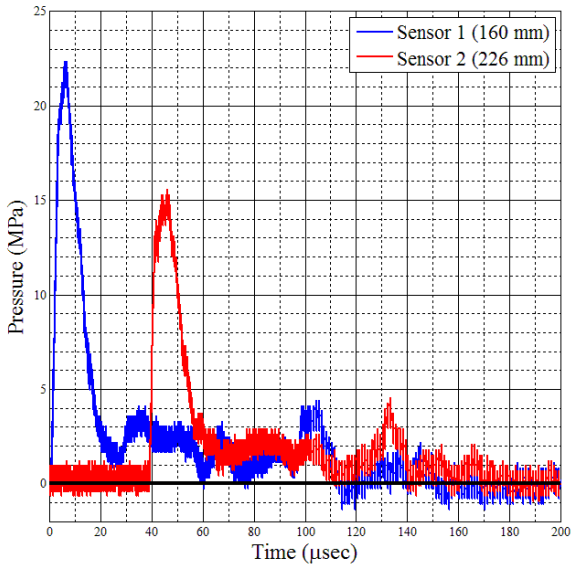

Figure 3.2.5.1-2: Overpressure histories, WWLT experiment 1

Post mortem damage included some delamination and minor fiber breakage around the boundaries, similar to that observed in the WW experiment set, but with more severe effects at the bottom boundary. This damage is illustrated in Figure 3.2.5.1-3.

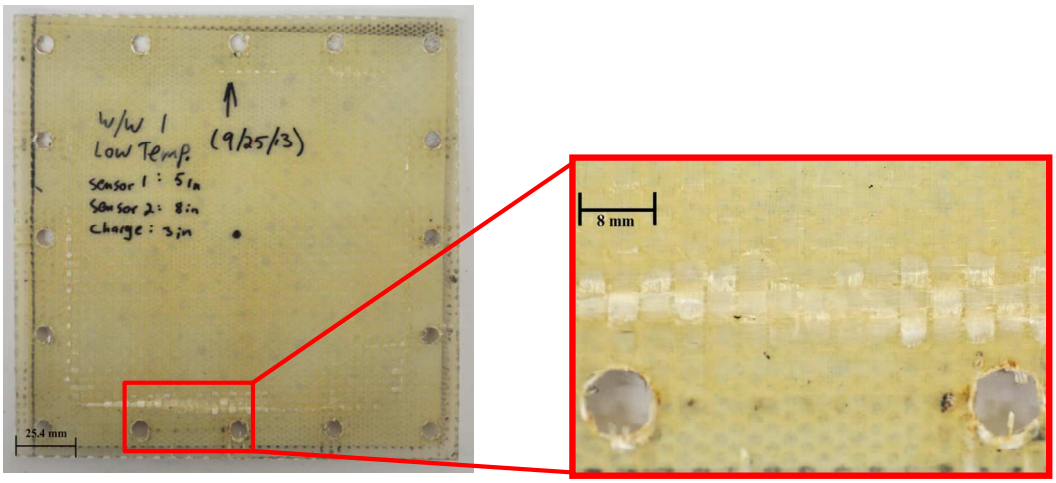

Figure 3.2.5.1-3: *Post mortem* damage typical of the WWLT series.

Side view imaging revealed that the bubble reached its maximum expansion by approximately 11.25 msec after detonation, before achieving full collapse and generating the first bubble pulse by approximately 22.7 msec. Key results of WALT experiment 1 are listed in Table 3.2.5.1-2.

Table 3.2.5.1-2: Key results from WWLT experiment 1

Parameter	Value	Elapsed Time
DIC Calibration Error	5.1%	-
Peak Overpresure, Sensor 1	21.7 MPa (3147 PSI)	6 µsec
Peak Overpresure, Sensor 2	16 MPa (2335 PSI)	39 µsec
200 µsec Panel Deflection	1.7 mm (0.07 in.)	-
Full Bubble Expansion	-	11.25 msec
Full Bubble Collapse	-	22.7 msec

3.2.5.2 WWLT Experiment 2

In the second WWLT experiment, the recording oscilloscope was again arranged with a sampling frequency of 100 MHz. The DIC camera stereo angle was 15°, and the

calibration error was found to be 4.6%. A side view camera with a 28 mm lens was employed, and appropriate illumination was supplied through the rear observation window. The cooling process was halted when the average registered temperature reached 3.3 ℃. Individual qualifying temperatures for each thermometer are given in Table 3.2.5.2-1.

Table 3.2.5.2-1: Qualifying temperatures for WWLT experiment 2

Thermometer	Temperature
1	4 ℃
2	3 ℃
3	4 ℃
4	3 ℃
5	2.6 ℃

Results for WWLT experiment 2 are shown in Figures 3.2.5.2-1 through -3. As seen in the figures, by 200 μsec the panel center point achieved a positive deflection of 1.6 mm (0.07 in.). This behavior is displayed in Figure 3.2.5.2-1.

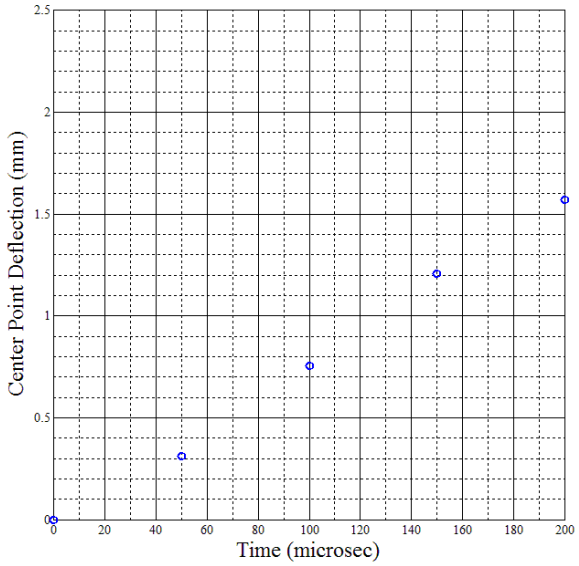

Figure 3.2.5.2-1: Outward center point deflection, WWLT experiment 2

Maximum overpressures for the event registered at approximately 22.3 MPa (3234.3 PSI) in sensor 1 at 6 μsec after initial contact with the shockwave, and at approximately 15.6 MPa (2262.6 PSI) in sensor 2 at 46 μsec after shockwave contact. These are depicted in Figure 3.2.5.2-2.

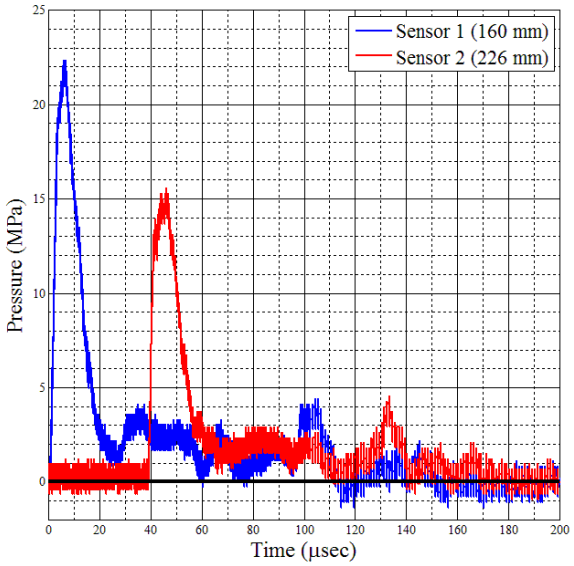

Figure 3.2.5.2-2: Overpressure histories, WWLT experiment 2

Post-mortem damage was similar to that exhibited by the specimen from WWLT 1, though with diminished severity at the bottom boundary. Side view imaging revealed that the bubble reached its maximum expansion by approximately 10.7 msec after detonation, before achieving full collapse and generating the first bubble pulse by approximately 22.8 msec. Key results of WALT experiment 1 are listed in Table 3.2.5.2-2.

Table 3.2.5.2-2: Key results from WWLT experiment 2

Parameter	Value	Elapsed Time
DIC Calibration Error	4.6%	-
Peak Overpresure, Sensor 1	22.3 MPa (3234.3 PSI)	6 μsec
Peak Overpresure, Sensor 2	15.6 MPa (2262.6 PSI)	46 μsec
200 μsec Panel Deflection	1.6 mm (0.07 in.)	-
Full Bubble Expansion	-	10.7 msec
Full Bubble Collapse	-	22.8 msec

3.2.6 High Temperature Water Immersion, Air Backing

Experiments were performed to investigate the response of the EVE composite specimen to an UNDEX event in an experimental environment characterized by water submersion and air backing at water temperatures of approximately 40 °C—an environment referred to hereafter as "WAHT." Because this experiment series bore exact likeness to the WALT series apart from the experimental water temperature, Table 3.2.4-1 may be referenced for key information related to the relevant preparation and set up. Because the high operating temperature that the WAHT series demanded exceeded the blast probes' working temperature, those sensors were not used and no pressure data was collected.

To achieve the required 40 °C water conditions, Equation 3.1.6.1-1 was used to obtain the required power input to raise the water temperature from 23 °C over a period of approximately 2 hours. The resulting power, just over 5 kW, was rounded to 5 kW due to electrical constraints in the experimental facility, as described in Section 3.1.6.1. Five 1-kW water heaters were suspended from rods above the water in the tank, with the heating elements fully submerged. Water circulation was achieved by an impeller. The water temperature was monitored by a network of five thermometers that were embedded in a small Styrofoam flotation raft. At any point during the heating process, the remaining heating duration could be ascertained by solving Equation 3.1.6.1-1 for Δt.

To prevent skin burns, measures were taken to avoid coming in contact with the hot water or the water heaters. Neoprene heat-resistant gloves were worn when

handling the water heaters, and the RP-503 explosive was inserted into the water via a small-bore copper tube. The explosive's lead wire was fed through the tube until the charge capsule was flush with it. The rigid tube provided an ideal means of directing the position of the explosive once placed in the water, and it was fastened in place simply by spanning a rod across the top of the water tank and taping the tube to the rod.

3.2.6.1 WAHT Experiment 1

In the first WAHT experiment, the DIC camera angles were 8° for the Master camera and 7° for the Slave 1 camera. The calibration error was found to be 7.3%. The heating process was halted when the average water temperature reached 41.5 °C. Individual qualifying temperatures for each thermometer are given in Table 3.2.6.1-1.

Table 3.2.6.1-1: Qualifying temperatures for WAHT experiment 1

Thermometer	Temperature
1	40 °C
2	42 °C
3	42 °C
4	42.5 °C
5	41.2 °C

Results for WAHT experiment 1 are shown in Figures 3.2.6.1-1 and -2. The panel center point achieved its maximum positive deflection of 28.7 mm (1.13 in.) at 1.25 msec before rebounding. A maximum negative displacement of -7.5 mm (-0.3 in.) was achieved by approximately 17.2 msec, before the effects of the first bubble pulse

forced the panel center to a local positive maximum of approximately 12.7 mm (0.5 in.) at 25 msec. This behavior is displayed in Figure 3.2.6.1-1.

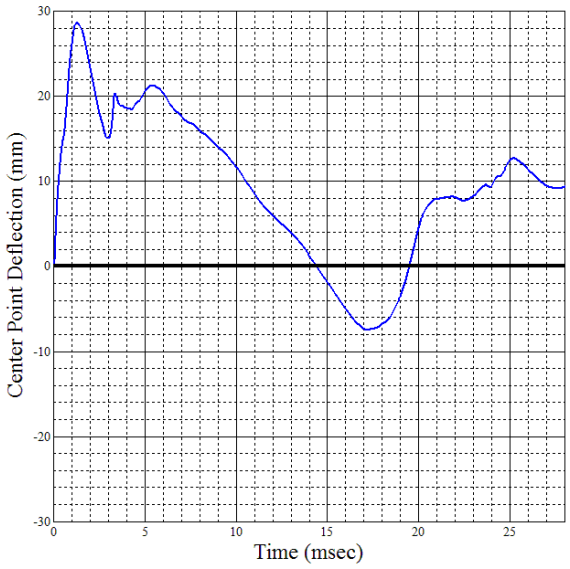

Figure 3.2.6.1-1: Outward center point deflection, WAHT experiment 1

Post mortem damage included some delamination, minor fiber breakage, as well as some matrix cracking in certain areas around the boundary. The damage severity was similar to that observed in the WA experiment set, but less pronounced. The *post-mortem* panel had a definite, easily-noticeable permanent concavity. A representative *post-mortem* specimen is illustrated in Figure 3.2.6.1-2.

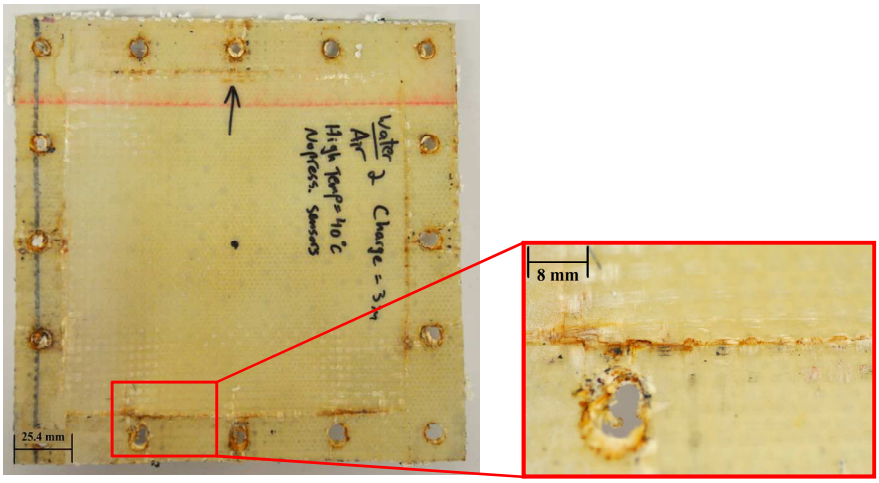

Figure 3.2.6.1-2: *Post mortem* damage typical of the WAHT series.

Key results of WALT experiment 1 are listed in Table 3.2.6.1-2.

Table 3.2.6.1-2: Key results from WAHT experiment 1

Parameter	Value	Elapsed Time
DIC Calibration Error	7.3%	-
Max. Positive Panel Deflection	28.7 mm (1.13 in.)	1.25 msec
Max. Negative Panel Deflection	-7.5 mm (-0.3 in.)	17.2 msec

3.2.6.2 WAHT Experiment 2

WAHT experiment 2 was performed immediately after WAHT experiment 1. Because of this, the DIC camera angles remained 8° for the Master camera and 7° for the Slave 1 camera. The calibration error also remained constant at 7.3%. The heating process was halted when the average water temperature reached 41.2 °C. Individual qualifying temperatures for each thermometer are given in Table 3.2.6.2-1.

Table 3.2.6.2-1: Qualifying temperatures for WAHT experiment 2

Thermometer	Temperature
1	40 °C
2	41 °C
3	42 °C
4	42 °C
5	41.1 °C

Results for WAHT experiment 2 are shown in Figure 3.2.6.2-1. The panel center point achieved its maximum positive deflection of 28.8 mm (1.13 in.) at 1.35 msec before rebounding. A maximum negative displacement of -23.7 mm (-0.93 in.) was achieved by approximately 19.1 msec, before the effects of the first bubble pulse forced the panel center to a local positive maximum of approximately 8.7 mm (0.34 in.) at 24 msec.

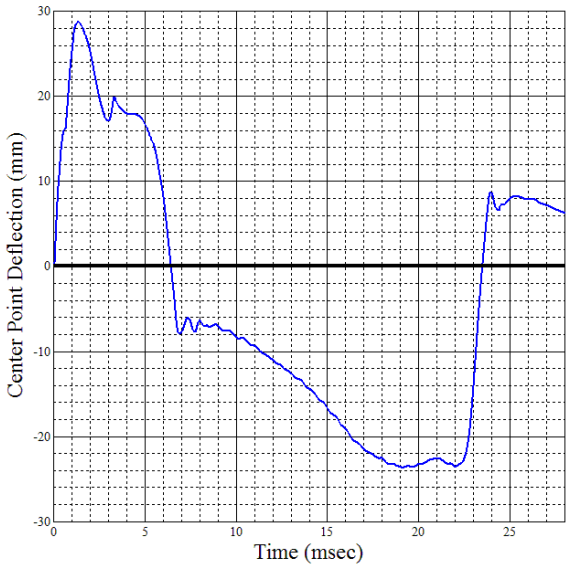

Figure 3.2.6.2-1: Outward center point deflection, WAHT experiment 2

Post mortem damage was very similar to that observed in the WAHT 1 specimen. Key results of WALT experiment 1 are listed in Table 3.2.6.2-2.

Table 3.2.6.2-2: Key results from WAHT experiment 2

Parameter	Value	Elapsed Time
DIC Calibration Error	7.3%	-
Max. Positive Panel Deflection	28.8 mm (1.13 in.)	1.35 msec
Max. Negative Panel Deflection	-23.7 mm (-0.93 in.)	19.1 msec

3.2.7 High Temperature Water Immersion, Water Backing

Experiments were performed to investigate the response of the EVE composite specimen to an UNDEX event in an experimental environment characterized by water submersion and water backing at water temperatures of approximately 40 °C—an environment referred to hereafter as "WWHT." As with the case between the WALT and WWLT series, setup and preparation for the WWHT experiment set bears great similarity to those for the WAHT set. Notable differences are limited to, again, the retracted location of the experimental fixture and the presence of thick cavitation in front of the specimen during the UNDEX event, permitting only the first 200 μsec of DIC data to be confidently processed.

3.2.7.1 WWHT Experiment 1

In the first WWHT experiment, the DIC camera angles were 8° for the Master camera and 7° for the Slave 1 camera, and the calibration error was found to be 4.4%.

The heating process was halted when the average water temperature reached 40.8 °C. Individual qualifying temperatures for each thermometer are given in Table 3.2.7.1-1.

Table 3.2.7.1-1: Qualifying temperatures for WWHT experiment 1

Thermometer	Temperature
1	38 °C
2	42 °C
3	42 °C
4	42 °C
5	39.8 °C

Results for WWHT experiment 1 are shown in Figures 3.2.7.1-1 and -2. By 200 μsec the panel center point achieved a positive deflection of 1.63 mm (0.06 in.).

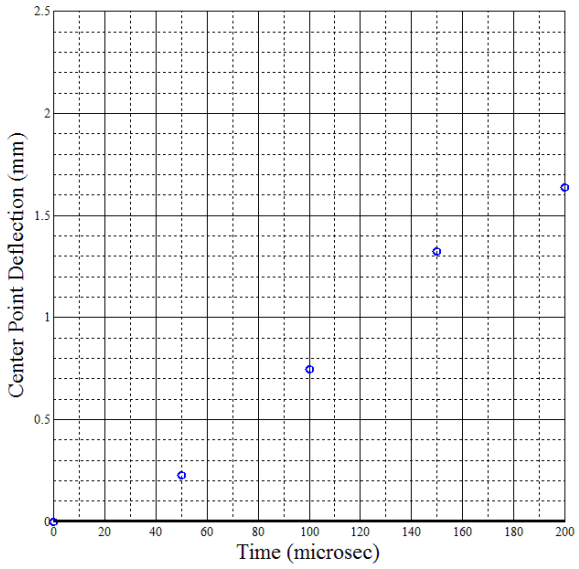

Figure 3.2.7.1-1: Outward center point deflection, WWHT experiment 1

Post mortem damage included some minor matrix cracking around the boundaries, as well as very minor localized delamination in certain areas, and the specimen had noticeable permanent concavity. A representative *post-mortem* specimen is illustrated in Figure 3.2.7.1-2.

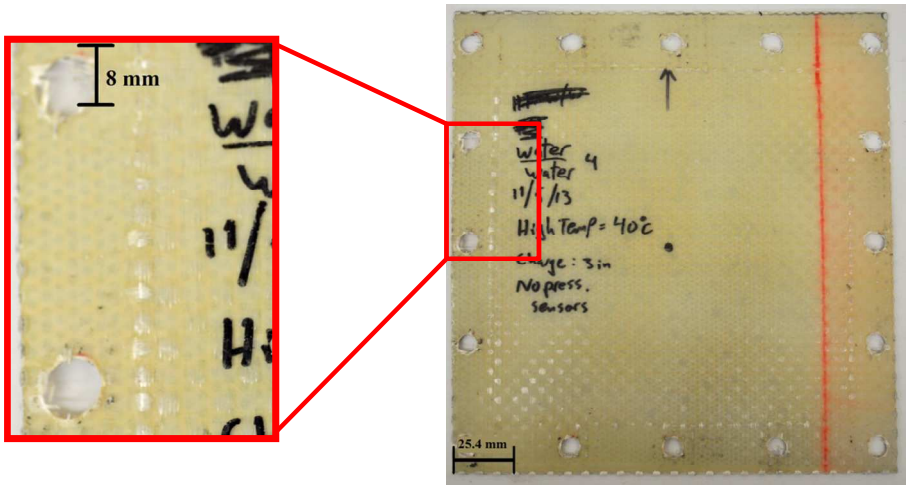

Figure 3.2.7.1-2: *Post mortem* damage typical of the WWHT series.

Key parameters from WWHT experiment 1 are listed in Table 3.2.7.1-2.

Table 3.2.7.1-2: Key results from WWHT experiment 1

Parameter	Value	Elapsed Time
DIC Calibration Error	4.4%	-
200 μsec Panel Deflection	1.63 mm (0.06 in.)	1.25 msec

3.2.6.2 WWHT Experiment 2

WWHT experiment 2 was performed immediately after WWHT experiment 1. Because of this, the DIC camera angles remained 8° for the Master camera and 7° for

the Slave 1 camera. The calibration error also remained constant at 4.4%. The heating process was halted when the average water temperature reached 40.8 °C. Individual qualifying temperatures for each thermometer are given in Table 3.2.7.2-1.

Table 3.2.7.2-1: Qualifying temperatures for WWHT experiment 2

Thermometer	Temperature
1	38 °C
2	42 °C
3	42 °C
4	42 °C
5	40 °C

Results for WWHT experiment 2 are shown in Figures 3.2.7.2-1 and -2. By 200 μsec the panel center point achieved a positive deflection of 1.74 mm (0.07 in.).

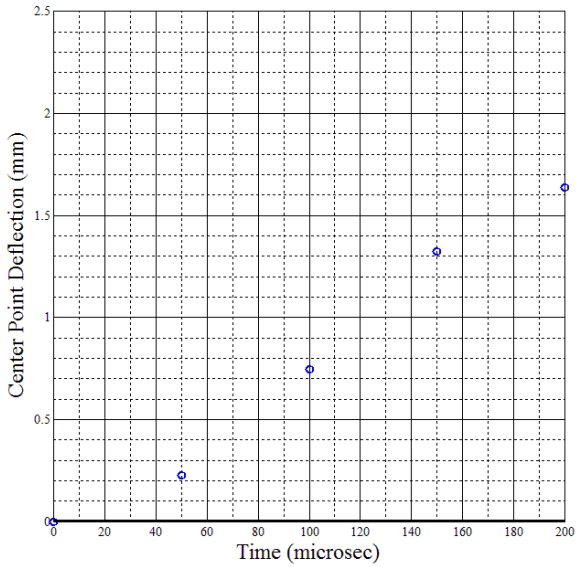

Figure 3.2.7.1-1: Outward center point deflection, WWHT experiment 2

Post mortem damage included some minor delamination, matrix cracking around the boundaries, and the specimen had a noticeable permanent concavity. Key parameters from WWHT experiment 2 are listed in Table 3.2.7.2-2.

Table 3.2.7.2-2: Key results from WWHT experiment 2

Parameter	Value	Elapsed Time
DIC Calibration Error	4.4%	-
200 μsec Panel Deflection	1.74 mm (0.06 in.)	-

CHAPTER 4: Findings

4.0 Discussion of Results

Pursuant to the goals of this study, the foregoing results provided insight to a number of questions. Some of these are discussed here.

4.1 Pressure Data

4.1.1 Air Pressure Decay

Especially owing to the intense noise encountered and the low signals detected, it was of interest to compare the recorded pressure decays in air with established theory. Smith and Hetherington give relations for shockwave pressure (in bar) as a function of standoff distance and explosive equivalent weight of TNT, with the caveat that, due to complex fluid flow processes close to the charge, the accuracy of pressure predictions in the near-field, "is somewhat lower than in the medium to far field" (Smith & Hetherington, 1994). These are expressed by Equations 4.1.1-1 and -2.

$$P_s = \frac{6.194}{Z} + \frac{0.326}{Z^2} + \frac{2.132}{Z^3} \qquad (4.1.1\text{-}1)$$

$$P_s = \frac{0.662}{Z} + \frac{4.05}{Z^2} + \frac{3.288}{Z^3} \qquad (4.1.1\text{-}2)$$

Here, Z is a scaled distance parameter expressed by $Z = \frac{R}{W^{1/3}}$. R is the standoff distance from the explosive in meters and W is the equivalent TNT charge weight in kilograms. Equation 4.1.1-1 may only be applied for $0.3 \leq Z \leq 1$, and Equation 4.1.1-2

may only be applied for $1 \leq Z \leq 10$. For the air blast pencil probe standoff distances of 234 mm (9.2 in.) and 310 mm (12.2 in.) then, the corresponding Z values are 2.3 and 3.1, respectively. Equation 4.1.1-2 was thus used to corroborate the experimental data. These theoretical pressures are given in Table 4.1.1-1.

Table 4.1.1-1: Calculated overpressures using Equation 4.1.1-2 for standoff distances of pencil probe transducers 1 (234 mm) and 2 (310 mm)

Standoff Distance	Pressure
234 mm (9.2 in.)	0.128 MPa (18.56 PSI)
310 mm (12.2 in.)	0.075 MPa (10.88 PSI)

For easy comparison, Table 4.1.1-2 reiterates the overpressure data collected during the AA series.

Table 4.1.1-2: Overpressures of the AA experiment set

Experiment	Pressure
AA 3, Sensor 1 (234 mm, 9.2 in.)	0.11 MPa (16 PSI)
AA 3, Sensor 2 (310 mm, 12.2 in.)	0.06 MPa (8.7 PSI)
AA 4, Sensor 1 (234 mm, 9.2 in.)	0.14 MPa (20.3 PSI)
AA 4, Sensor 2 (310 mm, 12.2 in.)	0.04 MPa (5.8 PSI)

The average overpressures from sensor 1 and sensor 2 are thus seen to have been 0.125 MPa and 0.05 MPa, respectively. From this it can be seen that the pencil probes

captured data that follow the theory to a reasonable degree, considering the propensity for error at such close standoff distances as proposed by Smith and Hetherington.

When calculating the pressure at the specimen distance of 76 mm (3 in.), the scaled distance parameter *Z* was seen to be 0.76. Thus Equation 4.1.1-1 was employed for ascertaining the overpressure at the panel specimen surface. Doing so gave 1.357 MPa (197 PSI).

Another notable pressure effect in the AA series occurred in the center point deflection profiles. It was seen that the maximum positive displacement of each experiment was of lesser magnitude than the maximum negative displacement. This seemingly counterintuitive phenomenon could be explained by the influence of the negative pressure phase as depicted in Figure 4.1.1-1, which details the filtered pressure decay seen in sensor 1 from AA experiments 3 and 4.

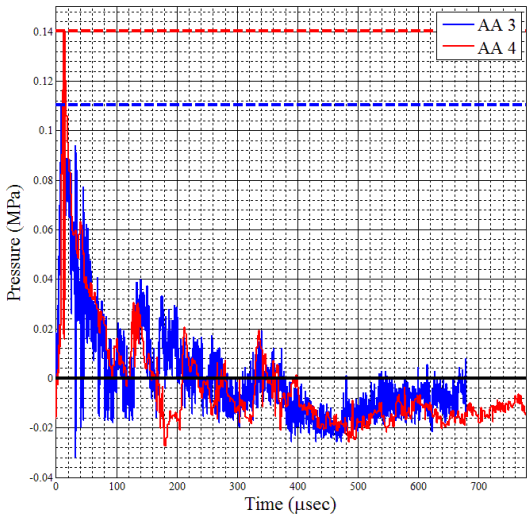

Figure 4.1.1-1: Pressure histories recorded by sensor 1, AA experiments 3 and 4.

In the figure, the onset of the negative pressure phase can be observed at approximately 100 msec. Extraneous wave reflections—perhaps from the bulky structure used to restrain the pencil probes—appear to have influenced the pressure transducer signal between 100 and 350 msec, but it's unlikely that these oscillations would have been experienced to any significant degree at the specimen interface. With this said, it can be reasonably stated that, absent the said reflections, the natural negative pressure phase began at approximately 100 msec and continued for a time duration beyond that which was recorded. This duration demonstrates the extent that the negative pressure "vacuum" could have influenced the panel specimen, as compared to the shorter positive phase. When considered over the whole explosion event, it is possible that the positive impulse applied to the panel by the shockwave was actually smaller than the negative impulse applied to the panel by the vacuum. This would explain why the maximum positive center point panel deflection was smaller than the maximum negative deflection.

4.1.2 Water Pressure Decay

The recorded pressure histories collected in water are illustrated in Figures 4.1.2-1 and -2, overlaid according to sensor.

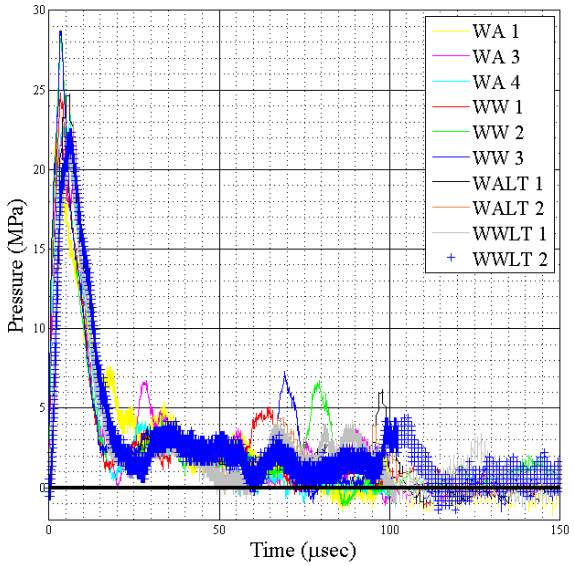

Figure 4.1.2-1: Overlaid pressure histories from tourmaline sensor 1

.

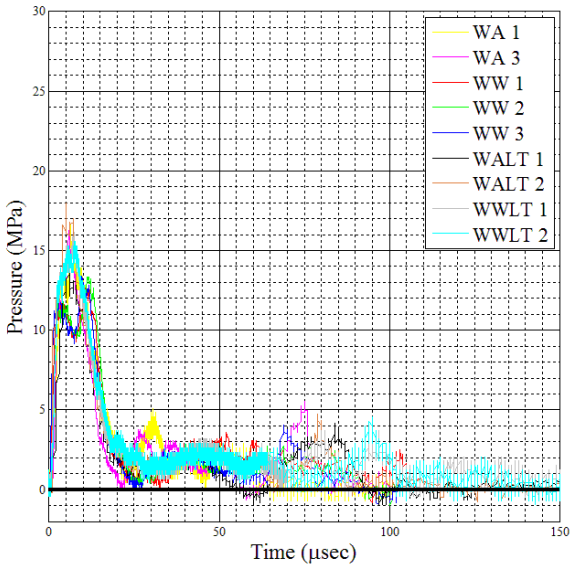

Figure 4.1.2-2: Overlaid pressure histories from tourmaline sensor 2

From these figures it can be seen that the durations of each detected pulse were quite repeatable and each resolved to approximately 0 MPa after about 150 μsec. The

rise behavior was largely consistent from experiment to experiment, except in the case of the WW series. Recalling Figures 3.2.2.1-4, 3.2.2.2-1, and 3.2.2.3-2, sensor 2 detected pulses unique to the WW series, pulses that looked slightly abnormal as compared to the other underwater pressure sets. This behavior may be explained by the sensors having been taped to metal stands, introducing the possibility that outside vibrations affected the signal. This does not, however, explain why this phenomenon occurred so noticeably for only the WW series. It is not clearly known what caused such behavior, but for analytical purposes the higher of the peaks shall be referenced as the peak overpressure for those pulses.

Taking all this into consideration, the peak overpressures for sensors 1 and 2 then are displayed in Table 4.1.2-1.

Table 4.1.2-1: Peak overpressures from UNDEX experiments

Experiment	Sensor 1 (160 mm) Overpressure, MPa	Sensor 2 (226 mm) Overpressure, MPa
WA 1	22.5	16.7
WA 3	22	16
WA 4	23	-
WW 1	24.8	12.8
WW 2	28.3	13.3
WW 3	28.7	13.4
WALT 1	25	14
WALT 2	23	18
WWLT 1	21.7	16
WWLT 2	22.3	15.6

The mean sensor 1 overpressure is then seen to have been 24 MPa, and the mean for sensor 2 is seen to have been 15 MPa. The extrapolated overpressures, based on the MATLAB-generated trend line function of $5429r^{-1.08}$, are listed in Table 4.1.2-2.

Table 4.1.2.2: Overpressures calculated from the MATLAB trend line function

Sensor 1 (160 mm) Overpressure, MPa	Sensor 2 (226 mm) Overpressure, MPa
22.6	15.6

The average experimental overpressures obviously came quite close to those generated by the MATLAB trend line function. Extrapolating the trend line function to the 76 mm (3 in.) standoff distance between the RP-503 explosive and the panel specimen gave 50.5 MPa (7324.4 PSI).

4.2 Environmental Effects

The central issue of this study was to examine particular environmental effects and their influence on the near-field blast response of the EVE composite. A variety of criteria could be selected to gauge the blast response of the panel specimen, but this study chiefly considered one criterion in particular, namely center point deflection. When considered over the whole duration of an UNDEX or air blast event, the panel center point experiences diverse forms of oscillatory behavior, which produce a range of deflections that could potentially be used to measure blast response. Of these, this study defined the maximum positive displacement as most significant and most indicative of resilience to the blast load. The maximum positive displacement was

recognized as being best suited to measure the immediate, direct effects of the shockwave on the panel. This blast response was investigated by varying two environmental characteristics, namely the backing medium and water temperature. Section 4.2 of this document will examine these effects by considering them in turn.

4.2.1 Effects of Backing Medium

Figures 4.2.1-1 through -3 display overlaid center point deflection plots for the WA, WW, and AA experiment sets.

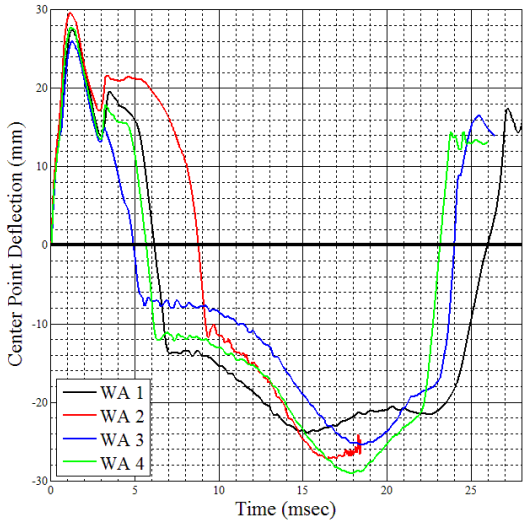

Figure 4.2.1-1: Overlaid center point deflections for the WA series

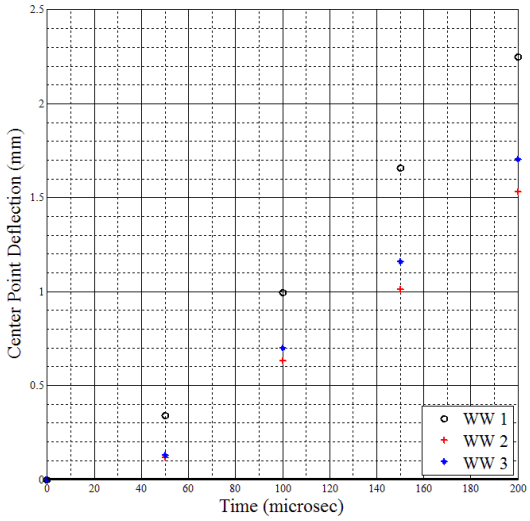

Figure 4.2.1-2: Overlaid center point deflections for the WW series

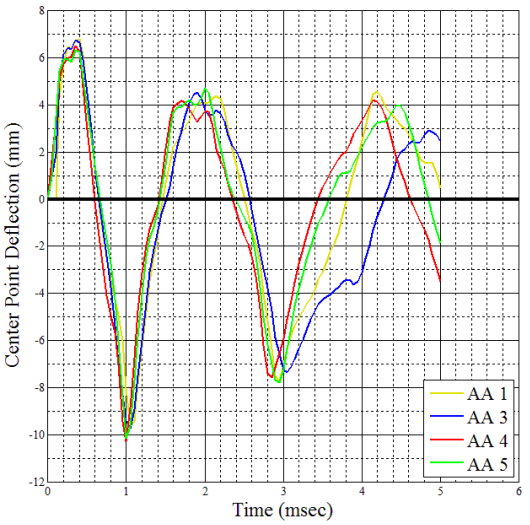

Figure 4.2.1-3: Overlaid center point deflections for the AA series

Inspection of these figures reveals the good repeatability of the data, the relevant results of which are included in Table 4.2.1-1.

Table 4.2.1-1: Recorded maximum positive center point deflections

Experiment	Max. Positive
WA 1	27.5 mm (1.08 in.)
WA 2	29.6 mm (1.17 in.)
WA 3	26 mm (1.02 in.)
WA 4	28 mm (1.1 in.)
WW 1 (200 μsec)	2.25 mm (0.09 in.)
WW 2 (200 μsec)	1.5 mm (0.06 in.)
WW 3 (200 μsec)	1.73 mm (0.07 in.)
AA 1	7 mm (0.27 in.)
AA 3	6.4 mm (0.25 in.)
AA 4	6.5 mm (0.26 in.)
AA 5	6.3 mm (0.25 in.)

These positive maxima were statistically analyzed using the Thompson's τ test, implemented by an original MATLAB file (see Appendix B), to identify and delete outlying data points. Only the 7 mm (0.27 in.) deflection of experiment AA 1 registered as an outlier within its data set, and it was accordingly deleted from further statistical consideration.

Inspection showed quite obviously that the WA environment produced the greatest center point deflection of the three, and even though the WW series could only be plotted up to 200 μsec, plotting the displacements from the WA 1 and AA 1 experiments over the 200 μsec range of WW 1 indicated that the WW series experienced the least deflection, as seen in Figure 4.2.1-4.

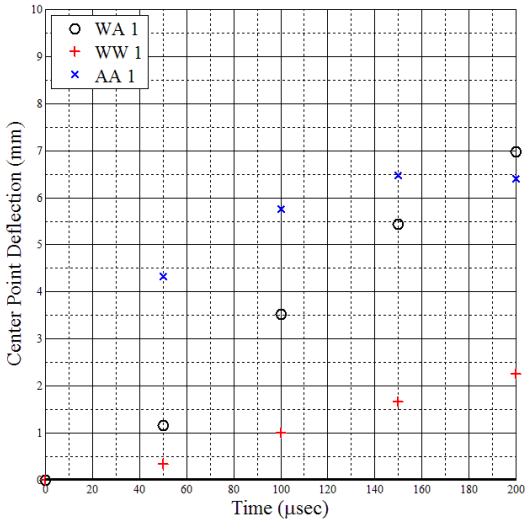

Figure 4.2.1-4: Abbreviated deflection plot of the WA 1, WW 1, and AA 1 experiments, up to 200 µsec.

Notice the anemic progression of the WW 1 displacement as compared to that of the WA 1 and AA 1 experiments. The most aggressive curve in Figure 4.2.1-4 is that of WA 1, which ultimately reaches its positive maximum of 27.5 mm (1.08 in.) by 1.3 msec. Meanwhile, as the WA 1 and WW 1 curves progress through the end of Figure 4.2.1-4, the AA 1 curve has almost reached its maximum positive deflection of 7 mm, which it achieves around 400 µsec. When examined with the *post mortem* damage from each experiment set, it can be reasonably deduced that the most debilitating blast environment was the WA arrangement, followed by the AA and then the WW arrangements.

It is believed that the significant differences in the maximum panel deflections were caused in large part by the differing characteristic acoustic impedances of water, air, and the composite material. Characteristic impedance is a material property that influences wave reflection and transmission between two media. Waves are

transmitted more easily between media with similar impedances than they are between media whose impedances are dissimilar. Equations 4.2.1-1 through -3 describe the relationship between wave amplitude and impedance, expressed as the product between a material's density, ρ, and longitudinal wave speed, c (LeBlanc et al., 2013)(Sadd, 2009)(Gracia, 2012)

$$A_2 = A_1 - A_4 \tag{4.2.1-1}$$

$$A_4 = (A_1 + A_2)\frac{c_{1A}\rho_A}{c_{1B}\rho_B} \tag{4.2.1-2}$$

$$\frac{A_1}{A_2} = \frac{1 + \frac{c_{1A}\rho_A}{c_{1B}\rho_B}}{1 - \frac{c_{1A}\rho_A}{c_{1B}\rho_B}} \tag{4.2.1-3}$$

where A_1, A_2, and A_4 are the amplitudes of the incident, reflected, and transmitted waves, respectively. LeBlanc et al describe a simple scenario to roughly approximate the magnitude of a reflected wave amplitude as a percentage of the incident wave. Given that the properties of the EVE composite in this study are similar to the baseline specimen considered by LeBlanc, those values were used here for a comparable rough approximation in a WA environment to demonstrate the general effects of impedance mismatches on reflected and transmitted wave amplitudes. Approximate values for wave speed and density are provided in Table 4.2.1-2 for air, water, and the EVE composite (LeBlanc et al., 2013).

Table 4.2.1-2: Densities and wave speeds for air, water, and the EVE composite.

	Density (kg/m^3)	Wave Speed (m/sec)
Air	1.204	343.3
Water	1000	1500
EVE Composite	1680	3060

For the approximation it was assumed that a plane dilatational wave made contact with a plane interface between water and the composite panel. Use of Equation 4.2.1-3 indicated that the ratio of the incident to reflected amplitude was 1.82, implying that the reflected amplitude was 55% of the incident amplitude. The transmitted wave, with an amplitude 45% of the incident amplitude, was assumed to propagate through the panel thickness and contact the interface between the panel and the air backing, at which point another reflection would occur, and so on. Table 4.2.1-3 lists rough approximations of reflected wave amplitudes as percentages of the incident wave, to assist in illustrating the effects of impedance mismatches on transmitted and reflected amplitudes.

Table 4.2.1-3: Rough approximations of reflected wave amplitudes

	Water → EVE	EVE → Air	Air → EVE	EVE → Water
Percentage Reflected	55%	~ 100%	~ 100%	55%

When this reasoning is applied to the WW, WA, and AA series, one can see how it is only logical that the WW environment exhibited the least damage and the most docile deflection behavior. In that series the shockwave passed through the most

benign interfaces: those between water and the composite, and between the composite and water. On the other hand, the WA and AA series both presented the most hostile interfaces for wave propagation, which led to higher reflected waves and in turn greater damage. However, between those two environments the AA series posed the more hostile interface. It would remain to be explained, then, how it follows that the maximum AA panel deflection would be considerably smaller than that of the WA series.

This can be explained by considering the impulse imparted to the specimen in those two environments. A pressure wave decays in air at a more drastic rate than it does in water. This can be learned from the literature (Cole, 1948)(Shin, 2004)(Batra & Hassan, 2007)(Smith & Hetherington, 1994)(Ngo et al., 2007), which provides empirical formulations of pressure decay as being functions of $1/r^3$ during air blasts and as high as $1/r^2$ during UNDEX events, and can also be interpreted from the pressure histories included in this document. As discussed previously in Section 4.1, the pressure at the target in an air blast event was roughly 1.357 MPa (197 PSI), a little more than 37 times less than the 50.5 MPa (7324.4 PSI) encountered at the target in an UNDEX event. *Ergo*, although the AA series presented an environment more hostile to wave propagation, the wave had dissipated to such a degree that the impulse applied to the panel specimen was considerably smaller. These results suggest that the wave dissipation effects dominate the impedance mismatch effects when considering explosions in water versus those in air.

4.2.2 Effects of Temperature

Figures 4.2.2-1 through -4 depict the center point deflection histories for the WALT, WWLT, WAHT, and WWHT experiment sets.

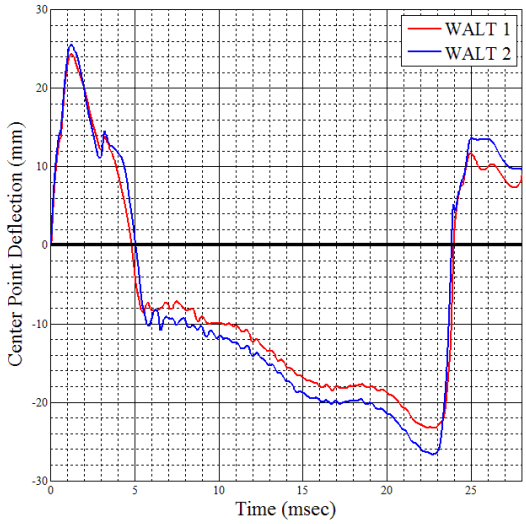

Figure 4.2.2-4: Overlaid center point deflections for the WALT series

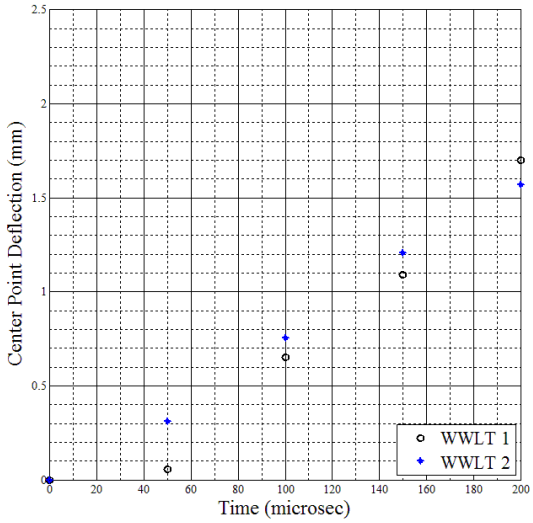

Figure 4.2.2-5: Overlaid center point deflections for the WWLT series

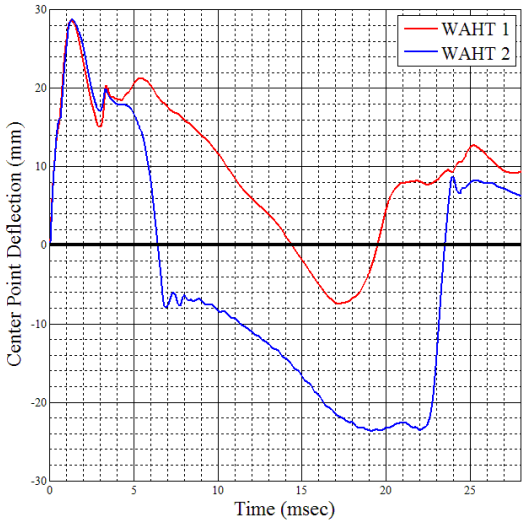

Figure 4.2.2-6: Overlaid center point deflections for the WAHT series

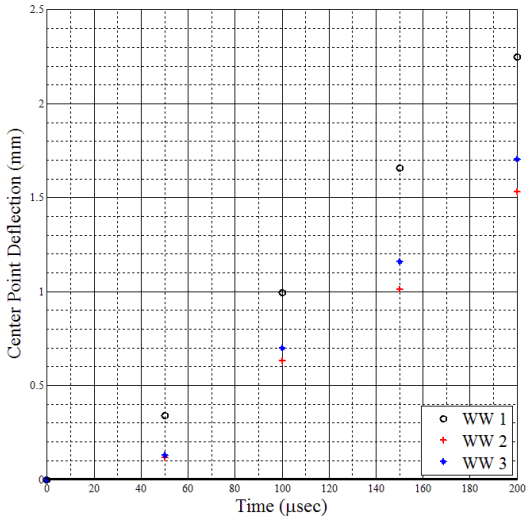

Figure 4.2.2-7: Overlaid center point deflections for the WWHT series

The collected does suggest that temperature influences center point deflection to a degree. Further insight is gleaned by comparing the overlaid average center point deflections of each series, as depicted in Figures 4.2.2-8 and -9.

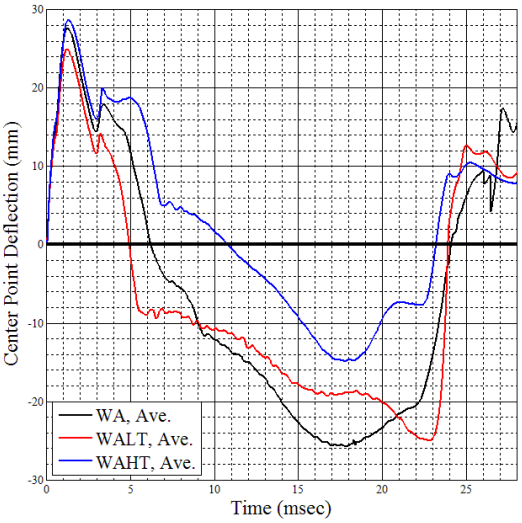

Figure 4.2.2-8: Overlaid average center point deflections for the WA, WALT, and WAHT experiment sets.

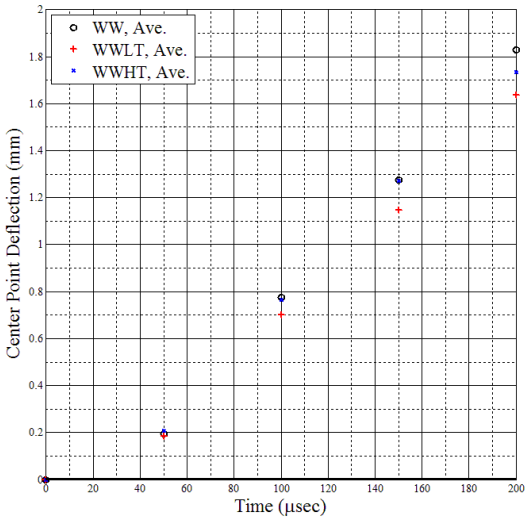

Figure 4.2.2-8: Overlaid average center point deflections for the WW, WWLT, and WWHT experiment sets.

There is insufficient data to examine the full effect of water temperature on the water backed environments (WW, WWLT, WWHT), but it is clear that, within the known 200 μsec range, there appears to be no influence of temperature.

The deflections exhibited by the panels from the air backed experiments (WA, WALT, WAHT) suggest a dependence between water temperature and center point deflection. The average maximum positive deflections from the air backed series are included in Table 4.2.2-1.

Table 4.2.2-1: Average maximum positive center point deflections from the water-backed series (WA, WALT, WAHT)

Experiment	Center Point Deflection
WA	27.8 mm (1.09 in.)
WALT	25 mm (0.98 in.)
WAHT	28.7 mm (1.13 in.)

These points were statistically analyzed using both ANOVA methods and an original MATLAB code at 90% confidence (see Appendix C). Both MATLAB and ANOVA indicated that, while the maximum positive WA and WAHT deflections were statistically the same, the maximum positive WALT deflection was statistically different than both the WA and WAHT deflections. These results are listed in Table 4.2.2-2.

Table 4.2.2-2: Results of statistical analysis

	MATLAB		ANOVA		
Data Comparison	t_o	$t_{\alpha/2}$	P	F	$F_{critical}$
WA/WAHT	0.91	2.13	0.41	0.83	4.54
WA/WALT	2.36	2.13	0.08	5.57	4.54
WAHT/WALT	6.17	2.92	0.03	38.04	8.53

Under the MATLAB scheme, t_o is a distribution parameter defined as

$$t_o = \frac{\overline{y_1} - \overline{y_2}}{S_p\sqrt{\frac{1}{n_1} + \frac{1}{n_2}}} \tag{4.2.2-1}$$

$$S_p^2 = \frac{(n_1 - 1)S_1^2 + (n_2 - 1)S_2^2}{n_1 + n_2 - 2} \tag{4.2.2-2}$$

where $n_{1,2}$ are the sample sizes of the experiments being compared, y is the sample mean, and $S_{1,2}$ are the sample variances. Additionally, $t_{\alpha/2}$ is an element of the t-distribution table, and is based on the sample size and desired confidence interval. Criteria for rejection of the null hypothesis—that any two corresponding experimental values are the same—is that t_o be greater than $t_{\alpha/2}$. Under the ANOVA scheme, P is the probability that variances and differences between two data sets would still exist if the null hypothesis were true. F is a ratio of cross-group variance to within-group variance. $F_{critical}$ is a threshold value of F beyond which two data sets are said to be statistically different.

With these statistical differences and similarities established, quantitative disparities among the data points in Table 4.2.2-1 were more readily appreciated.

Using the room temperature average center point deflection as a baseline for comparison, it can be seen that the average high temperature center point deflection was increased by 3%, while the average low temperature center point deflection was decreased by 10%. Bearing these points in mind, it is seen that, over the temperature range studied, and though the influence does not appear to be extraordinarily great, temperature influence on center point deflection did appear to manifest itself as the water was made colder.

4.3 Effects of Environment on Damage Mechanisms

4.3.1 Effects of Backing Conditions

The backing conditions greatly influenced the damage mechanisms exhibited in the panel specimens. Backing condition effects were evaluated by cross-comparing room temperature *post mortem* damage.

4.3.1.1 WA Post Mortem

Post mortem damage in the WA series occurred predominantly at the clamped boundary and manifested itself chiefly as fiber breakage and delamination. In some cases the fiber breakage propagated through the panel thickness along a seam. Through thickness breakages were not severe, though. Matrix cracking also existed in localized areas across the panel surface. Permanent deflection was observable and the panels had visible concavity.

To be expected, boundary effects apparently encouraged the development of high stress areas along the clamped edge, thus leading to pronounced fiber breakage and

delamination in those areas. The Matrix cracking was likely induced by the contorted vibration modes that the panel experienced during the UNDEX event.

4.3.1.2 WW Post Mortem

The WW series specimens experienced mostly matrix cracking around their boundaries and exhibited only sparse, highly-localized occurrences of delamination at the boundary. Small amounts of matrix cracking were typical of the WW specimens, which occurred towards the panel center. The panels had almost no visible permanent deflection, and virtually no concavity was observed in them.

4.3.1.3 AA Post Mortem

The prevailing damage mechanism in the AA series was impact damage from flying shrapnel produced when the RP-503 capsule exploded. The AA panels exhibited no visible delamination around their boundaries, which instead was pock-marked with impact craters from shrapnel. Some craters were black, indicative of resin singeing after plastic shrapnel became embedded between the specimen mounting bracket and the panel. A burned laceration was marked horizontally along the whole panel surface, across which there was near-continuous fiber breakage, much of which was through-thickness. This cleft appeared as a demarcation line, below which was a dense field of burned pockmarks and impact damage, and above which was a much sparser, unburned field of impact damage. It is believed that the dense impact damage below the demarcation line could be indicative of the explosive shrapnel being

deflected towards one area by the charge geometry or by other components in the blasting cap of the RP-503 charge.

4.3.2 Effects of Temperature on Damage Mechanisms

Damage mechanisms were not observed to have changed significantly as a function of temperature. Damage mechanisms in the high and low temperature specimens were evaluated and compared with room temperature mechanisms.

4.3.2.1 WALT Post Mortem

Although the specimen for WALT experiment 2 tore completely across a long seam on its bottom clamped edge, the prevailing damage mechanisms on both of the WALT panels caused that occurrence to be considered anomalous. The tearing, which occurred as a result of the first bubble pulse, could have been caused more fundamentally by quality variations during manufacturing. There was less-pronounced delamination around the WALT panels' boundaries and only superficial fiber breakage in those areas, apart from the tear in WALT specimen no. 2. Matrix cracking occurred in largely the same manner as it did in the WA series. Permanent concavity was noticeably lower than that of the WA series.

4.3.2.2 WAHT Post Mortem

The WAHT panels exhibited somewhat more delamination around the clamped boundary than was seen in the WALT series, but still less than exhibited in the WA series. As before, matrix cracking appeared in much the same way as it had in the WA

series. The WAHT panels exhibited the most pronounced permanent concavity of all the specimens in this study.

4.3.2.3 WWLT Post Mortem

WWLT panels exhibited very little delamination around the clamped edge, except in the case of WWLT specimen 1, which exhibited quite noticeable delamination along about half of its boundary. Very faint matrix cracking was observed in areas across the panel face, and neither panel exhibited any visible concavity.

4.3.2.4 WWHT Post Mortem

WWHT specimens exhibited more concavity than did the WWLT specimens, and also displayed some matric cracking and sparse delamination around the clamped edge. Otherwise they exhibited no further unique damage mechanisms.

From these results it should be noted that water temperature appeared only to significantly influence the permanent concavity of the panels.

4.4 WA Correlation with the Gas Bubble

The air backed deflections followed a pattern indicative of heavy dependence on the progress of the gas bubble. Given the repeatability of the experiments, and given the similar displacement trends for each of the water temperatures, WA experiment 3 will suffice as a representative case for discussion. In WA experiment 3, the maximum expansion of the bubble between approximately 11 and 14 msec coincided with the initiation of the panel's final inward flex to its global negative maximum; the center

point's steep outward rebound at ~23 msec initiated at approximately the same time as the bubble's final collapse at ~22.15 msec. These observations are depicted in Figure 4.4-1.

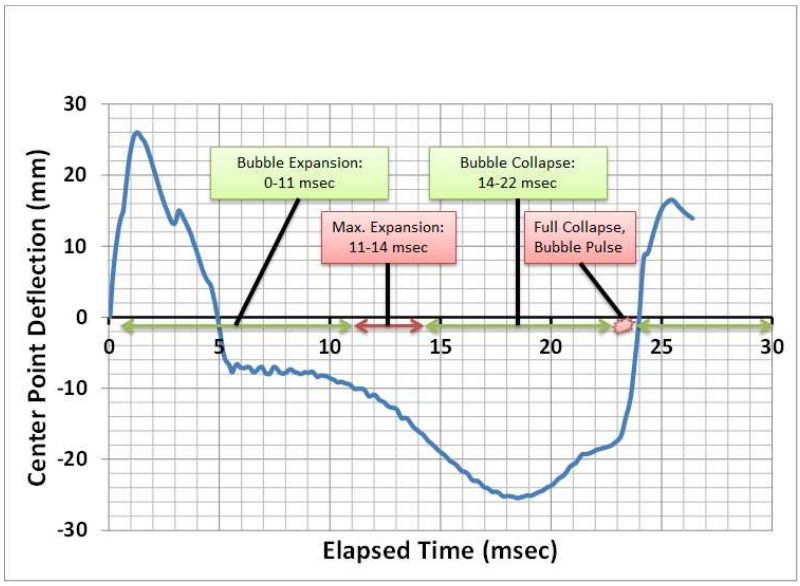

Figure 4.4-1: Detail of the relationship between bubble expansion/contraction and panel center point deflection, as exhibited by WA experiment 3.

The figure shows a notable phenomenon in the panel deflection activity around 5 msec. In the preceding approximate 3 msec, it can be seen that the center point fell steeply away from its maximum outward displacement and tended precipitously towards the epicenter of the explosion. Very shortly after 5 msec the panel displacement flat-lined, remaining at a near-constant negative deflection of -8.5 to -9 mm until approximately 10 msec, at which point the panel gradually initiated its final retraction to the maximum negative displacement. This peculiar movement would seem counterintuitive given that the gas bubble, still expanding from 0–11 msec, presumably would interact in such a way as to cause reversal—instead of a

sustainment—of the panel's direction at ~5.5 msec. This behavior could be explained by considering a different account of the bubble's influence on panel movement, as follows:

1. Initial contact between the shockwave and the panel forced the panel to its maximum positive center point deflection.
2. The elastic response of the E-glass fiber reinforcement reversed the panel motion after the maximum positive deflection was achieved, initiating the panel's steep negative velocity towards the epicenter of the explosion.
3. By approximately 5 msec elapsed time, the panel encountered a barrier of water (Figure 4.4-2) separating it from the explosive gas bubble, which at that moment was in the throes of expansion.
4. As a result of the bubble's expansion, inertial effects on the surrounding water barrier damped the panel's deflection like a fluid "pillow"—arresting its movement, dissipating some of its kinetic energy, and compressing it.
5. The panel's movement was arrested until the bubble radius increased to such an extent that the inertial effects on the surrounding water were reduced due to the gradual slowing of the bubble growth and its reversal to collapsing motion.
6. As the bubble's internal pressure dropped to, and fell below, ambient conditions, its reversal into collapse began dragging the surrounding water in the collapse direction. This not only created a suction current towards

the bubble's center, but also relieved the compressive force the water barrier and the panel.

7. The bubble subsequently initiated its collapse period from 14–23 msec.
8. This change in fluid dynamics permitted the gradual ebb in panel deflection towards its negative maximum, observable from approximately 10–18.5 msec. After achieving its negative maximum at ~18.5 msec, the elastic response of the E-glass fiber reinforcement again reversed the panel motion away from the bubble center.
9. This reversal of panel motion, due to the concurrent bubble collapse and its associated flow dynamics towards the bubble center, developed only modestly and the panel's velocity slowed until a point just before 23 msec.
10. At approximately 23 msec, the bubble achieved full collapse and emitted its first bubble pulse. The pulse interfaced with the panel very shortly afterward, forcing the panel's final outward displacement ~25 msec.

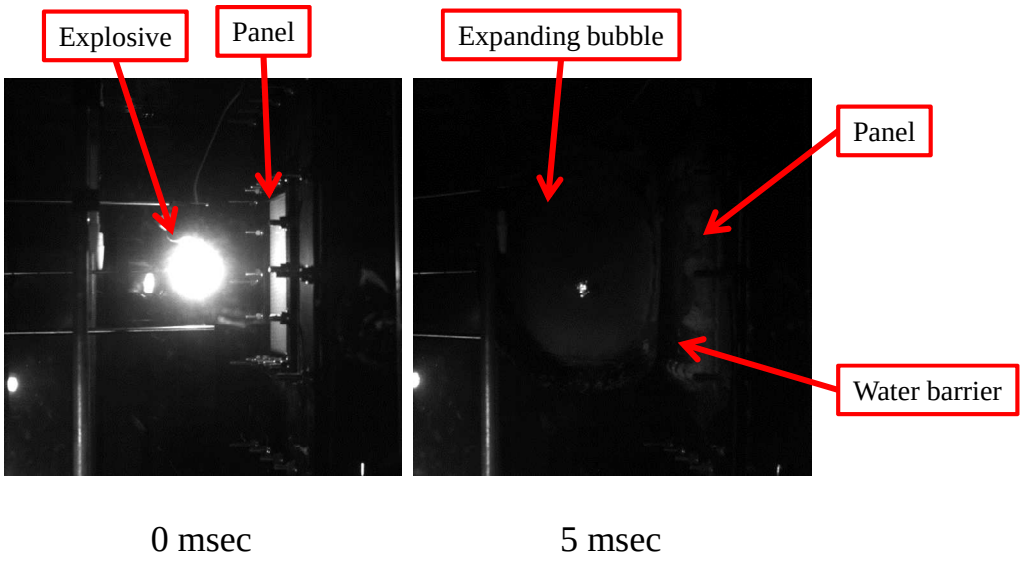

Figure 4.4-2: Side view images of the explosion area at 0 and 5 msec. At 0 msec, the explosion is seen, illuminating the panel specimen. At 5 mesc, the water barrier may be observed between the panel specimen and the expanding bubble.

CHAPTER 5: Conclusion

5.0 Conclusions

Based on the forgoing results and analyses, it was concluded that immersion environment contributes significantly to the blast response of the EVE marine composite, including the exhibited damage mechanisms, damage severity, and center point deflection. The WA, WALT, and WAHT series exhibited the greatest center point deflections and most severe damage mechanisms, including abundant instances of fiber breakage and sometimes considerable delamination. After the WA, WALT, and WAHT experiments, the AA series experienced the highest center point deflection, and exhibited significant evidence of impact damage from flying pieces of the explosive capsule after detonation. Although there was not sufficient DIC data available to draw comparable conclusions about its exact center point deflections, available information, including *post mortem* damage and early event DIC data, suggested that the WW, WWLT, and WWHT series experienced the least center point deflections and most benign damage mechanisms. The disparity in blast response was attributed to differences in characteristic impedance between the panel material and the immersion environment, but that, although the AA series experienced the most hostile environment from an acoustics standpoint, the water/air backed series (WA, WALT, WAHT) ultimately experienced the greatest environmental punishment due to water's ability to sustain pressure wave intensity.

Experimental results indicated that water temperature influenced panel blast response over the range of temperatures from 0 °C to 40 °C, based on available DIC

data for the WA, WALT, and WAHT series. WAHT experiments displayed only 3% greater average maximum center point deflection than the room temperature WA series. In contrast, WALT experiments displayed average maximum center point deflections that not only were 10% smaller than those exhibited by the WA series, but also were proven to be statistically different than the corresponding deflections from the WAHT and WA series by two independent statistical analyses. *Post mortem* results for those specimens indicated no appreciable temperature influence on damage mechanisms, apart from permanent concavity. The available DIC data for the WW, WWLT, and WWHT series suggested no difference in center point deflection across temperatures; but since the available DIC data pertained to only the first 200 μsec of the blast event on account of dense cavitation, it's unclear what can be conclusively inferred from it. Minor variations in *post mortem* damage were insufficient by themselves to imply temperature dependent damage mechanisms.

5.1 Recommendations for Future Work

Having stated the conclusions of this study, there also are some ways that the research may be advanced in future work. Some of these are as follows:

1. Correlations may be drawn between the applied overpressure and the maximum positive panel center point displacement. These correlations may be developed by conducting similar experiments to those of this study, while varying the explosive standoff distance.

2. Greater insight regarding the temperature dependence of center point deflection and damage mechanisms may be gleaned by the following:
    a. Increasing the range of water temperatures, especially to investigate why the high- and room-temperature maximum center point deflections were statistically the same, whereas the low- and room-temperature deflections were statistically different.
    b. Drastically raising the temperature of the panel specimen above that of the environment, to simulate blast effects on a structure heated by prolonged exposure to direct sunlight.
3. Experiments may be conducted in an environment characterized by air immersion with water backing, to simulate the blast effects of a detonation beside the interior bulkhead of a ship or submerged structure.

APPENDIX A

EVE Composite Panel Manufacturing Report

Date of manufacture: August 22-24, 2012

Business trips to TPI Composites in Warren, R.I. were taken on August 22, 23, and 24 (Wednesday, Thursday, Friday), 2012.

Wednesday, August 22, 2012:

Departed URI at 7:30 A.M. Arrived at TPI Composites around 8:30 A.M. Work of the day consisted of the following:

1. All work was performed while wearing safety glasses.

2. Preparation work was undertaken on a large glass table.
    a. The table surface was scraped using razor blades clamped in vice-grip clamp pliers. From previous use in the past, the table was damaged in several places, which were subsequently avoided.
    b. After scraping, the table was polished using TR Mold Release wax, specially designed for high temperatures. After the wax was applied, the polished areas were buffed using rags (old undershirts). Nitrile gloves were worn during the application and buffing of wax.

3. A large spool of plain woven glass fiber sheet, areal density of 0.61 kg/m^2 (18 oz/yd^2), oriented at 0°/90°, was moved to a separate drafting table. A 36” x 36” area on the sheet was measured and prepared for cutting.
    a. The perimeter of the 36” x 36” area was identified using measuring tape.
    b. Conveniently, two of the perimeter faces were actually the perpendicular side edges of the glass fiber sheet.

c. Along the other two perimeter faces, in turn, a single weave of the glass sheet was removed using scissors. The absence of this weave from the sheet provided a clear line along which to cut with scissors.

d. This process was repeated for another 36” x 36” sheet, thus making two plies of 0°/90° oriented glass fabric.

4. The two sheets were laid on top of each other on the glass table.

5. A fine mesh fabric, called Peel Ply, was measured, cut, and laid on top of the glass sheets. The Peel Ply was measured so as to cover more than the glass sheets by about 4”.

6. A thick double-sided tape, called Tacky Tape, was laid around the perimeter of the Peel Ply, standing off about 2 inches from the Peel Ply.

7. Half of the Peel Ply was carefully folded up and off of the glass sheets, whereafter 3M Super 77 spray-on adhesive was applied to the folded half of the Peel Ply, to the glass sheets, and to the glass table. The Peel Ply was then re-laid on top of the glass sheets and was smoothed over, thus neatly adhering the components together. This process was repeated for the other side.

8. A coarse mesh material, called Flow Media, was measured, cut, and laid on top of the Peel Ply.

a. Two parallel, opposite edges of the flow media were measured to be 2” shorter than the edges of the glass fiber sheets; the remaining two edges of the flow media were measured to be 1” shorter than the glass fiber sheets (Figure A.1-1).

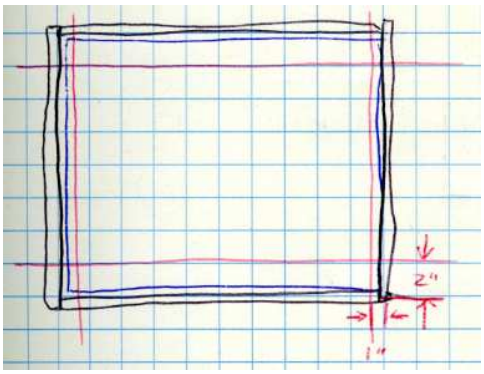

Figure A.1-1: Top view detail of flow media trimming. Red lines indicate 2” and 1” offsets (Image courtesy of Payam Fahr)

b. The flow media’s mesh was oriented such that the diamonds’ lengthwise direction was facing to the right in Figure A.1-1. This was done to encourage the flow of resin across the whole of the glass sheets.
c. The flow media was adhered to the peel ply in a similar manner as described in bullet 7.

9. Scrap material (glass fabric), approximately 7” wide, was adhered to the edges of the Peel Ply for which the flow media stood off 2” (top and bottom edges of Figure A.1-1). Rope of approximately 0.5” diameter was laid in the middle of the scrap material, running lengthwise. The scrap material was folded over the rope so as to envelop it, and was

adhered in place using the 3M spray adhesive. On both edges, a small end portion of the scrap material was not adhered so as to allow the connection of vacuum tubes later on.

10. A spring coil, enveloped within a flow media sleeve, was laid across the middle of the flow media sheet described in bullet 8 (tacky tape was applied to potential sharp edges of the spring coil to prevent the puncturing of the vacuum bag, applied later on). The flow media sleeve, enveloping the spring coil, was taped in place with small periodic applications of Tacky Tape.

11. Vacuum tubes were inserted over the rope contained within the scrap material, as depicted in Figure A.1-2.

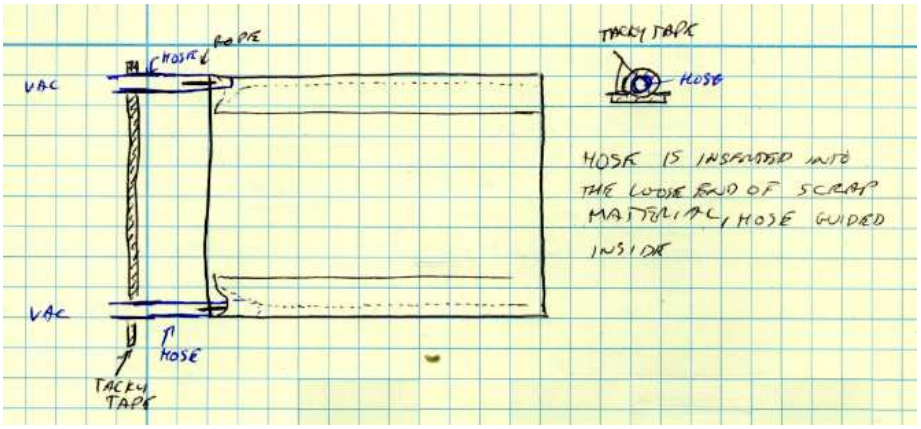

Figure A.1-2: Top view detail of vacuum tubes being inserted over the ropes laid within the scrap material (Image courtesy of Payam Fahr).

The vacuum tubes were laid over the Tacky Tape surrounding the glass sheet/Peel Ply setup. A resin feed tube was also inserted into the spring coil described in bullet 10.

12. A plastic sheet was measured and cut to serve as the vacuum tube for the panel manufacture. The vacuum bag was measured to fit comfortably over the Tacky Tape perimeter, with comfortable excess.

13. The Tacky Tape adhesive backing was gradually removed, and the vacuum bag was in turn pressed against the tape, leaving pleads (bunny ears) in strategic places to ensure an air-tight fit with Tacky Tape later on. This process is depicted in Appendix A.1.

Similar considerations were made for Nate Gardner's composite panels.

Departed TPI Composites at 2:30 P.M. and returned to URI at 3:30 P.M.

Thursday, August 23, 2012:

Departed URI at 7:30 A.M. Arrived at TPI Composites around 8:30 A.M. Work of the day consisted of the following:

1. A pressure drop test was performed so as to ensure an air-tight seal.
    a. The vacuum tubes were connected to a vacuum chamber, and the resin feed tube was clamped shut using a vice grip clamp.
    b. The vacuum chamber was connected to the company's low pressure air mains. The vacuum valve was switched into the flow position.
    c. Low pressure was induced at 15 inHg. Any audible leaks were closed by pressing the vacuum bag harder into the Tacky Tape.

d. After audible leaks were closed the low pressure was switched to 30 inHg. Once the vacuum pressure reached a steady state, the peak pressure was recorded and the vacuum chamber valve was closed. After 2 minutes the pressure was recorded again.
e. Final pressure must be above 27 inHg to qualify for a good enough seal.

2. The vacuum was left running while the resin was mixed.
    a. The weight of the glass fiber sheets was determined from its area and areal density. The sheets were both 36" x 36", or 1 yd^2. By the areal density described in bullet 3 of the August 22 notes (18 oz/yd^2), the total weight of the two glass panels was 18 oz + 18 oz = 36 oz. Simple conversion yielded 2.25 lb.
    b. The amount of resin used was approximately 5 lb.
    c. The type of resin used was Ashland Derakane 8084 Vinyl Ester resin.
    d. Additives to the resin were mixed according to weight ratios: 15% cobalt, 1.8% MEKP 925 (Methyl Ethyl Keytone Peroxide). The MEKP level had to be below 2%.

3. The resin feed tube was inserted into the resin bucket, the vacuum pressure was turned on, and the feed tube was unclamped.

4. The 36" x 36" panels infused properly and without error.

5. Nate Gardner's panel infused improperly and had to be completely reconstructed and infused that afternoon.

Departed TPI Composites at 3:00 P.M. and returned to URI at 4:00 P.M.

Friday, August 24, 2012:

Departed URI at 7:30 A.M. Arrived at TPI Composites around 9:00 A.M., due to traffic. Work of the day consisted of the following:

1. Composite specimens were cut using a 1/8”-thick diamond-edged saw. The 36” x 36” composite panel was cut into sixteen 8” x 8” specimens. Extra material was also collected for possible use in sundry analysis later on.

2. Similar actions were performed for Nate Gardner’s panels.

Departed TPI Composites at 10:30 A.M. and returned to URI at 11:30 A.M.

APPENDIX A.1

Notes Collected by Payam Fahr on 8/22 and 8/23

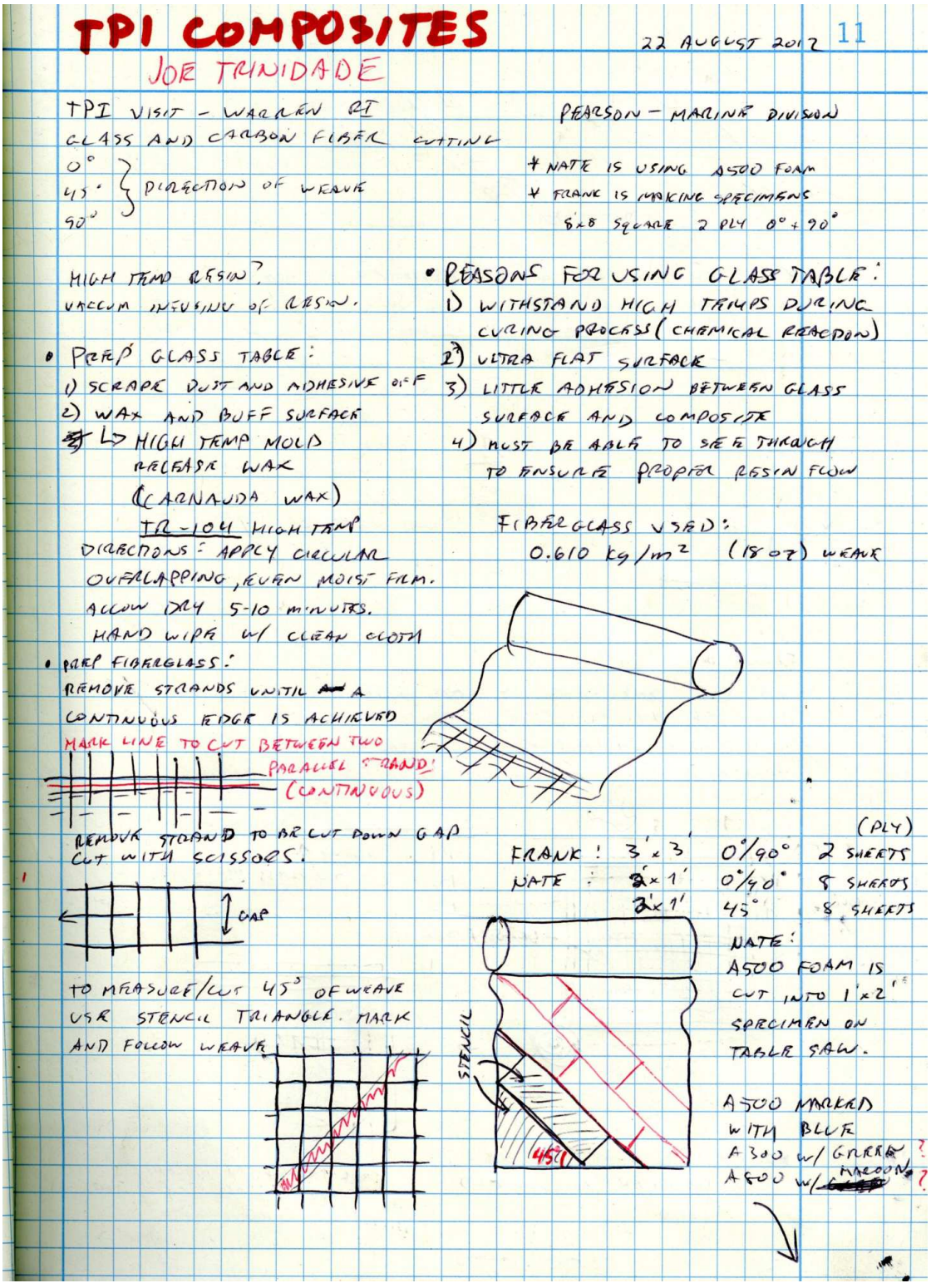

Figure A.1.1-1: Page 1 of the notes from the TPI Composites Trip, courtesy of Mr. Payam Fahr.

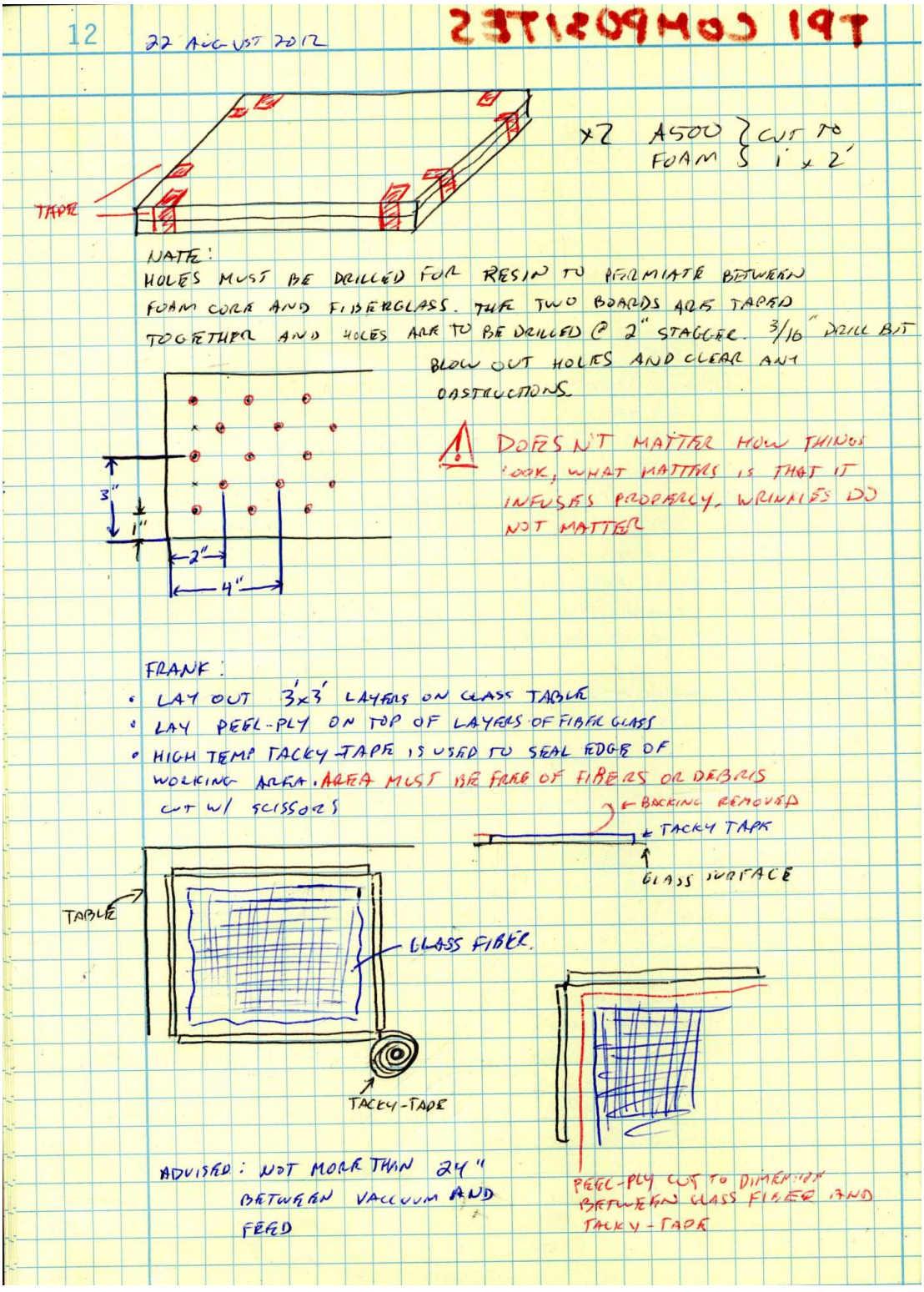

Figure A.1.1-2: Page 2 of the notes from the TPI Composites Trip, courtesy of Mr. Payam Fahr.

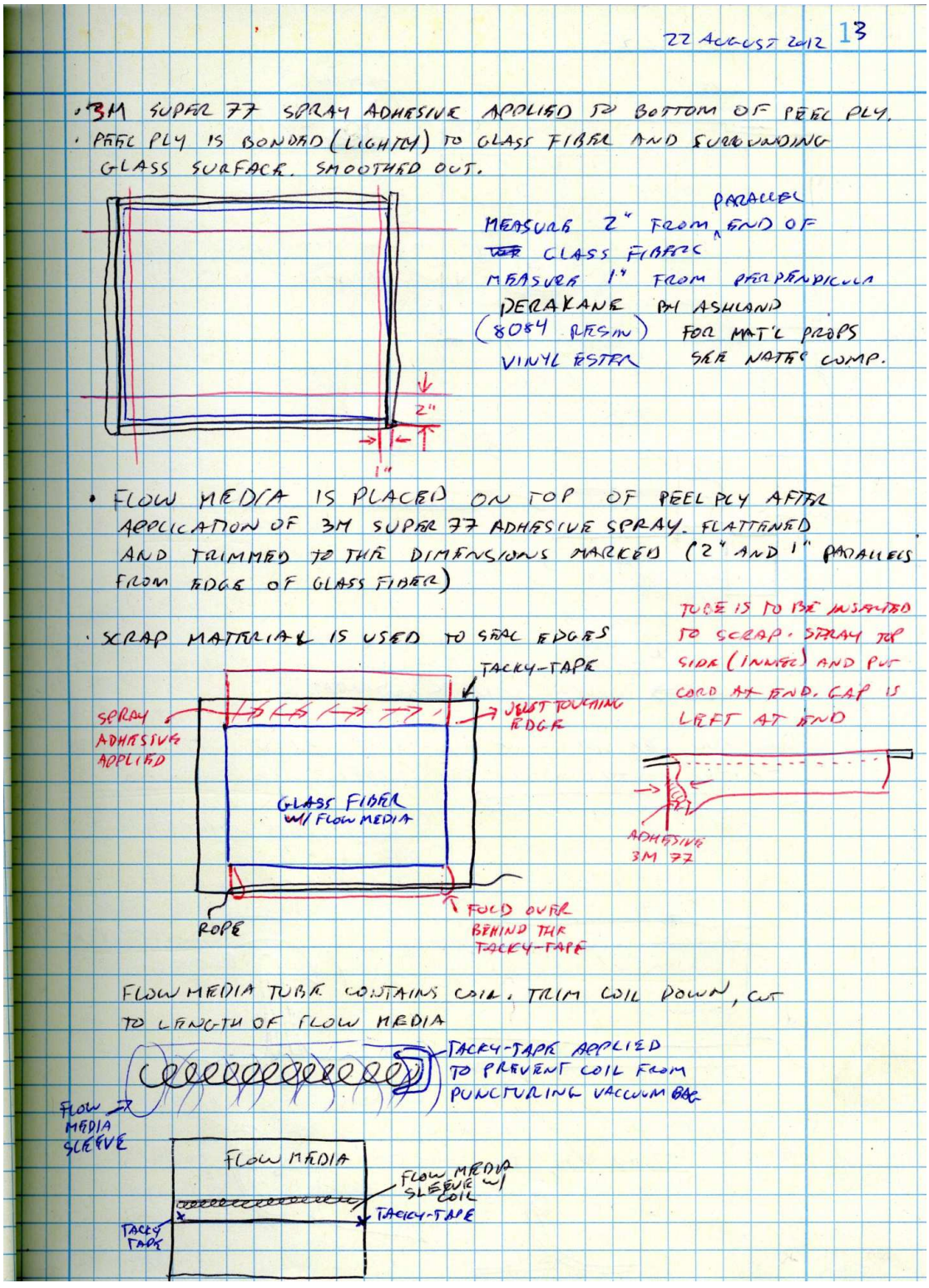

Figure A.1.1-3: Page 3 of the notes from the TPI Composites Trip, courtesy of Mr. Payam Fahr.

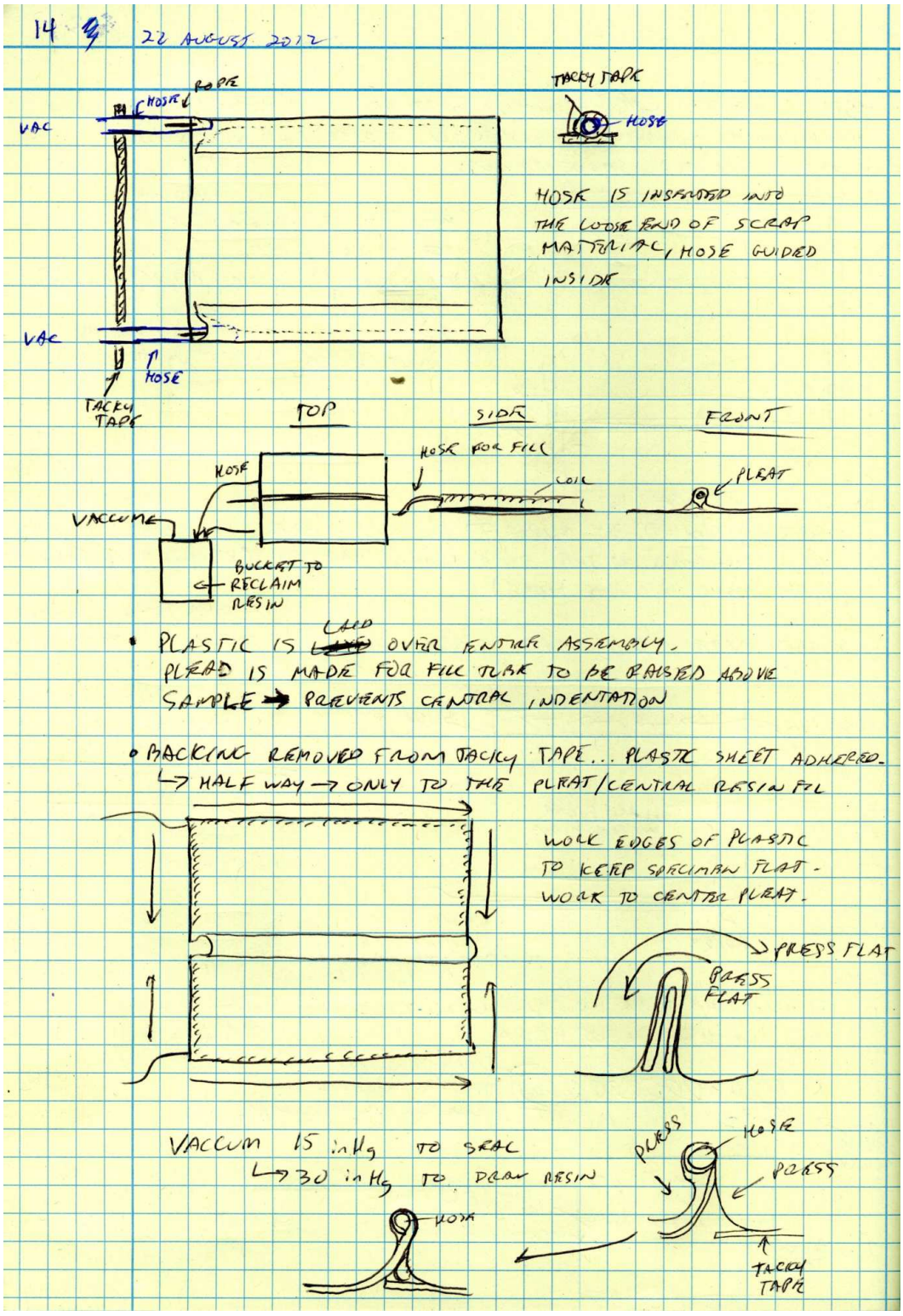

Figure A.1.1-4: Page 4 of the notes from the TPI Composites Trip, courtesy of Mr. Payam Fahr.

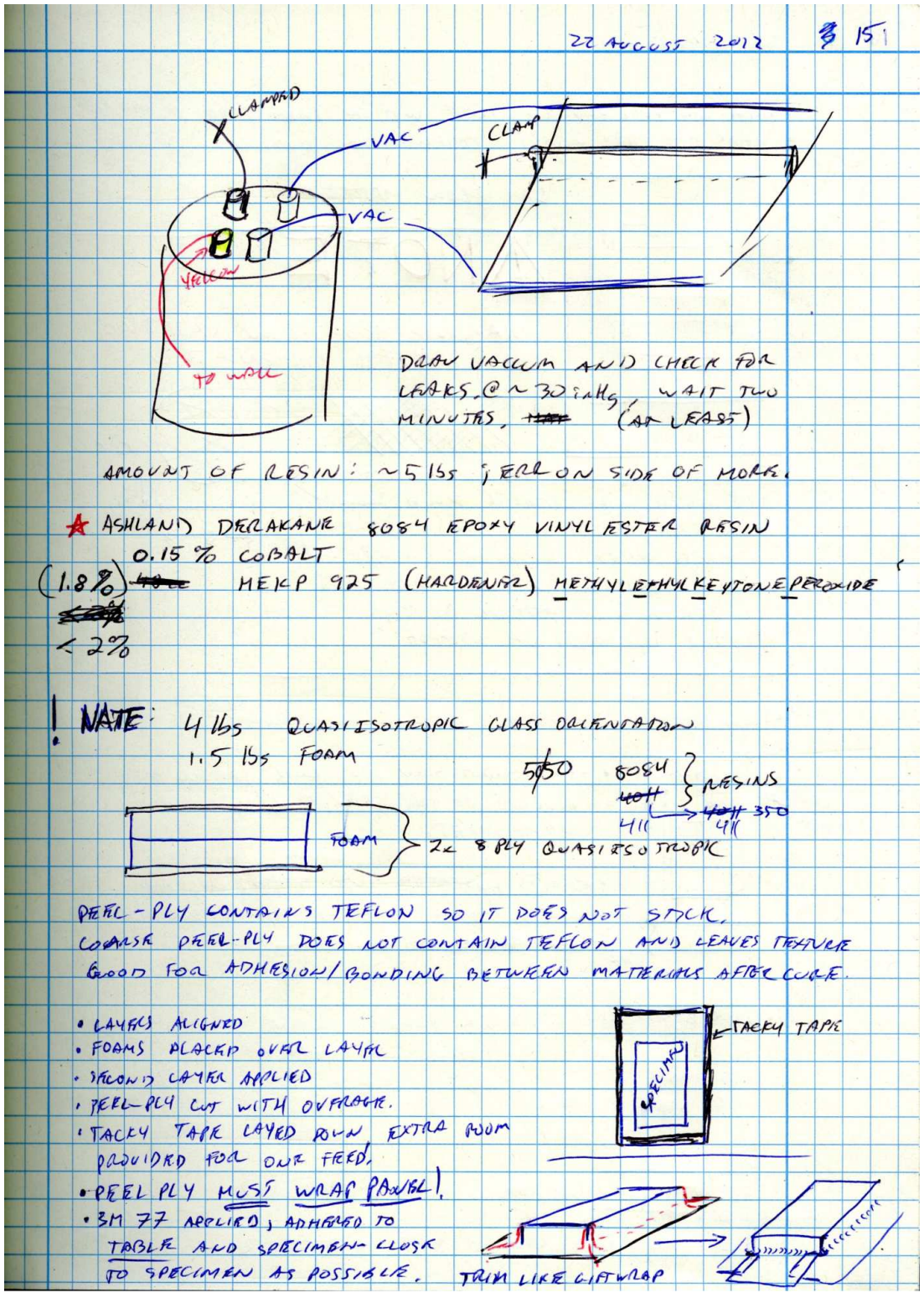

Figure A.1.1-5: Page 5 of the notes from the TPI Composites Trip, courtesy of Mr. Payam Fahr.

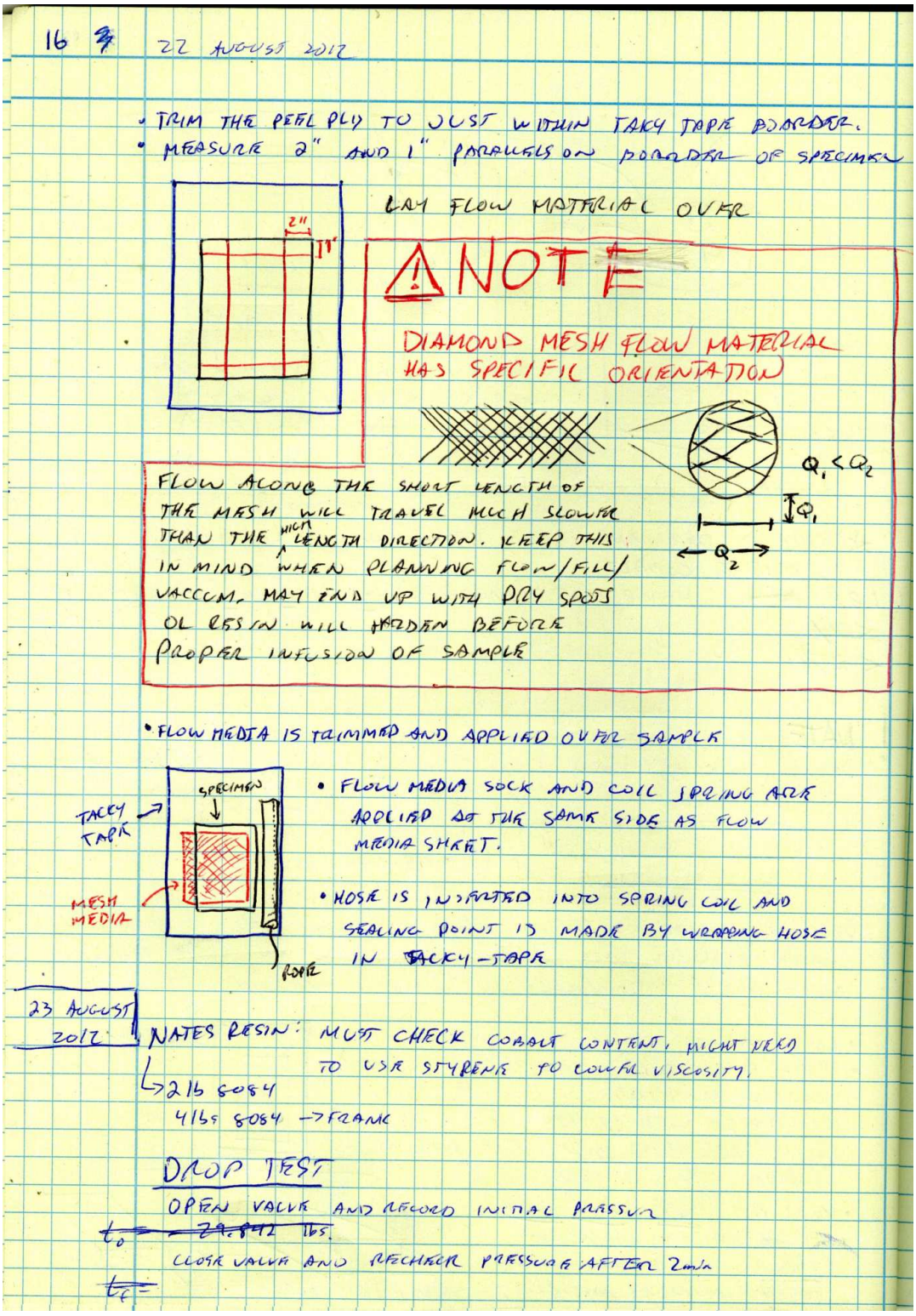

Figure A.1.1-6: Page 6 of the notes from the TPI Composites Trip, courtesy of Mr. Payam Fahr.

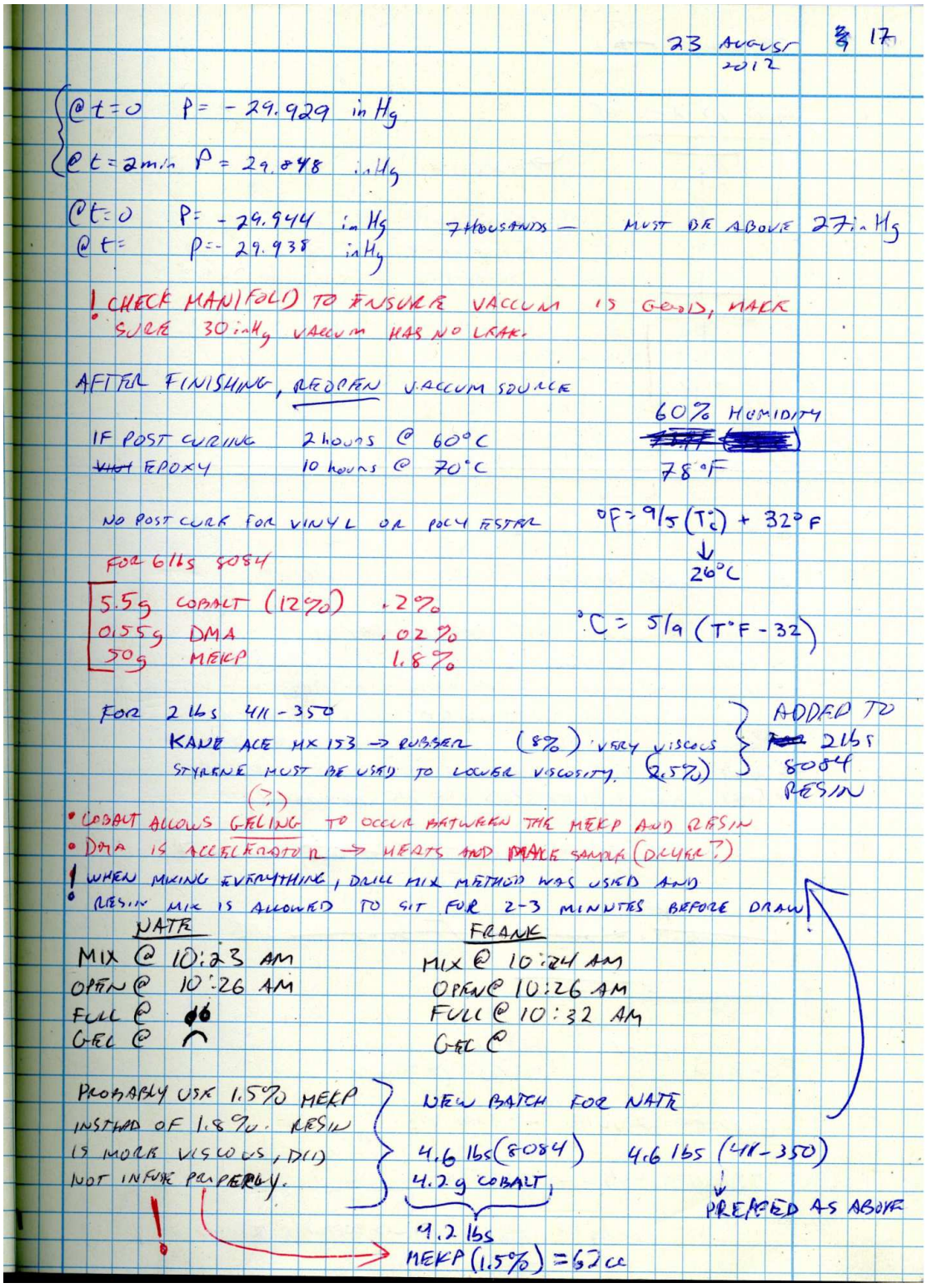

Figure A.1.1-7: Page 7 of the notes from the TPI Composites Trip, courtesy of Mr. Payam Fahr.

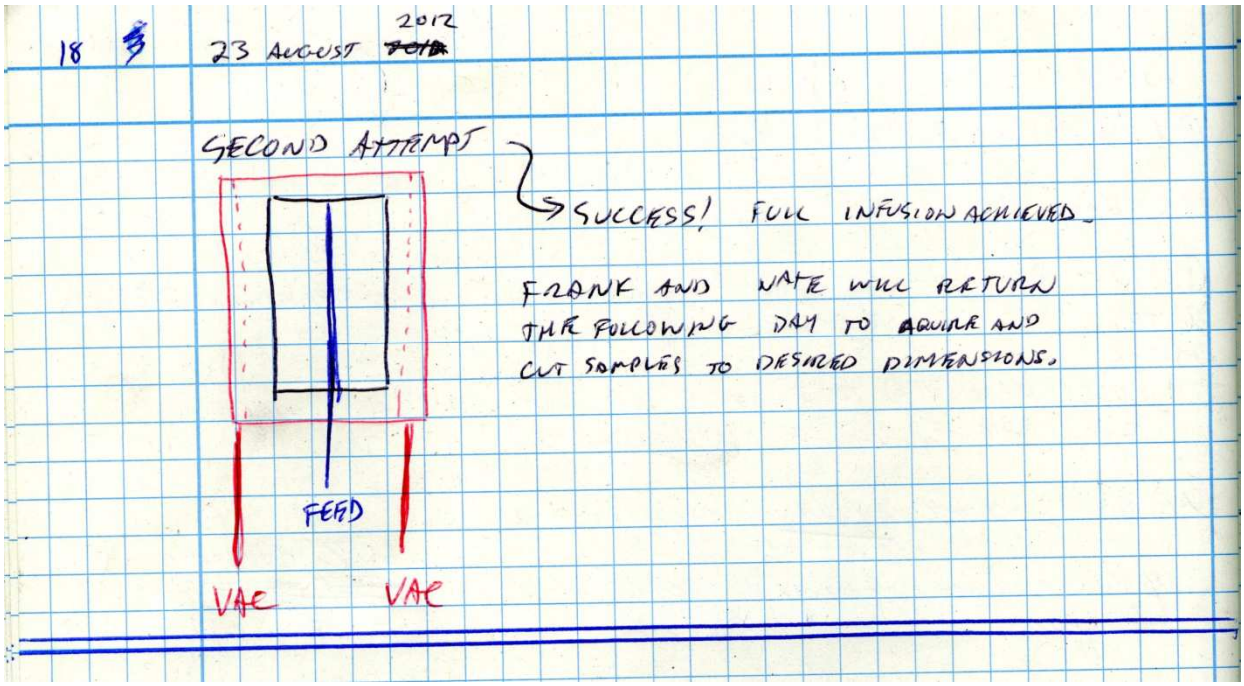

Figure A.1.1-8: Page 8 of the notes from the TPI Composites Trip, courtesy of Mr. Payam Fahr.

APPENDIX B

MATLAB Outlying Data Points Filter

```
%Outlying data points filter
%Response of Marine Composites Subjected to Near-Field Blast Loading
%Frank LiVolsi

clear all
clc
format short

SAMPLE=input('please enter the vector of data points: ');
SAMPLE1=SAMPLE; %SAMPLE1 is an array into which the data points are
dumped, and from which the outlying data points will be deleted later
on.

n=length(SAMPLE); %n is the number of data points in the sample.
THOMPSON=[0 0 1.150 1.393 1.572 1.656 1.711 1.749 1.777 1.798 1.815
1.829 1.840 1.849 1.858 1.865 1.871 1.876 1.881 1.885 1.889 1.893
1.896 1.899 1.902 1.904 1.906 1.908 1.910 1.911 1.913 1.914 1.916
1.917 1.919 1.920 1.921 1.922 1.923 1.924];
%THOMPSON is a vector of tau values for sample sizes ranging from 3-
40. For samples sizes of 1 and 2, tau is assumed to be zero.

%Part A: Use Thompson's "tau" technique to determine if there are any
%outliers; if there are, reject them.

Mean=mean(SAMPLE);
StandDev=std(SAMPLE);

j=1; %j is a "while" loop index that's used to terminate the loop as
soon as values no longer need to be deleted from the sample.
i=1; %i is the index for the array "DELETE"; it's used to create a
vector of the values that are deleted from the sample.
DELETE=[]; %DELETE is the vector of deleted data points from SAMPLE1
(see code below).

while j<2; %This loop will continue until all outlying data points
are deleted, after which time j will be increased to 2 and the loop
will break.

    n=length(SAMPLE1); %Redefine n to be the number of data points in
the ammended vector SAMPLE1.
    StandDev=std(SAMPLE1); %Redefine the standard deviation based on
the updated SAMPLE1
    Mean=mean(SAMPLE1); %Redefine the mean of the updated SAMPLE1

    Max=max(SAMPLE1); %Since maxima and minima are the first
candidates for elimination, identify the maximum in SAMPLE1.
    Min=min(SAMPLE1); %Since maxima and minima are the first
candidates for elimination, identify the minimum in SAMPLE1.

    Delt1=abs(Max-Mean); %Determine the absolute difference between
the maximum in SAMPLE1 and the mean of SAMPLE1
    Delt2=abs(Min-Mean); %Determine the absolute difference between
the minimum in SAMPLE1 and the mean of SAMPLE1
```

```
    DELT=[Delt1 Delt2]; %Put the two resulting differences into a
vector, for comparing against each other.
    Larger=max(DELT); %Assign the variable "Larger" to be the larger
value of the above two differences.

    Thomp=THOMPSON(n)*StandDev; %Evaluate the product between the
Thompson "tau" value (that corresponds to the sample size) and the
standard deviation.


    if Thomp < Larger; %If the product is smaller than the larger
difference value, then the data point corresponding to that
difference is an outlier and needs to be deleted.

        SAMPLE2=SAMPLE1; %SAMPLE2 is an arbitrary duplicate of
SAMPLE1, and is referenced later on by the DELETE vector after
SAMPLE1 has been ammended. SAMPLE2 serves only to allow DELETE to
reference data points from SAMPLE1 that have already been eliminated.

        Plus=(round((Mean+Larger)*1.0e36))/1.0e36;
        index=find(SAMPLE1==(Plus)); %To identify which outlying data
point corresponds to the larger difference, first add the difference
to the mean and search SAMPLE1 for any matches.
        SAMPLE1(index)=[]; %If a match is found, it is deleted.

        if length(SAMPLE1)==length(SAMPLE2); %If no data point from
SAMPLE1 was identified for deletion, then enter a sub-if-statement to
look elsewhere+

            Minus=(round((Mean-Larger)*1.0e36))/1.0e36;
            index=find(SAMPLE1==(Minus)); %If no match was found
above, subtract the difference from the mean and search SAMPLE1 for
any matches, and place any match in a variable "f."
            SAMPLE1(index)=[]; %If a match is found, it is deleted.

        end

        DELETE(i)=SAMPLE2(index(1,1)); %DELETE is the vector of
deleted data points from SAMPLE1.

        n=n-1; %Redefine n, for future calculation of tau.
        i=i+1;

    else
        j=2; %If no other outlying data points are found, j is
increased to 2 and the while loop is broken.
    end
end

fprintf('An outlying data point is: %4.2f\n',DELETE(:))

%*****************************************************************
*****
```

```
%Determine the confidence interval:

n=length(SAMPLE1); %n is equal to the number of samples in the
filtered data set
Confidence1=input('\nTo calculate the first confidence interval,
please enter the \nappropriate percent in decimal form (0.80, 0.90,
0.95, 0.98, 0.99): '); %"Confidence1" establishes the first percent
confidence interval.
Confidence2=input('\nTo calculate the second confidence interval,
please enter the \nappropriate percent in decimal form (0.80, 0.90,
0.95, 0.98, 0.99): '); %"Confidence2" establishes the second percent
confidence interval.
Alpha1=1-Confidence1;
Alpha2=1-Confidence2;
Nu=n-1; %Nu is equal to the degress of freedom.

if Alpha1 >= 0.1950 && Alpha1 <= 0.2050 %Alpha for 80% confidence
    AlphaIndex1=1; %The various "AlphaIndexes" correspond to the
different columns in the t-distribution table.
elseif Alpha1 >= 0.0950 && Alpha1 <= 0.1050 %Alpha for 90% confidence
    AlphaIndex1=2;
elseif Alpha1 >= 0.0450 && Alpha1 <= 0.0550 %Alpha for 95% confidence
    AlphaIndex1=3;
elseif Alpha1 >= 0.0195 && Alpha1 <= 0.0250 %Alpha for 98% confidence
    AlphaIndex1=4;
elseif Alpha1 >= 0.0050 && Alpha1 <= 0.0150 %Alpha for 99% confidence
    AlphaIndex1=5;
end

if Alpha2 >= 0.1950 && Alpha2 <= 0.2050 %Alpha for 80% confidence
    AlphaIndex2=1; %The various "AlphaIndexes" correspond to the
different columns in the t-distribution table.
elseif Alpha2 >= 0.0950 && Alpha2 <= 0.1050 %Alpha for 90% confidence
    AlphaIndex2=2;
elseif Alpha2 >= 0.0450 && Alpha2 <= 0.0550 %Alpha for 95% confidence
    AlphaIndex2=3;
elseif Alpha2 >= 0.0195 && Alpha2 <= 0.0250 %Alpha for 98% confidence
    AlphaIndex2=4;
elseif Alpha2 >= 0.0050 && Alpha2 <= 0.0150 %Alpha for 99% confidence
    AlphaIndex2=5;
end

T_TABLE=[3.078 6.314 12.706 31.823 63.658; 1.886 2.920 4.303 6.964
9.925
    1.638 2.353 3.182 4.541 5.841; 1.533 2.132 2.776 3.747 4.604
    1.476 2.015 2.571 3.365 4.032; 1.440 1.943 2.447 3.143 3.707
    1.415 1.895 2.365 2.998 3.499; 1.397 1.860 2.306 2.896 3.355
    1.383 1.833 2.262 2.821 3.250; 1.372 1.812 2.228 2.764 3.169
    1.363 1.796 2.201 2.718 3.106; 1.356 1.782 2.179 2.681 3.054
    1.350 1.771 2.160 2.650 3.012; 1.345 1.761 2.145 2.624 2.977
    1.341 1.753 2.131 2.602 2.947; 1.337 1.746 2.120 2.583 2.921
    1.333 1.740 2.110 2.567 2.898; 1.330 1.734 2.101 2.552 2.878
    1.328 1.729 2.093 2.539 2.861; 1.325 1.725 2.086 2.528 2.845
    1.323 1.721 2.080 2.518 2.831; 1.321 1.717 2.074 2.508 2.819
    1.319 1.714 2.069 2.500 2.807; 1.318 1.711 2.064 2.492 2.797
    1.316 1.708 2.060 2.485 2.787; 1.315 1.706 2.056 2.479 2.779
```

```
    1.314 1.703 2.052 2.473 2.771; 1.313 1.701 2.048 2.467 2.763
    1.311 1.699 2.045 2.463 2.756; 1.310 1.697 2.042 2.457 2.750];
%student t-distribution table.

t1_a2=T_TABLE(Nu,AlphaIndex1); %t1_a2 is the t value derived from the
t-distribution table for 95% confidence, based on corresponding
values of Nu and AlphaIndex1.
t2_a2=T_TABLE(Nu,AlphaIndex2); %t2_a2 is the t value derived from the
t-distribution table for 99% confidence, based on corresponding
values of Nu and AlphaIndex2.

Uncert1=t1_a2*(StandDev/sqrt(n)); %Estimate of population mean
uncertainty
Uncert2=t2_a2*(StandDev/sqrt(n)); %Estimate of population mean
uncertainty

clc
if length(DELETE)>0
fprintf('An outliying data point is %4.2f, which can be deleted from
the sample space\n',DELETE)
fprintf('\nThe filtered sample, which includes no outlying data
points, is: ');
SAMPLE1
end
display(' ')

%Part B: Find the Sample Mean:
fprintf('The sample mean is %4.2f\n',Mean)
 %Part C: Find the sample standard deviation:
fprintf('The sample standard deviation is %4.2f\n',StandDev)

fprintf('The %.0f percent confidence interval is %4.2f +/-
%4.4f\n',Confidence1*100,Mean,Uncert1)
fprintf('The %.0f percent confidence interval is %4.2f +/-
%4.4f\n',Confidence2*100,Mean,Uncert2)
```

APPENDIX C

MATLAB Statistical Analysis Code: Null Hypothesis Tests

```
clear all
clc
format long
set(0,'defaultAxesFontName', 'Times New Roman')
%Use the command "c = listfonts" to return a sorted list of available
system fonts.

%PART 1: Sorting the data and establishing variables:

load DeflectionOutPutAA1.TXT
TimeAA1=DeflectionOutPutAA1(:,1); %Column Vector of time data points
in milliseconds, starting from zero.
DefAA1=DeflectionOutPutAA1(:,2); %Column Vector of center point
deflection values, in millimeters.

load DeflectionOutPutAA3.TXT
TimeAA3=DeflectionOutPutAA3(:,1); %Column Vector of time data points
in milliseconds, starting from zero.
DefAA3=DeflectionOutPutAA3(:,2); %Column Vector of center point
deflection values, in millimeters.

load DeflectionOutPutAA4.TXT
TimeAA4=DeflectionOutPutAA4(:,1); %Column Vector of time data points
in milliseconds, starting from zero.
DefAA4=DeflectionOutPutAA4(:,2); %Column Vector of center point
deflection values, in millimeters.

load DeflectionOutPutAA5.TXT
TimeAA5=DeflectionOutPutAA5(:,1); %Column Vector of time data points
in milliseconds, starting from zero.
DefAA5=DeflectionOutPutAA5(:,2); %Column Vector of center point
deflection values, in millimeters.

load DeflectionOutPutWA1.TXT
TimeWA1=DeflectionOutPutWA1(:,1); %Column Vector of time data points
in milliseconds, starting from zero.
DefWA1=DeflectionOutPutWA1(:,2); %Column Vector of center point
deflection values, in millimeters.

load DeflectionOutPutWA2.TXT
TimeWA2=DeflectionOutPutWA2(:,1); %Column Vector of time data points
in milliseconds, starting from zero.
DefWA2=DeflectionOutPutWA2(:,2); %Column Vector of center point
deflection values, in millimeters.

load DeflectionOutPutWA3.TXT
TimeWA3=DeflectionOutPutWA3(:,1); %Column Vector of time data points
in milliseconds, starting from zero.
DefWA3=DeflectionOutPutWA3(:,2); %Column Vector of center point
deflection values, in millimeters.

load DeflectionOutPutWA4.TXT
TimeWA4=DeflectionOutPutWA4(:,1); %Column Vector of time data points
in milliseconds, starting from zero.
```

```
DefWA4=DeflectionOutPutWA4(:,2); %Column Vector of center point
deflection values, in millimeters.

load DeflectionOutPutWAHT1.TXT
TimeWAHT1=DeflectionOutPutWAHT1(:,1); %Column Vector of time data
points in milliseconds, starting from zero.
DefWAHT1=DeflectionOutPutWAHT1(:,2); %Column Vector of center point
deflection values, in millimeters.

load DeflectionOutPutWAHT2.TXT
TimeWAHT2=DeflectionOutPutWAHT2(:,1); %Column Vector of time data
points in milliseconds, starting from zero.
DefWAHT2=DeflectionOutPutWAHT2(:,2); %Column Vector of center point
deflection values, in millimeters.

load DeflectionOutPutWALT1.TXT
TimeWALT1=DeflectionOutPutWALT1(:,1); %Column Vector of time data
points in milliseconds, starting from zero.
DefWALT1=DeflectionOutPutWALT1(:,2); %Column Vector of center point
deflection values, in millimeters.

load DeflectionOutPutWALT2.TXT
TimeWALT2=DeflectionOutPutWALT2(:,1); %Column Vector of time data
points in milliseconds, starting from zero.
DefWALT2=DeflectionOutPutWALT2(:,2); %Column Vector of center point
deflection values, in millimeters.

load DeflectionOutPutWW1.TXT
TimeWW1=DeflectionOutPutWW1(:,1); %Column Vector of time data points
in milliseconds, starting from zero.
DefWW1=DeflectionOutPutWW1(:,2); %Column Vector of center point
deflection values, in millimeters.

load DeflectionOutPutWW2.TXT
TimeWW2=DeflectionOutPutWW2(:,1); %Column Vector of time data points
in milliseconds, starting from zero.
DefWW2=DeflectionOutPutWW2(:,2); %Column Vector of center point
deflection values, in millimeters.

load DeflectionOutPutWW3.TXT
TimeWW3=DeflectionOutPutWW3(:,1); %Column Vector of time data points
in milliseconds, starting from zero.
DefWW3=DeflectionOutPutWW3(:,2); %Column Vector of center point
deflection values, in millimeters.

load DeflectionOutPutWWHT1.TXT
TimeWWHT1=DeflectionOutPutWWHT1(:,1); %Column Vector of time data
points in milliseconds, starting from zero.
DefWWHT1=DeflectionOutPutWWHT1(:,2); %Column Vector of center point
deflection values, in millimeters.

load DeflectionOutPutWWHT2.TXT
TimeWWHT2=DeflectionOutPutWWHT2(:,1); %Column Vector of time data
points in milliseconds, starting from zero.
```

```
DefWWHT2=DeflectionOutPutWWHT2(:,2); %Column Vector of center point
deflection values, in millimeters.

load DeflectionOutPutWWLT1.TXT
TimeWWLT1=DeflectionOutPutWWLT1(:,1); %Column Vector of time data
points in milliseconds, starting from zero.
DefWWLT1=DeflectionOutPutWWLT1(:,2); %Column Vector of center point
deflection values, in millimeters.

load DeflectionOutPutWWLT2.TXT
TimeWWLT2=DeflectionOutPutWWLT2(:,1); %Column Vector of time data
points in milliseconds, starting from zero.
DefWWLT2=DeflectionOutPutWWLT2(:,2); %Column Vector of center point
deflection values, in millimeters.



%Designate the maximum positive and negative displacements in the
Air/Air
%experiment set:
MaxPos_AA1=max(DefAA1); %Identify the maximum positive displacement
of the Air/Air 1 panel.
MaxNeg_AA1=min(DefAA1); %Identify the maximum negative displacement
of the Air/Air 1 panel.
MaxPos_AA3=max(DefAA3); %Identify the maximum positive displacement
of the Air/Air 3 panel.
MaxNeg_AA3=min(DefAA3); %Identify the maximum negative displacement
of the Air/Air 3 panel.
MaxPos_AA4=max(DefAA4); %Identify the maximum positive displacement
of the Air/Air 4 panel.
MaxNeg_AA4=min(DefAA4); %Identify the maximum negative displacement
of the Air/Air 4 panel.
MaxPos_AA5=max(DefAA5); %Identify the maximum positive displacement
of the Air/Air 5 panel.
MaxNeg_AA5=min(DefAA5); %Identify the maximum negative displacement
of the Air/Air 5 panel.
fprintf('The maximum positive deflection in the Air/Air 1 Panel is
%.4f mm\n',MaxPos_AA1)
fprintf('The maximum positive deflection in the Air/Air 3 Panel is
%.4f mm\n',MaxPos_AA3)
fprintf('The maximum positive deflection in the Air/Air 4 Panel is
%.4f mm\n',MaxPos_AA4)
fprintf('The maximum positive deflection in the Air/Air 5 Panel is
%.4f mm\n\n',MaxPos_AA5)
fprintf('The maximum negative deflection in the Air/Air 1 Panel is
%.4f mm\n',MaxNeg_AA1)
fprintf('The maximum negative deflection in the Air/Air 3 Panel is
%.4f mm\n',MaxNeg_AA3)
fprintf('The maximum negative deflection in the Air/Air 4 Panel is
%.4f mm\n',MaxNeg_AA4)
fprintf('The maximum negative deflection in the Air/Air 5 Panel is
%.4f mm\n\n',MaxNeg_AA5)

%Calculate the average maximum positive displacement in the Air/Air
%experiment set:
```

```
SAMPLE_AA=[MaxPos_AA1 MaxPos_AA3 MaxPos_AA4 MaxPos_AA5];
MaxPosAA_Ave=mean(SAMPLE_AA);
fprintf('The mean positive deflection in the Air/Air Panels is %.4f
mm\n',MaxPosAA_Ave)

%Calculate the standard deviation of the maximum positive
displacements in
%the Air/Air experiment set:
StandDevAA=std(SAMPLE_AA);
fprintf('The standard devistion of the positive deflections in the
Water/Air Panels is %.4f mm\n\n',StandDevAA)
fprintf('**************************************************************
***********\n\n')

%**************************************************************************
***************

%Designate the maximum positive and negative displacements in the
Water/Air
%experiment set:
MaxPos_WA1=max(DefWA1); %Identify the maximum positive displacement
of the Water/Air 1 panel.
MaxNeg_WA1=min(DefWA1); %Identify the maximum negative displacement
of the Water/Air 1 panel.
MaxPos_WA2=max(DefWA2); %Identify the maximum positive displacement
of the Water/Air 2 panel.
MaxNeg_WA2=min(DefWA2); %Identify the maximum negative displacement
of the Water/Air 2 panel.
MaxPos_WA3=max(DefWA3); %Identify the maximum positive displacement
of the Water/Air 3 panel.
MaxNeg_WA3=min(DefWA3); %Identify the maximum negative displacement
of the Water/Air 3 panel.
MaxPos_WA4=max(DefWA4); %Identify the maximum positive displacement
of the Water/Air 4 panel.
MaxNeg_WA4=min(DefWA4); %Identify the maximum negative displacement
of the Water/Air 4 panel.
fprintf('The maximum positive deflection in the Water/Air 1 Panel is
%.4f mm\n',MaxPos_WA1)
fprintf('The maximum positive deflection in the Water/Air 2 Panel is
%.4f mm\n',MaxPos_WA2)
fprintf('The maximum positive deflection in the Water/Air 3 Panel is
%.4f mm\n',MaxPos_WA3)
fprintf('The maximum positive deflection in the Water/Air 4 Panel is
%.4f mm\n\n',MaxPos_WA4)
fprintf('The maximum negative deflection in the Water/Air 1 Panel is
%.4f mm\n',MaxNeg_WA1)
fprintf('The maximum negative deflection in the Water/Air 2 Panel is
%.4f mm\n',MaxNeg_WA2)
fprintf('The maximum negative deflection in the Water/Air 3 Panel is
%.4f mm\n',MaxNeg_WA3)
fprintf('The maximum negative deflection in the Water/Air 4 Panel is
%.4f mm\n\n',MaxNeg_WA4)

%Calculate the average maximum positive displacement in the Water/Air
%experiment set:
SAMPLE_WA=[MaxPos_WA1 MaxPos_WA2 MaxPos_WA3 MaxPos_WA4];
```

```
AVEMaxPosWA=mean(SAMPLE_WA);
fprintf('The mean positive deflection in the Water/Air Panels is %.4f
mm\n',AVEMaxPosWA)

%Calculate the standard deviation of the maximum positive
displacements in
%the Water/Air experiment set:
StandDevWA=std(SAMPLE_WA);
fprintf('The standard devistion of the positive deflections in the
Water/Air Panels is %.4f mm\n\n\n',StandDevWA)
fprintf('**********************************************************
**********\n\n')

%**********************************************************************
***************

%Designate the maximum positive and negative displacements in the
high
%temperature Water/Air experiment set:
MaxPos_WAHT1=max(DefWAHT1); %Identify the maximum positive
displacement of the high temperature Water/Air 1 panel.
MaxNeg_WAHT1=min(DefWAHT1); %Identify the maximum negative
displacement of the high temperature Water/Air 1 panel.
MaxPos_WAHT2=max(DefWAHT2); %Identify the maximum positive
displacement of the high temperature Water/Air 2 panel.
MaxNeg_WAHT2=min(DefWAHT2); %Identify the maximum negative
displacement of the high temperature Water/Air 2 panel.
fprintf('The maximum positive deflection in the high temperature
Water/Air 1 Panel is %.4f mm\n',MaxPos_WAHT1)
fprintf('The maximum positive deflection in the high temperature
Water/Air 2 Panel is %.4f mm\n\n\n',MaxPos_WAHT2)
fprintf('The maximum negative deflection in the high temperature
Water/Air 1 Panel is %.4f mm\n',MaxNeg_WAHT1)
fprintf('The maximum negative deflection in the high temperature
Water/Air 2 Panel is %.4f mm\n\n\n',MaxNeg_WAHT2)

%Calculate the average maximum positive displacement in the high
temperature Water/Air
%experiment set:
SAMPLE_WAHT=[MaxPos_WAHT1 MaxPos_WAHT2];
AVEMaxPosWAHT=mean(SAMPLE_WAHT);
fprintf('The mean positive deflection in the high temperature
Water/Air Panels is %.4f mm\n',AVEMaxPosWAHT)

%Calculate the standard deviation of the maximum positive
displacements in
%the high temperature Water/Air experiment set:
StandDevWAHT=std(SAMPLE_WAHT);
fprintf('The standard devistion of the positive deflections in the
hightemperature Water/Air Panels is %.4f mm\n\n\n',StandDevWAHT)
fprintf('**********************************************************
**********\n\n')

%**********************************************************************
***************
```

```
%Designate the maximum positive and negative displacements in the low
%temperature Water/Air experiment set:
MaxPos_WALT1=max(DefWALT1); %Identify the maximum positive
displacement of the low temperature Water/Air 1 panel.
MaxNeg_WALT1=min(DefWALT1); %Identify the maximum negative
displacement of the low temperature Water/Air 1 panel.
MaxPos_WALT2=max(DefWALT2); %Identify the maximum positive
displacement of the low temperature Water/Air 2 panel.
MaxNeg_WALT2=min(DefWALT2); %Identify the maximum negative
displacement of the low temperature Water/Air 2 panel.
fprintf('The maximum positive deflection in the low temperature
Water/Air 1 Panel is %.4f mm\n',MaxPos_WALT1)
fprintf('The maximum positive deflection in the low temperature
Water/Air 2 Panel is %.4f mm\n\n',MaxPos_WALT2)
fprintf('The maximum negative deflection in the low temperature
Water/Air 1 Panel is %.4f mm\n',MaxNeg_WALT1)
fprintf('The maximum negative deflection in the low temperature
Water/Air 2 Panel is %.4f mm\n\n',MaxNeg_WALT2)

%Calculate the average maximum positive displacement in the low
temperature Water/Air
%experiment set:
SAMPLE_WALT=[MaxPos_WALT1 MaxPos_WALT2];
AVEMaxPosWALT=mean(SAMPLE_WALT);
fprintf('The mean positive deflection in the low temperature
Water/Air Panels is %.4f mm\n',AVEMaxPosWALT)

%Calculate the standard deviation of the maximum positive
displacements in
%the low temperature Water/Air experiment set:
StandDevWALT=std(SAMPLE_WALT);
fprintf('The standard devistion of the positive deflections in the
low temperature Water/Air Panels is %.4f mm\n\n',StandDevWALT)
fprintf('**********************************************************
**********\n\n')

%**************************************************************
***************

%PART 2: Test to see if the Water/Air displacements are statistically
different from each
%other, across temperatures:

fprintf('Null hypothesis 1: The average displacements of the room
temperature \nWater/Air environment and high temperature Water/Air
\nenvironment are statistically the same.\n\n')
disp('Alternate hypothesis 1: Those displacements are not the same.')
disp(' ')
fprintf('Null hypothesis 2: The average displacements of the room
temperature \nWater/Air environment and low temperature Water/Air
\nenvironment statistically are the same.\n\n')
disp('Alternate hypothesis 2: Those displacements are not the same.')
disp(' ')
```

```
fprintf('Null hypothesis 3: The average displacements of the low
temperature \nWater/Air environment and high temperature Water/Air
\nenvironment are the same.\n\n')
disp('Alternate hypothesis 3: Those displacements are not the same.')
disp(' ')
disp('**********************************************************
***')
disp(' ')

n2=length(SAMPLE_WA); %n2 is the number of data points associated
with the Water/Air environment.
n4=length(SAMPLE_WAHT); %n4 is the number of data points associated
with the high temperature Water/Air environment.
n8=length(SAMPLE_WALT); %n8 is the number of data points associated
with the low temperature Water/Air environment.

%FIRST HYPOTHESIS TEST:
disp('FIRST HYPOTHESIS TEST:')

Nu24=n2+n4-2; %Calculate the degrees of freedom

Var2=StandDevWA^2; %Calculate the variance for the Water/Air
environment.
Var4=StandDevWAHT^2; %Calculate the variance for the high temperature
Water/Air environment.

PopVar24=sqrt(((n2-1)*Var2+(n4-1)*Var4)/Nu24); %Calculate the
population variance.
to_24=(abs(AVEMaxPosWA-
AVEMaxPosWAHT))/(PopVar24*sqrt((1/n2)+(1/n4))); %Hypothetical "t"
value.

AlphaIndex=2; %Desired confidence interval is 90%; so alpha is 0.1,
alpha over 2 is 0.05, and the corresponding column in the "t" table
is 2.

T_TABLE=[3.078 6.314 12.706 31.823 63.658; 1.886 2.920 4.303 6.964
9.925
    1.638 2.353 3.182 4.541 5.841; 1.533 2.132 2.776 3.747 4.604
    1.476 2.015 2.571 3.365 4.032; 1.440 1.943 2.447 3.143 3.707
    1.415 1.895 2.365 2.998 3.499; 1.397 1.860 2.306 2.896 3.355
    1.383 1.833 2.262 2.821 3.250; 1.372 1.812 2.228 2.764 3.169
    1.363 1.796 2.201 2.718 3.106; 1.356 1.782 2.179 2.681 3.054
    1.350 1.771 2.160 2.650 3.012; 1.345 1.761 2.145 2.624 2.977
    1.341 1.753 2.131 2.602 2.947; 1.337 1.746 2.120 2.583 2.921
    1.333 1.740 2.110 2.567 2.898; 1.330 1.734 2.101 2.552 2.878
    1.328 1.729 2.093 2.539 2.861; 1.325 1.725 2.086 2.528 2.845
    1.323 1.721 2.080 2.518 2.831; 1.321 1.717 2.074 2.508 2.819
    1.319 1.714 2.069 2.500 2.807; 1.318 1.711 2.064 2.492 2.797
    1.316 1.708 2.060 2.485 2.787; 1.315 1.706 2.056 2.479 2.779
    1.314 1.703 2.052 2.473 2.771; 1.313 1.701 2.048 2.467 2.763
    1.311 1.699 2.045 2.463 2.756; 1.310 1.697 2.042 2.457 2.750];
%T_TABLE represents the student t-distribution table.
```

```
t1_24=T_TABLE(Nu24,AlphaIndex); %t1_24 is the t value derived from
the t-distribution table for 90% confidence, based on corresponding
values of Nu24 and AlphaIndex.

if abs(to_24) > t1_24
    fprintf('Since the "t" for the null hypothosis (%.4f)
exceeds\n',to_24)
    fprintf('that for the desired 90 percent confidence interval
(%.4f),\n',t1_24)
    fprintf('the null hypothesis must be rejected: room temperature
and high temperature displacements are not the same\n')
    j1=5;
end

if abs(to_24) <= t1_24
    fprintf('Since the "t" for the null hypothosis (%.4f) does not
exceed\n',to_24)
    fprintf('that for the desired 90 percent confidence interval
(%.4f),\n',t1_24)
    fprintf('the null hypothesis must be accepted: room temperature
and high temperature displacements are the same\n')
    j1=15;
end

disp(' ')
disp('**************************************************************
***')
disp(' ')

%SECOND HYPOTHESIS TEST:
disp('SECOND HYPOTHESIS TEST:')

Nu28=n2+n8-2; %Calculate the degrees of freedom

Var2=StandDevWA^2; %Calculate the variance for the Water/Air
environment.
Var8=StandDevWALT^2; %Calculate the variance for the low temperature
Water/Air environment.

PopVar28=sqrt(((n2-1)*Var2+(n8-1)*Var8)/Nu28); %Calculate the
population variance.
to_28=(abs(AVEMaxPosWA-
AVEMaxPosWALT))/(PopVar28*sqrt((1/n2)+(1/n8))); %Hypothetical "t"
value.

AlphaIndex=2; %Desired confidence interval is 90%; so alpha is 0.1,
alpha over 2 is 0.05, and the corresponding column in the "t" table
is 2.

T_TABLE=[3.078 6.314 12.706 31.823 63.658; 1.886 2.920 4.303 6.964
9.925
    1.638 2.353 3.182 4.541 5.841; 1.533 2.132 2.776 3.747 4.604
    1.476 2.015 2.571 3.365 4.032; 1.440 1.943 2.447 3.143 3.707
    1.415 1.895 2.365 2.998 3.499; 1.397 1.860 2.306 2.896 3.355
    1.383 1.833 2.262 2.821 3.250; 1.372 1.812 2.228 2.764 3.169
```

```
    1.363 1.796 2.201 2.718 3.106; 1.356 1.782 2.179 2.681 3.054
    1.350 1.771 2.160 2.650 3.012; 1.345 1.761 2.145 2.624 2.977
    1.341 1.753 2.131 2.602 2.947; 1.337 1.746 2.120 2.583 2.921
    1.333 1.740 2.110 2.567 2.898; 1.330 1.734 2.101 2.552 2.878
    1.328 1.729 2.093 2.539 2.861; 1.325 1.725 2.086 2.528 2.845
    1.323 1.721 2.080 2.518 2.831; 1.321 1.717 2.074 2.508 2.819
    1.319 1.714 2.069 2.500 2.807; 1.318 1.711 2.064 2.492 2.797
    1.316 1.708 2.060 2.485 2.787; 1.315 1.706 2.056 2.479 2.779
    1.314 1.703 2.052 2.473 2.771; 1.313 1.701 2.048 2.467 2.763
    1.311 1.699 2.045 2.463 2.756; 1.310 1.697 2.042 2.457 2.750];
%T_TABLE represents the student t-distribution table.

t1_28=T_TABLE(Nu28,AlphaIndex); %t1_28 is the t value derived from
the t-distribution table for 90% confidence, based on corresponding
values of Nu28 and AlphaIndex.

if abs(to_28) > t1_28
    fprintf('Since the "t" for the null hypothosis (%.4f)
exceeds\n',to_28)
    fprintf('that for the desired 90 percent confidence interval
(%.4f),\n',t1_28)
    fprintf('the null hypothesis must be rejected: room temperature
and low temperature displacements are not the same\n')
    j2=5;
end

if abs(to_28) <= t1_28
    fprintf('Since the "t" for the null hypothosis (%.4f) does not
exceed\n',to_28)
    fprintf('that for the desired 90 percent confidence interval
(%.4f),\n',t1_28)
    fprintf('the null hypothesis must be accepted: room temperature
and low temperature displacements are the same\n')
    j2=15;
end

disp(' ')
disp('**************************************************************
***')
disp(' ')

%THIRD HYPOTHESIS TEST:
disp('THIRD HYPOTHESIS TEST:')

Nu48=n4+n8-2; %Calculate the degrees of freedom

Var4=StandDevWAHT^2; %Calculate the variance for the high temperature
Water/Air environment.
Var8=StandDevWALT^2; %Calculate the variance for the low temperature
Water/Air environment.

PopVar48=sqrt(((n4-1)*Var4+(n8-1)*Var8)/Nu48); %Calculate the
population variance.
```

```
to_48=(abs(AVEMaxPosWAHT-
AVEMaxPosWALT))/(PopVar48*sqrt((1/n4)+(1/n8))); %Hypothetical "t"
value.

AlphaIndex=2; %Desired confidence interval is 90%; so alpha is 0.1,
alpha over 2 is 0.05, and the corresponding column in the "t" table
is 2.

T_TABLE=[3.078 6.314 12.706 31.823 63.658; 1.886 2.920 4.303 6.964
9.925
    1.638 2.353 3.182 4.541 5.841; 1.533 2.132 2.776 3.747 4.604
    1.476 2.015 2.571 3.365 4.032; 1.440 1.943 2.447 3.143 3.707
    1.415 1.895 2.365 2.998 3.499; 1.397 1.860 2.306 2.896 3.355
    1.383 1.833 2.262 2.821 3.250; 1.372 1.812 2.228 2.764 3.169
    1.363 1.796 2.201 2.718 3.106; 1.356 1.782 2.179 2.681 3.054
    1.350 1.771 2.160 2.650 3.012; 1.345 1.761 2.145 2.624 2.977
    1.341 1.753 2.131 2.602 2.947; 1.337 1.746 2.120 2.583 2.921
    1.333 1.740 2.110 2.567 2.898; 1.330 1.734 2.101 2.552 2.878
    1.328 1.729 2.093 2.539 2.861; 1.325 1.725 2.086 2.528 2.845
    1.323 1.721 2.080 2.518 2.831; 1.321 1.717 2.074 2.508 2.819
    1.319 1.714 2.069 2.500 2.807; 1.318 1.711 2.064 2.492 2.797
    1.316 1.708 2.060 2.485 2.787; 1.315 1.706 2.056 2.479 2.779
    1.314 1.703 2.052 2.473 2.771; 1.313 1.701 2.048 2.467 2.763
    1.311 1.699 2.045 2.463 2.756; 1.310 1.697 2.042 2.457 2.750];
%T_TABLE represents the student t-distribution table.

t1_48=T_TABLE(Nu48,AlphaIndex); %t1_48 is the t value derived from
the t-distribution table for 90% confidence, based on corresponding
values of Nu48 and AlphaIndex.

if abs(to_48) > t1_48
    fprintf('Since the "t" for the null hypothosis (%.4f)
exceeds\n',to_48)
    fprintf('that for the desired 90 percent confidence interval
(%.4f),\n',t1_48)
    fprintf('the null hypothesis must be rejected: high temperature
and low temperature displacements are not the same\n')
    j3=5;
end

if abs(to_48) <= t1_48
    fprintf('Since the "t" for the null hypothosis (%.4f) does not
exceed\n',to_48)
    fprintf('that for the desired 90 percent confidence interval
(%.4f),\n',t1_48)
    fprintf('the null hypothesis must be accepted: high temperature
and low temperature displacements are the same\n')
    j3=15;
end

disp(' ')
disp('**************************************************************
***')
disp(' ')
```

```
%*****************************************************************
**
%PART 3: Determine random error for each sample mean:

%Room tmperature Water/Air environment:
Nu2=n2-1;
t2=T_TABLE(Nu2,AlphaIndex);
P2=t2*(StandDevWA/sqrt(n2));
fprintf('The mean maximum positive deflection for the room
temperature Water/Air environment (at 90 percent confidence)\n')
fprintf('is equal to %4.2f, plus or minus %4.2f mm\n',AVEMaxPosWA,P2)
disp(' ')

%High temperature Water/Air environment:
Nu4=n4-1;
t4=T_TABLE(Nu4,AlphaIndex);
P4=t4*(StandDevWAHT/sqrt(n4));
fprintf('The mean maximum positive deflection for the high
temperature temperature Water/Air environment (at 90 percent
confidence)\n')
fprintf('is equal to %4.2f, plus or minus %4.2f
mm\n',AVEMaxPosWAHT,P4)
disp(' ')

%Low temperature Water/Air environment:
Nu8=n8-1;
t8=T_TABLE(Nu8,AlphaIndex);
P8=t8*(StandDevWALT/sqrt(n8));
fprintf('The mean maximum positive deflection for the low temperature
Water/Air environment (at 90 percent confidence)\n')
fprintf('is equal to %4.2f, plus or minus %4.2f
mm\n',AVEMaxPosWALT,P8)
disp(' ')
```

BIBLIOGRAPHY

Batra, R. C., & Hassan, N. M. (2007). Response of fiber reinforced composites to underwater explosive loads. *Composites Part B: Engineering*, *38*(4), 448–468.

Batra, R. C., & Hassan, N. M. (2008). Blast resistance of unidirectional fiber reinforced composites. *Composites Part B: Engineering*, *39*(3), 513–536.

Brinkley, S. R., & Kirkwood, J. G. (1945). *Tables and Graphs of the Theoretical Peak Pressures, Energies, and Impulses of Shock Waves from Explosives Sources in Sea Water*. Office of Scientific Research and Development.

Cichocki, K. (1999). Effects of underwater blast loading on structures with protective elements. *International Journal of Impact Engineering*, *22*(6), 609–617.

Cole, R. H. (1948). *Underwater explosions*. Princeton Univ. Press.

Espinosa, H. D., Lee, S., & Moldovan, N. (2006). A Novel Fluid Structure Interaction Experiment to Investigate Deformation of Structural Elements Subjected to Impulsive Loading. *Experimental Mechanics*, *46*(6), 805–824.

Gracia, D. (2012). *Underwater Blast Loading Performance of Composite Panels*. University of Rhode Island.

Haile, M. A., Yin, W., & Ifju, P. G. (2009). MATLAB® based Image PreProcessing and Digital Image Correlation of Objects in Liquid. In *Proceedings of the SEM Annual Conference*. Albuquerque, New Mexico, USA.

Hartmann, G. K., & Laboratory, N. S. W. C. W. O. (1976). *Wave making by an underwater explosion*. Naval Surface Weapons Center, White Oak Laboratory.

LeBlanc, J., Gardner, N., & Shukla, A. (2013). Effect of polyurea coatings on the response of curved E-Glass/Vinyl ester composite panels to underwater explosive loading. *Composites Part B: Engineering*, *44*(1), 565–574.

LeBlanc, J., & Shukla, A. (2011). Dynamic response of curved composite panels to underwater explosive loading: Experimental and computational comparisons. *Composite Structures*, *93*(11), 3072–3081.

Ngo, T., Mendis, P., Gupta, A., & Ramsay, J. (2007). Blast Loading and Blast Effects on Structures - An Overview. *Eectronic Journal of Structural Engineering*, (Special Issue: Loading on Structures), 76–91.

Rajendran, R., & Lee, J. M. (2009). Blast Loaded Plates. *Marine Structures*, *22*(2), 99–127.

Rajendran, R., & Narasimhan, K. (2001). Damage prediction of clamped circular plates subjected to contact underwater explosion. *International Journal of Impact Engineering*, *25*(4), 373–386.

Sadd, M. (2009). *Wave Motion and Vibration in Continuous Media*. University of Rhode Island.

Shin, Y. S. (2004). Ship shock modeling and simulation for far-field underwater explosion. *Computers & Structures*, *82*(23–26), 2211–2219.

Shukla, A., & Dally, J. W. (2010). *Experimental solid mechanics*. Knoxville, Tenn.: College House Enterprises.

Smith, P., & Hetherington, J. (1994). *Blast and Ballistic Loading of Structures*. CRC Press.

Spranghers, K., Vasilakos, I., Lecompte, D., Sol, H., & Vantomme, J. (2012). Full-Field Deformation Measurements of Aluminum Plates Under Free Air Blast Loading. *Experimental Mechanics*, *52*(9), 1371–1384.

Sutton, M. A., Orteu, J. J., & Schreier, H. (2009). *Image Correlation for Shape, Motion and Deformation Measurements: Basic Concepts,Theory and Applications* (2009 edition.). Springer.

Torabizadeh, M. (2013). Tensile, compressive and shear properties of unidirectional glass/epoxy composites subjected to mechanical loading and low temperature services. *Indian Journal of Engineering & Materials Sciences*, *20*, 299–309.

Van Lear, B. T. (2008). *Underwater Explosions with Fluid-Structure Interactions*. University of Minnesota.

Wang, Z., Zhou, Y., & Mallick, P. (2002). Effects of Temperature and Strain Rate on the Tensile Behavior of Short Fiber Reinforced Polyamide-6. *Polymer Composites*, *23*(5), 858–871.

Zakrisson, B., Wikman, B., & Häggblad, H.-Å. (2011). Numerical simulations of blast loads and structural deformation from near-field explosions in air. *International Journal of Impact Engineering*, *38*(7), 597–612.